Adding insult to injury: mechanistic basis for how AmpC mutations allow *Pseudomonas aeruginosa* to accelerate cephalosporin hydrolysis and evade avibactam

by

Cole Lee Slater

A Thesis submitted to the Faculty of Graduate Studies of

The University of Manitoba

in partial fulfillment of the requirements for the degree of

Master of Science

Department of Microbiology

University of Manitoba

Winnipeg, Manitoba, Canada

Abstract

Pseudomonas aeruginosa is a leading cause of nosocomial infections worldwide and notorious for its broad-spectrum resistance to antibiotics. A key mechanism that confers extensive resistance to β-lactam antibiotics is the inducible expression of AmpC, a highly efficient Ambler class C β-lactamase enzyme. Unfortunately, several *P. aeruginosa* clinical isolates expressing mutated forms of AmpC have been found to be clinically resistant to the novel antipseudomonal β-lactam/β-lactamase inhibitor (BLI) combinations ceftolozane/tazobactam and ceftazidime/avibactam. The objective of this thesis was to investigate the enzymatic activity of four of these reported AmpC mutants, E247K, G183D, T96I, and ΔG229–E247 (alongside wild-type (WT) AmpC from *P. aeruginosa* PAO1), to gain detailed insights into how these mutations circumvent these clinically vital antibiotic/inhibitor combinations. The effect of these mutations on the catalytic cycle of AmpC was found to be two-fold. First, they reduced the stability of the enzyme, which presumably increased its flexibility. This appeared to accelerate deacylation of the enzyme-bound β-lactam, which resulted in greater catalytic efficiencies towards ceftolozane and ceftazidime. Second, these mutations reduced the affinity of avibactam for AmpC by increasing the apparent activation energy barrier of the enzyme acylation step. The catalytic turnover of ceftolozane and ceftazidime was not influenced by this significantly, as deacylation was found to be the rate-limiting step for the breakdown of these antibiotics. It is remarkable that these mutations enhance the catalytic efficiency of AmpC towards ceftolozane and ceftazidime while simultaneously reducing susceptibility to inhibition by avibactam. It is our hope that the knowledge gained from the molecular analysis of these and other AmpC resistance mutants will aid the design of β-lactams and BLIs with reduced susceptibility to mutational resistance.

Acknowledgements

First and foremost, I would like to thank my supervisor, Dr. Brian Mark, for conceptualizing this intriguing research project and allowing me the opportunity to challenge it. His guidance and unwavering support throughout these past two years aided my academic success and development as a researcher. I would also like to thank the members of my advisory committee, Dr. Ayush Kumar and Dr. Frank Schweizer, for their frequent encouragement and valuable insight, as well as the Canadian Institute for Health Research (CIHR) for providing the financial support that made this research possible.

I want to extend my sincerest gratitude towards Dr. Judith Winogrodzki for all the time and energy she spent towards formally training and educating me in molecular biology, enzyme kinetics, and protein crystallography. Her knowledge of and dedication to scientific research helped shape this project into what it is today. I am incredibly grateful for her guidance.

I would also like to acknowledge Dr. Mazdak Khajehpour for offering his expertise and extensive knowledge in enzymology, as it helped me tremendously with both the analysis and interpretation of the overwhelming amounts of kinetic data collected for this project.

I am also thankful for all the members of the Mark lab, who continue to provide a safe, friendly, and positive work environment. The same can be said for the rest of the students and faculty members within the Department of Microbiology, including the helpful support staff.

Last, but certainly not least, I want to thank my family: mom, dad, Brennan, and Emily. Their unconditional love, support, and patience has helped me more than they will ever know. I wholeheartedly dedicate this thesis to them.

Table of Contents

List of Tables

List of Figures

List of Acronyms

AA	Amino acid
Ala	Alanine
Asn	Asparagine
AVI	Avibactam
BLI	β-lactamase inhibitor
bp	Base Pair
BSA	Bovine serum albumin
˚C	Degrees celsius
CAZ	Ceftazidime
DBO	Diazabicyclooctane
DNA	Deoxyribonucleic acid
DSF	Differential scanning fluorimeter
EDTA	Ethylenediaminetetraacetic acid
FDA	Food and Drug Administration
FPLC	Fast protein liquid chromatography
Gen	Gentamycin
GlcNAc	*N*-acetylglucosamine
Glu	Glutamic acid
Gly	Glycine
HEPES	4-(2-hydroxyethyl)-1-piperazineethanesulfonic acid
hrs	Hours
IPTG	Isopropyl-β-D-1-thiogalactopyranoside
k_{off}^{app}	Apparent rate constant for inhibitor dissociation (s^{-1})
k_{on}^{app}	Apparent rate constant for inhibitor binding (M^{-1} s^{-1})
Kan	Kanamycin
k_{cat}	Enzyme turnover number (catalytic rate constant) (s^{-1})
k_{cat}/K_m	Specificity constant (catalytic efficiency)
kDa	kiloDaltons
$K_{I\text{-}binding}$	Apparent inhibition binding constant (M)
K_m	Michaelis constant (substrate affinity)
k_{obs}	Pseudo-first order rate constant (s^{-1})
Lys	Lysine
M	Molar
MDR	Multidrug-resistant
µg	Microgram
mg	Milligram
µl	Microlitre
ml	Millilitre
µM	Micromolar
mM	Millimolar
MIC	Minimum inhibitory concentration
MW	Molecular weight
MWCO	Molecular weight cut-off
MurNAc	*N*-acetylmuramic acid
N/A	Not applicable

NEB	New England Biolabs
ND	Not determined
ng	Nanogram
nm	Nanometre
nM	Nanomolar
OD	Optical density
ORF	Open reading frame
PBP	Penicillin binding protein
PCR	Polymerase chain reaction
PDB	Protein data bank
PDC	*Pseudomonas*-derived cephalosporinase
PG	Peptidoglycan
pI	Isoelectric point
PMSF	Phenylmethanesulphonylfluoride
RT	Room temperature
rpm	Revolutions per minute
s	Seconds
SANC*	Structural Alignment-based Numbering of class C β-lactamases
SD	Standard deviation
SDS	Sodium dodecyl sulfate
SDS–PAGE	Sodium dodecyl sulfate polyacrylamide gel electrophoresis
SE	Standard error
Ser	Serine
TAZO	Tazobactam
TB	Terrific broth
TCAG	The Centre for Applied Genomics
Thr	Threonine
T_m	Melting temperature
TOL	Ceftolozane
Tyr	Tyrosine
UDP	Uridine diphosphate
UV	Ultraviolet
V_{max}	Maximum enzyme velocity
WT	Wild-type

* The numbering of all AmpC residues discussed throughout this thesis represents their positions in the immature form of the enzyme (i.e., signal peptide included), and is consistent with the SANC scheme, proposed by Mack *et al.* (2019). Any mention of the "SANC position" of a residue indicates its position in the mature form of the enzyme (e.g., the SANC position of the AmpC catalytic serine, Ser90, is 64).

1. Introduction

1.1. Antibiotics: discovery and development of resistance

Antibiotics are small molecule compounds that reduce or inhibit the growth of microorganisms. Naturally, environmental microbes like saprophytic bacteria and fungi produce antibiotics as a means of protection (Holmes *et al.* 2016). The discovery of these compounds led to their use (and eventual misuse) in clinical medicine. Indeed, antibiotic therapy continues to be a predominant strategy for combatting infections caused by numerous pathogens, including *Staphylococcus aureus*, *Streptococcus pneumoniae*, *Acinetobacter baumannii*, and, most relevant to this thesis, *Pseudomonas aeruginosa* (Aslam *et al.* 2018). While antibiotics have undoubtedly revolutionized healthcare throughout the last century, the rates of novel drug discovery and development have slowed dramatically since the 1980s (de la Fuente-Nunez 2019). Indeed, the last discovery of a novel molecular scaffold informing a new class of antibiotics was nearly 30 years ago (de la Fuente-Nunez 2019). Moreover, although antibiotic design and development remains a vigorous, multi-billion-dollar scientific venture, its progress is pale in comparison to that of the evolution of antibiotic resistance (Aslam *et al.* 2018). This is attributed to the excessive use and misuse of antibiotics in clinics and livestock farming, increased international travel, and inadequate sanitization. These practices provide the selection pressure that promotes the development of multidrug-resistant (MDR) bacterial pathogens, which navigate rather effortlessly between animals, humans, and the environment. Indeed, prolonged and repeated antibiotic exposure has facilitated the evolution of numerous bacterial defense mechanisms, including inhibition of drug entry or distribution, enzymatic modification of the drug target, and drug inactivation, to name a few (Aslam *et al.* 2018).

1.2. *Pseudomonas aeruginosa*

While there are numerous bacterial pathogens currently threatening human health and rapidly evolving resistance mechanisms against the antibiotics targeting them, the organism of particular interest to this thesis is the Gram-negative Gammaproteobacterium, *Pseudomonas aeruginosa*. *P. aeruginosa* is a leading opportunistic pathogen notorious for establishing chronic and often fatal nosocomial infections in immunocompromised cancer patients and burn victims (Lister *et al.* 2009). It also contributes significantly to the frequent occurrence and spread of chronic respiratory infections in cystic fibrosis patients (Talwalkar and Murray 2016). Not surprisingly, the morbidity and mortality rates associated with this organism are among the highest of all clinically relevant Gram-negative pathogens (Thaden *et al.* 2017). This is attributed, in part, to its extensive intrinsic multidrug resistance profile (Lister *et al.* 2009), a feature that has helped to establish it as one of the World Health Organization's top three priority pathogens for research and discovery of new antibiotics (WHO, 2017). This resistance profile protects *P. aeruginosa* against a suite of antibiotic classes, including aminoglycosides and quinolones (Hancock and Speert 2000); however, this thesis is focused specifically on its ability to circumvent the bactericidal effects of β-lactam antibiotics.

1.3. β-lactam antibiotics

1.3.1. Mechanism of action of β-lactam antibiotics

Among the myriad of drugs used to combat *P. aeruginosa* infections are the β-lactam antibiotics (Lister *et al.* 2009). These drugs are defined by their β-lactam ring, a highly reactive, four-membered cyclic amide (Gilchrist 1987; Mandell and Perti 1996). All β-lactam antibiotics function to impede cell wall synthesis by interfering with peptidoglycan cross-linking (Mandell

and Perti 1996). It is necessary to discuss the mechanism of peptidoglycan synthesis in order to understand how β-lactams interfere with this process. To begin, peptidoglycan is a mesh-like network of alternating β-1,4-linked *N*-acetylglucosamine (GlcNAc) and *N*-acetylmuramic acid (MurNAc) sugars cross-linked by short peptides (Holtje 1998). It is used to construct the cell wall, a defining feature of bacterial cells that, in addition to providing shape and structure, confers protection and regulates osmotic pressure (Vollmer and Holtje 2001). Bacteria employ an assortment of enzymes to accomplish the synthesis, maturation, and recycling of peptidoglycan. Specifically, transglycosylases polymerize the glycan strand by linking together the GlcNAc and MurNAc sugars of peptidoglycan precursor molecules, while DD–transpeptidases catalyze peptide bond formation between the *meso*-diaminopimelic acid (*meso*-DAP) of the acceptor GlcNAc-MurNAc-pentapeptide and the D-alanine (D-Ala) of the donor pentapeptide (Sauvage *et al.* 2008). This peptide bond is hydrolyzed by DD–endopeptidases during peptidoglycan recycling and repair (Vollmer *et al.* 2008). Finally, DD–carboxypeptidases cleave the terminal D-Ala from the peptidoglycan precursor molecules (Frère 2004).

Most relevant to this discussion are the DD–transpeptidases, also known as penicillin binding proteins (PBPs), as they are the target enzymes of β-lactam antibiotics (Mandell and Perti 1996). The process of peptidoglycan cross-linking begins with PBP acylation, whereby the PBP obtains a GlcNAc-MurNAc-pentapeptide molecule to deliver to the growing peptidoglycan sacculus (Holtje 1998) (**Fig. 1.1**). This is accomplished when the catalytic serine of the PBP launches a nucleophilic attack on the carbonyl carbon of the penultimate D-Ala of this peptidoglycan precursor, releasing the terminal D-Ala. The acylated PBP then catalyzes the formation of a peptide bond between the D-Ala to which it is covalently bound and the *meso*-DAP of the acceptor GlcNAc-MurNAc-pentapeptide of the nascent peptidoglycan chain (Holtje

1998). The function of β-lactams is to block PBP acylation and therefore prevent PBPs from delivering peptidoglycan precursors to the growing cell wall (Mandell and Perti 1996). To do this, the β-lactam presents a carbonyl carbon to the PBP that mimics the D-Ala–D-Ala peptide bond on which this enzyme naturally launches a nucleophilic attack (Mandell and Perti 1996). The PBP "mistakenly" attacks this carbonyl carbon, which opens up the β-lactam ring and results in the formation of a highly stable acyl–enzyme complex. Since PBPs are mostly incapable of hydrolytic deacylation (Knox *et al.* 1996), dissociation of this complex is very slow. This renders the PBP inactive and therefore unavailable to facilitate peptidoglycan cross-linking. As the β-lactam molecules continue to outcompete the donor GlcNAc-MurNAc-pentapeptides for PBP acylation, cell wall synthesis slows down and the sacculus weakens. If the cell lacks the appropriate mechanisms to combat the β-lactam drug, it eventually lyses, as its fragile inner membrane is unequipped to handle osmotic pressure (Vollmer and Holtje 2001).

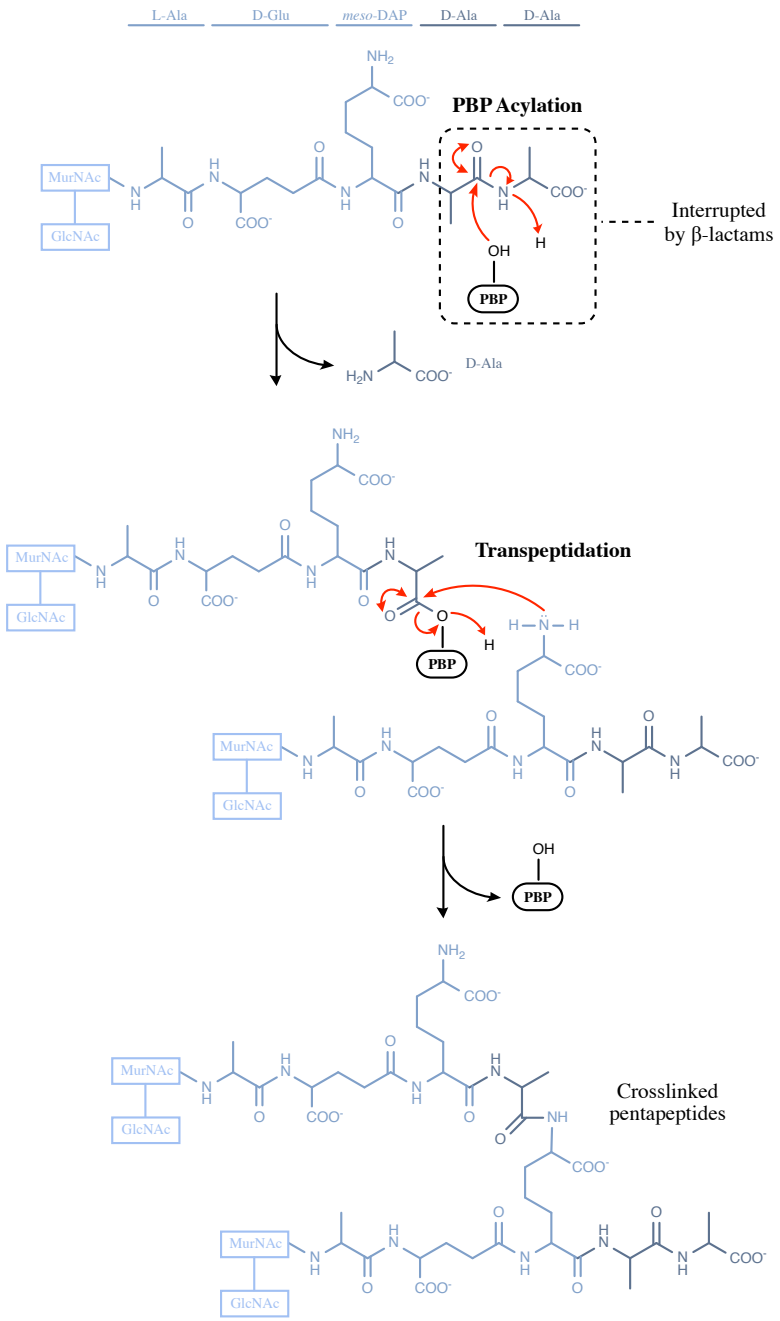

Figure 1.1 – Mechanism of peptidoglycan crosslinking. **(A)** PBP Acylation. The catalytic serine of the DD–transpeptidase (PBP) launches a nucleophilic attack on the carbonyl carbon of the penultimate D-Ala of the donor GlcNAc-MurNAc-pentapeptide, releasing the terminal D-Ala. **(B)** Transpeptidation. The *meso*-DAP of the acceptor GlcNAc-MurNAc-pentapeptide is then covalently linked to the D-Ala of the donor and the PBP is released. The function of β-lactam antibiotics is to disrupt peptidoglycan crosslinking by interrupting PBP acylation. The PBP "mistakenly" attacks the carbonyl carbon of the β-lactam ring instead of that of the donor GlcNAc-MurNAc-pentapeptide, rendering it inactive and unavailable for crosslinking. This figure was adapted from "A 1.2-Å snapshot of the final step of bacterial cell wall biosynthesis" by Lee *et al.* (2001) in PNAS, **98(4):**1427–1431 © United States National Academy of Sciences.

1.3.2. Classification of β-lactam antibiotics

There are four main classes of β-lactam antibiotics, each with a unique β-lactam nucleus (**Fig. 1.2**). All four types of nuclei contain the characteristic β-lactam ring, so the distinguishing feature is the five- or six-membered ring to which it is fused. The presence of a secondary ring provides room for additional substituents or functional groups that protect the drug against β-lactamase-mediated hydrolysis and/or provide clinically beneficial properties such as increased stability or weak convulsion-inducing potential (Mandell and Perti 1996). A brief description of each β-lactam class is below.

Monobactams. These are the least structurally sophisticated of the β-lactam classes, as their β-lactam ring is not fused to a secondary ring (i.e., monocyclic). The C-3 atom of the ring, however, can be substituted with large functional groups, while the nitrogen atom is linked to sulfonic acid. The absence of a ring fusion accounts for the relatively low spectrum of activity and high β-lactamase susceptibility observed in these antibiotics, leaving them infrequently prescribed (Bush and Bradford 2016). In fact, aztreonam is the only monobactam approved for therapeutic use. Fortunately, it is effective against *P. aeruginosa* (Bush and Bradford 2016).

Penams. More commonly regarded as penicillins, these antibiotics are characterized by the fusion of a sulfur-containing 5-membered ring to the β-lactam ring. Benzylpenicillin (penicillin G), the first β-lactam ever discovered and approved for clinical use, is a defining member of this class (Rammelkamp and Keefer 1943). Most penams, including ampicillin and amoxicillin, do not possess intrinsic stability against β-lactamases, and are therefore co-administered with β-lactamase inhibitors to enhance their efficacy (Bush and Bradford 2016).

Carbapenems. Like the penams, the β-lactam ring of carbapenems is fused to a 5-membered ring; however, this ring contains a C-2–C-3 double bond, and the sulfur atom at

position 1 is replaced by a carbon atom, providing space for an additional functional group (Papp-Wallace *et al.* 2011). Of all the β-lactam classes, carbapenems exhibit the broadest spectrum of activity and the greatest potency against both Gram-negative and Gram-positive bacteria (Papp-Wallace *et al.* 2011). As such, they are often used as last-resort treatment options for infections caused by MDR bacteria. Their reliance on outer membrane porins (OMPs) for entry into cells, however, presents an opportunity for the development of resistance (Martinez-Martinez 2008) (see section 1.4). Examples include imipenem and meropenem.

Cephalosporins. This class of antibiotics began with the discovery of cephalosporin C from the fungus *Cephalosporium acremonium* (Abraham and Newton 1961). The bulkiness of the 6-membered dihydrothiazine ring of the β-lactam nucleus increases steric hindrance and therefore broadens its spectrum of activity compared to the monobactams and penams (O'Callaghan 1979). Of particular interest to this thesis are the novel antipseudomonal cephalosporins ceftazidime and ceftolozane (**Fig. 1.3**). These β-lactams share an R1 side chain composed of three distinct moieties: (1) an aminothiadiazole ring that enhances activity against Gram-negative bacilli like *P. aeruginosa*; (2) an oxime moiety that confers stability against β-lactamases; (3) a dimethyl acetic acid moiety that heightens antipseudomonal activity (Zhanel *et al.* 2014). They are distinguishable only by the R2 side chain, which is a methyl-pyridinium ring in ceftazidime (Caprile 1988) and a 2-methyl-3-aminopyrazolium substituent in ceftolozane (Toda *et al.* 2008). Notably, ceftolozane and ceftazidime are among the most effective β-lactam antibiotics used to treat infections caused by MDR *P. aeruginosa* (van Duin and Bonomo 2016).

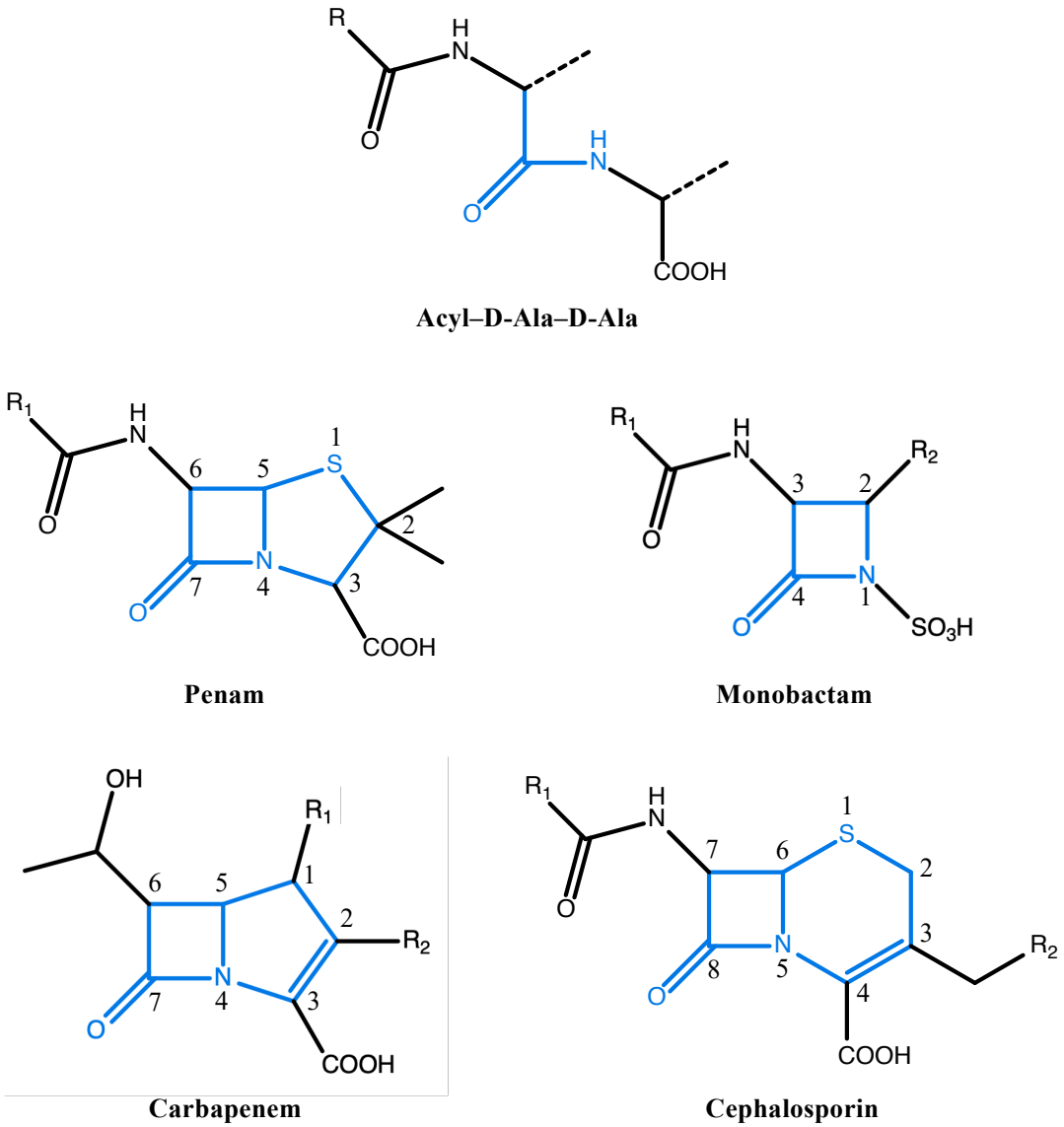

Figure 1.2 – Chemical structures of the four classes of β-lactam antibiotics. The nucleus of each β-lactam class is outlined in blue. The defining feature of all β-lactam antibiotics is the four-membered β-lactam ring, which is an analogue of the D-Ala–D-Ala of the GlcNAc-MurNAc-pentapeptide used in peptidoglycan biosynthesis (included for comparison) (Mandell and Perti 1996).

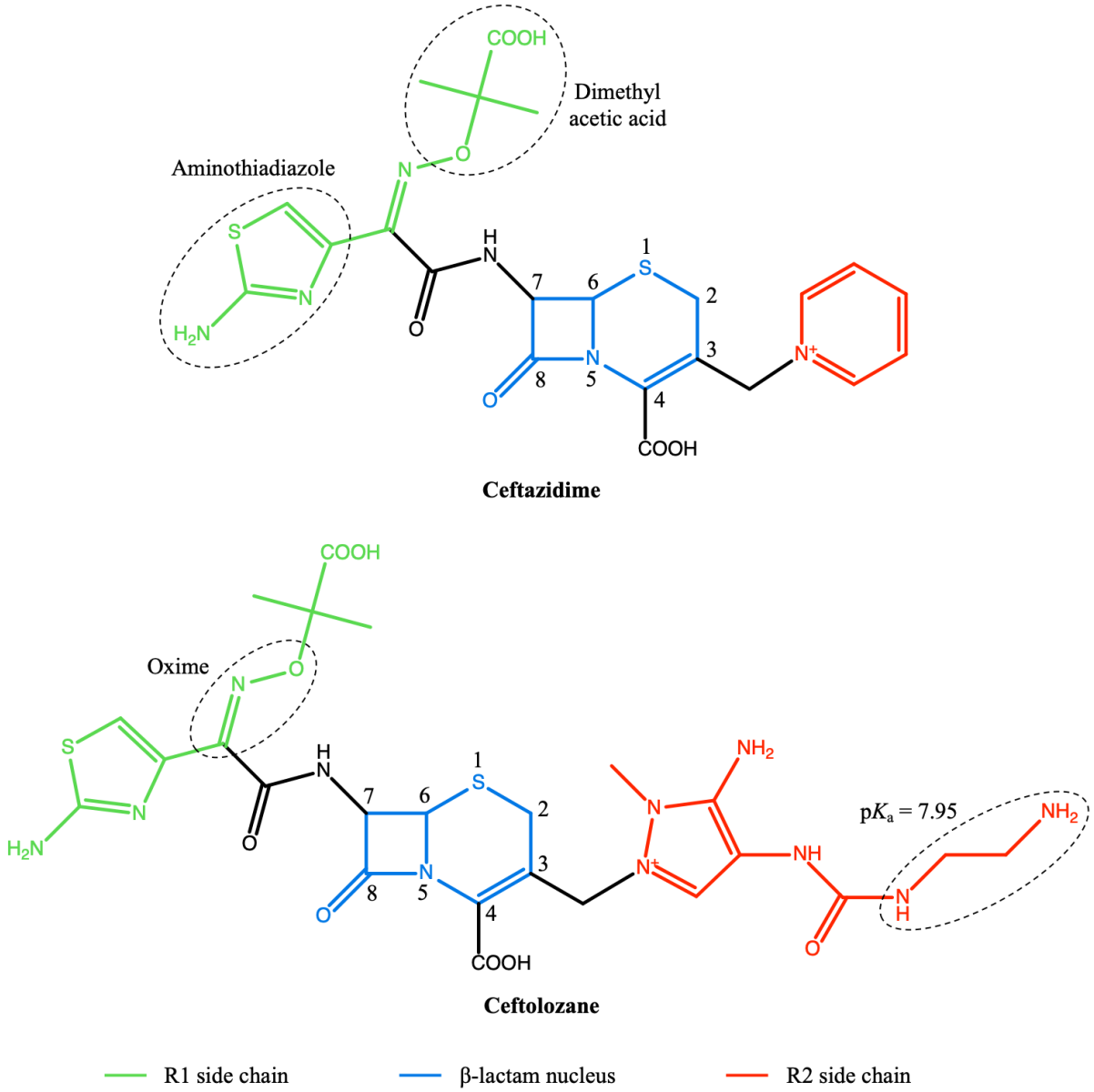

Figure 1.3 – Chemical structures of ceftazidime and ceftolozane. These cephalosporins have the same R1 (7-position) side chain (green) and β-lactam nucleus (blue). The R1 side chain has three main components: (1) an aminothiadiazole ring that enhances activity against Gram-negative bacilli; (2) an oxime moiety that confers stability against β-lactamases; (3) a dimethyl acetic acid moiety that heightens antipseudomonal activity. The R2 (3-position) side chain (red) is what distinguishes these antibiotics. Ceftazidime contains a methyl-pyridinium functional group that also exhibits antipseudomonal activity. Ceftolozane, on the other hand, contains a 2-methyl-3-aminopyrazolium moiety harbouring a 2-aminoethylureido group which provides bulkiness and a net positive charge to the drug (pK_a = 7.95) (Zhanel *et al.* 2014).

1.4. Resistance to β-lactam antibiotics

A defining feature of *P. aeruginosa* is its remarkable multidrug resistance profile, which unfortunately extends to include the β-lactam antibiotics. Indeed, this pathogen readily combats these drugs through an array of acquired, adaptive, and intrinsic resistance mechanisms (Babic *et al.* 2006). Acquired β-lactam resistance includes horizontal transfer of resistance genes (Breidenstein *et al.* 2011), while adaptive resistance commonly manifests as biofilm formation in the lungs of infected patients. This robust microbial consortium provides a diffusion barrier that slows the invasion of β-lactams into the cells (Drenkard 2003). It also aids in the development of MDR persister cells, which cause long-lasting or recurrent infections in people battling cystic fibrosis (Mulcahy *et al.* 2010). Of particular concern, however, are the four primary intrinsic resistance mechanisms. These are described below.

Reduced expression of OMPs. PBPs, the target enzymes of β-lactams, reside in the periplasm; therefore, β-lactams must traverse the outer membrane and/or peptidoglycan layer to reach them. While zwitterionic β-lactams like the cephalosporins cefepime and cefpirome can rapidly diffuse through the outer membrane (Nikaido *et al.* 1990), bulkier drugs like carbapenems must travel through outer-membrane porins (OMPs). *P. aeruginosa* exploits this requirement by reducing the expression of OMPs (or selecting for spontaneous mutations in them) in an attempt to decrease membrane permeability. A common example is the Q142X mutation of the OprD porin, which has been shown to confer robust carbapenem resistance (Livermore 2001). While effective in reducing the periplasmic levels of certain β-lactams, this mechanism is typically accompanied by β-lactamase expression (Jacoby *et al.* 2004).

Efflux pumps. The presence of β-lactams in the periplasm of *P. aeruginosa* may also trigger overexpression of efflux systems, which consist of a series of membrane pumps that

function to rapidly expel β-lactams out of the cell and into the surrounding environment (Poole 2004). The MexA-MexB-OprM system is among the most common and effective efflux strategies employed by *P. aeruginosa* (Li *et al.* 2000). In fact, this is a common feature of MDR *P. aeruginosa* strains, as it also reduces susceptibility to protein synthesis inhibitors like tetracycline and chloramphenicol (Li *et al.* 2000).

Active site modifications of PBPs. Another strategy that *P. aeruginosa* employs to defend against β-lactams is the modification of PBP active sites. Selecting for mutations that reduce the affinity of PBPs for β-lactams allows these enzymes to evade inhibition while still maintaining peptidoglycan homeostasis (Drawz and Bonomo 2010). In some cases, however, spontaneous inactivation of non-essential DD–peptidases like PBP4 has been reported in *P. aeruginosa* in response to imipenem or piperacillin treatment in cystic fibrosis patients (Strateva and Yordanov 2009).

Production of β-lactamases. The fourth resistance mechanism, β-lactamase production, is the one most relevant to this thesis and will be described in more detail in the following section (1.5). Briefly, β-lactamases are enzymes that inactivate β-lactam-based antibiotics through hydrolysis of the β-lactam ring (Jacoby 2009). Concerningly, β-lactamase expression has been – and continues to be – the leading resistance mechanism employed by *P. aeruginosa* and other Gram-negative bacterial pathogens (Neu 1990; Prabaker and Weinstein 2011).

1.5. β-lactamases

1.5.1. Catalytic mechanism of β-lactamases

As mentioned above, β-lactamases are bacterial enzymes that function to inactivate β-lactam-based antibiotics through hydrolysis of the β-lactam ring (Jacoby 2009). β-lactam

hydrolysis proceeds by a mechanism involving acylation and subsequent deacylation of the β-lactamase (**Fig. 1.4**). (Some β-lactamases accomplish β-lactam inactivation without acylation – see section 1.5.2). Acylation occurs when the catalytic serine launches a nucleophilic attack on the β-lactam carbonyl carbon, forming a high-energy acylation intermediate. This leads to opening of the β-lactam ring and the formation of a low-energy acyl–enzyme complex. Deacylation occurs when a catalytic water attacks this complex, facilitating the formation of a high-energy deacylation intermediate that promotes the release of the inactive β-lactam product from the enzyme (Minasov *et al.* 2002). The active site is regenerated, enabling continued hydrolysis of the antibiotic molecules (Drawz and Bonomo 2010).

There is sufficient genetic and mechanistic evidence to suggest that β-lactamases evolved from PBPs (Knox *et al.* 1996; Urbach *et al.* 2009; Morar and Wright 2010). One major difference between PBPs and (serine) β-lactamases, however, is the addition of a basic residue in the β-lactamase active site. Depending on the type or "class" of β-lactamase, this residue may be a tyrosine (Tyr150) or glutamic acid (Glu166) (see section 1.5.2) (Knox *et al.* 1996; Tomanicek *et al.* 2011). This extra functional residue confers mechanistic versatility to β-lactamases, specifically by facilitating hydrolytic deacylation (which, as described above, is the final step of the β-lactam catalysis mechanism). While the lysine-serine dyad of PBPs is effective in facilitating peptidase activity for cell wall biosynthesis, the absence of a general base from this catalytic motif renders it insufficient to hydrolyze β-lactam antibiotics (Knox *et al.* 1996).

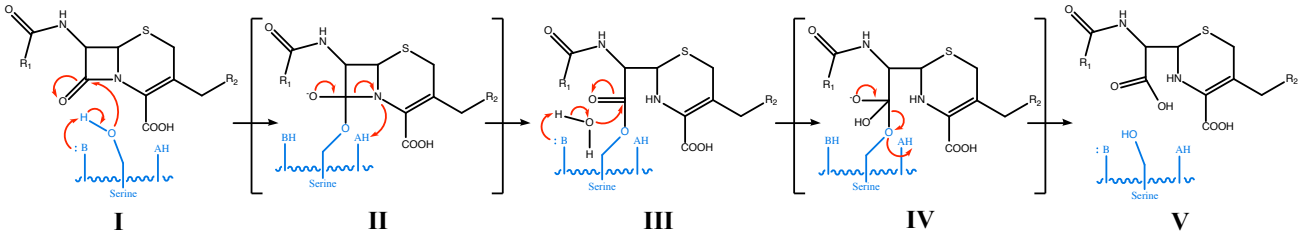

Figure 1.4 – Schematic of β-lactam hydrolysis by serine β-lactamases. β-lactam hydrolysis proceeds by a mechanism involving acylation and deacylation of the β-lactamase. Acylation occurs when the catalytic serine (Ser90 in class C β-lactamases [SANC position 64]) launches a nucleophilic attack on the β-lactam carbonyl carbon **(I)**, forming a high-energy acylation intermediate **(II)** that leads to opening of the β-lactam ring and the formation of a low-energy acyl–enzyme complex **(III)**. Deacylation occurs when a catalytic water attacks the acyl–enzyme complex **(IV)**, facilitating the formation of a high-energy deacylation intermediate that promotes the release of the inactive β-lactam product from the enzyme **(V)**. A lysine residue (Lys93 in class C β-lactamases [SANC position 67]) functions as the general acid (A), and depending on the class of β-lactamase, the general base (B) is glutamic acid or tyrosine (Minasov *et al.* 2002). This figure was adapted with permission from "The deacylation mechanism of AmpC β-lactamase at ultrahigh resolution" by Chen *et al.* (2006) in J. Am. Chem. Soc., **128(9):**2970–2976 © American Chemical Society.

1.5.2. Classification of β-lactamases

There are two primary classification schemes for β-lactamases: (1) the Ambler classification scheme, which is based on amino acid sequence homology and places β-lactamases into one of four classes, A through D (i.e., structural classification) (Ambler 1980); (2) the Bush–Jacoby–Medeiros classification scheme, which categorizes β-lactamases into groups 1 through 4 according to substrate preference and susceptibility to β-lactamase inhibitors (i.e., functional classification) (Bush *et al.* 1995). While both schemes are useful, the former is less convoluted and as such will be used for this review. A brief description of each class is below.

Class A: Serine penicillinases. As the name suggests, these enzymes predominantly hydrolyze penicillins (but also some cephalosporins) by a mechanism involving a catalytic serine residue (Bush and Jacoby 2009). Although classes C and D also hydrolyze β-lactams by a serine-based mechanism, class A β-lactamases are unique in that their catalytic cycle relies on a glutamic acid residue (Glu166) to activate the hydrolytic water during deacylation (Herzberg and Moult 1987). Representative enzymes include KPC-2 (*Klebsiella pneumoniae* carbapenemase) and *Escherichia coli* TEM-1, the first plasmidic β-lactamase (Datta and Kontomichalou 1965).

Class B: Metallo-β-lactamases. The defining feature of this class of β-lactamases is the absence of a catalytic serine in the active site. Instead, these enzymes utilize a pair of Zn^{2+} ions, which coordinate with the hydroxyl group of a water molecule, to directly hydrolyze the β-lactam. Concerningly, class B β-lactamases inactivate most β-lactams, including carbapenems (Walsh *et al.* 2005). Representative enzymes include IMP-1 and VIM-1 (Bush and Jacoby 2009).

Class C: Cephalosporinases. Mechanistically, these enzymes are highly similar to class A β-lactamases; however, a tyrosine residue (Tyr150) is used as the general activating base for deacylation rather than glutamic acid (Drawz and Bonomo 2010). Moreover, their predominant

β-lactam targets are the cephalosporins. A representative enzyme is AmpC, which is the β-lactamase investigated in this thesis. This enzyme is discussed in greater detail in section 1.6.

Class D: Oxacillinases. These serine β-lactamases were named for their ability to hydrolyze oxacillin, a narrow-spectrum penicillin, considerably faster than class A and C serine β-lactamases (Danel *et al.* 2007). Uniquely, their catalytic mechanism centers around the carboxylation of the active-site lysine (Lys70). Ionization of the carbamic acid of this lysine yields a carbamate anion that interacts with the catalytic serine (Ser67) via hydrogen bonding. This carboxylated lysine functions as the general base by activating both Ser67 and a catalytic water (for acylation and deacylation, respectively) (Golemi *et al.* 2001). Representative enzymes include OXA-1 and OXA-10, as well as OXA-50, which is constitutively expressed in *P. aeruginosa* (Walther-Rasmussen and Hoiby 2006; Bush and Jacoby 2009).

1.6. AmpC β-lactamases

1.6.1. Overview

AmpC is a particularly robust group 1, Ambler class C β-lactamase enzyme (Bush and Jacoby 2010; Ambler 1980) capable of hydrolyzing a wide range of β-lactams – including penicillins, monobactams, and cephalosporins – with remarkable efficiency (Jacoby 2009). Indeed, these enzymes hydrolyze many β-lactams at their diffusion limit (Bulychev and Mobashery 1999). Specifically, at their most efficient, AmpC β-lactamases can exhibit catalytic efficiencies towards their preferred β-lactam substrates (cephalosporins) of 10^7 to 10^8 M^{-1} s^{-1} (Dubus *et al.* 1996). Moreover, they are resistant to inhibition by the clinically relevant β-lactamase inhibitors clavulanic acid, sulbactam, and tazobactam; in fact, these compounds often behave as inducers of AmpC expression (Mark *et al.* 2011) (see section 1.7.2).

Historically, these cephalosporinases were expressed chromosomally by *P. aeruginosa* and are therefore often regarded as *Pseudomonas*-derived cephalosporinases (PDCs). AmpC enzymes were also initially found among members of the Enterobacteriaceae family, particularly *Enterobacter* spp., *C. freundii*, and *S. marcescens*; however, they have begun to disperse among Enterobacteriaceae on plasmids (Munier *et al.* 2010). These plasmid-borne AmpC enzymes are classified as cephamycinases due to their ability to also hydrolyze cephamycins (Bush and Bradford 2016). The focus of this thesis, however, is on the AmpC β-lactamase from *P. aeruginosa*, as its production is among the most prevalent and effective mechanisms employed by this pathogen to obtain clinically relevant levels of β-lactam resistance (Jacoby 2009).

1.6.2. Regulation of AmpC expression

Expression of *ampC* (or bla_{PDC}), the chromosomal gene encoding the AmpC enzyme, is regulated by the Gram-negative peptidoglycan recycling pathway (Park and Uehara 2008) (**Fig. 1.5**). As previously discussed, peptidoglycan is a network of alternating GlcNAc and MurNAc sugars cross-linked by short peptides (Holtje 1998) (**Fig. 1.1**). During normal cellular growth, hydrolytic enzymes called autolysins excise fragments of peptidoglycan (Vollmer *et al.* 2008), generating a series of GlcNAc-1,6-anhydroMurNAc-peptides (i.e., tri-, tetra-, and penta-peptides) (Park and Uehara 2008). The inner membrane permease, AmpG, then transports these muropeptides into the cytosol (Dietz *et al.* 1996; Cheng and Park 2002), where their GlcNAc sugars are removed by the glycoside hydrolase, NagZ (Cheng *et al.* 2000; Votsch and Templin 2000). This produces a pool of 1,6-anhydroMurNAc-peptide molecules, which are converted into UDP–MurNAc-peptides for cell wall anabolism (Park and Uehara 2008).

While the UDP–MurNAc-pentapeptides are thought to repress *ampC* transcription (Jacobs *et al.* 1997), the 1,6-anhydroMurNAc-pentapeptides are believed to induce it (Dietz *et al.* 1997). Specifically, these peptidoglycan metabolites compete for binding to the tetrameric transcriptional regulator, AmpR (Jacobs *et al.* 1997), and their relative quantities are influenced by the presence of β-lactams (Park and Uehara 2008). In the absence of β-lactams (i.e., during normal cellular growth), the *N*-acetyl-muramyl-L-alanine amidase, AmpD, separates the peptides from the 1,6-anhydroMurNAc sugars of the 1,6-anhydroMurNAc-pentapeptides (Holtje *et al.* 1994; Jacobs *et al.* 1995). Through a series of steps, these peptides are converted into UDP–MurNAc-pentapeptide molecules, which accumulate and out-compete the 1,6-anhydroMurNAc-pentapeptides for binding to AmpR, resulting in repression of *ampC* transcription (Holtje *et al.* 1994; Jacobs *et al.* 1995). Exposure to β-lactam antibiotics, on the other hand, leads to increased peptidoglycan fragmentation, leading to the accumulation of 1,6-anhydroMurNAc-pentapeptides (Dietz *et al.* 1997). This promotes displacement of the UDP–MurNAc-pentapeptides from AmpR, allowing the 1,6-anhydroMurNAc-pentapeptides to bind it instead, thereby activating *ampC* transcription (Dietz *et al.* 1997; Jacobs *et al.* 1997). The resulting AmpC enzyme is then delivered to the periplasm, where it inactivates the β-lactam antibiotic molecules in an attempt to re-establish peptidoglycan homeostasis (Rice 2009).

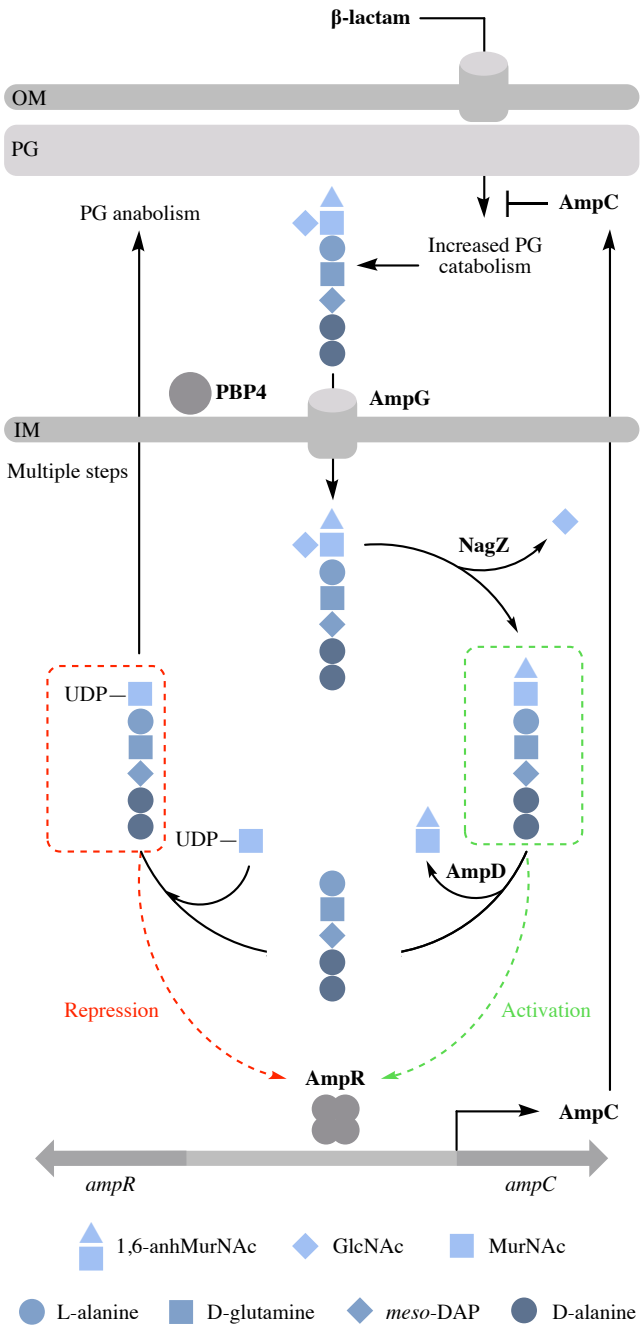

Figure 1.5 – Regulation of *ampC* expression. During normal cell growth, UDP-MurNAc-pentapeptides dominate the peptidoglycan metabolite pool and therefore bind AmpR, repressing *ampC* transcription. Introduction of β-lactam antibiotics to the cell increases peptidoglycan fragmentation, leading to the accumulation of 1,6-anhydroMurNAc-pentapeptides, which outcompete the UDP-MurNAc-pentapeptides for binding to AmpR, thereby relieving repression and permitting *ampC* transcription. The AmpC enzyme then enters the periplasm, where it hydrolyzes the antibiotic. This figure was adapted with permission from "The β-lactamase gene regulator AmpR is a tetramer that recognizes and binds the D-Ala–D-Ala motif of its repressor UDP-*N*-acetylmuramic acid (MurNAc)-pentapeptide" by Vadlamani *et al.* (2015) in J. Biol. Chem., **290(5):**2630–2643 © the American Society for Biochemistry and Molecular Biology.

Not surprisingly, several facets of this complex regulatory pathway have already been exploited by *P. aeruginosa* to strengthen its β-lactam resistance to clinically relevant levels. Indeed, selection of chromosomal *ampD* (AmpD) and *dacB* (PBP4) null mutations promote constitutive hyperproduction of AmpC. Specifically, loss of AmpD function promotes the accumulation of cytosolic 1,6-anhydroMurNAc-pentapeptides, which again act as inducers of *ampC* expression through the removal of AmpR repression (Holtje *et al.* 1994; Juan *et al.* 2006). Uniquely, *P. aeruginosa* contains three *ampD* homologues which are thought to be differentially expressed to balance *ampC* "derepression" and peptidoglycan recycling (Juan *et al.* 2006). This is a common occurrence in people battling cystic fibrosis or bloodstream nosocomial infections (Henrichfreise *et al.* 2007; Hocquet *et al.* 2007). Spontaneous inactivation of the non-essential endopeptidase PBP4, on the other hand, helps slow down peptidoglycan catabolism in order to minimize the effects of β-lactam-mediated inactivation of anabolic PBPs (Vollmer and Holtje 2004). It is worth mentioning that, while AmpR point mutants have also been found to promote constitutive hyperproduction of AmpC (Kuga *et al.* 2000), their occurrence is far less common than that of AmpD and PBP4 null mutants (Juan *et al.* 2005). This is likely because, in addition to regulating *ampC* expression, AmpR controls the transcription of many other genes in *P. aeruginosa* (Kong *et al.* 2005). Therefore, compromising its functionality would likely interfere with the expression of genes related to virulence and/or fitness (Mark *et al.* 2011).

1.7. β-lactamase inhibitors

1.7.1. Mechanism of action of β-lactamase inhibitors

The discovery of β-lactamases necessitated the development of β-lactamase inhibitors (BLIs). These small-molecule compounds are co-administered with specific β-lactam antibiotics

and, as the name suggests, function to inhibit β-lactamases (Drawz and Bonomo 2010). Most BLIs contain the same carbonyl carbon that β-lactamases target in β-lactams, and in this way, disguise themselves as substrates for these enzymes; however, the acyl–enzyme complexes that these BLIs form with β-lactamases undergo intramolecular rearrangements that prevent engagement with catalytic residues. This strongly disfavours hydrolytic deacylation of the inhibitor, allowing it to remain bound to the β-lactamase, rendering it inactive (Helfand *et al.* 2003). Consequently, hydrolysis of the β-lactam antibiotic is prevented, allowing it to inhibit PBPs and in turn disrupt cell wall biosynthesis. In this way, BLIs indirectly enhance the efficacy of their partner β-lactams (Drawz and Bonomo 2010).

1.7.2. Classification of β-lactamase inhibitors

There are four classes of BLIs, each with a unique pharmacophore (i.e., the moiety responsible for β-lactamase acylation) (**Fig. 1.6**). A brief description of each class is below.

Clavams. The defining BLI of this class is clavulanic acid, the first BLI employed in clinical medicine. It was first isolated from *Streptomyces clavuligerus* nearly 50 years ago (Reading and Cole 1977). Like the penam antibiotics, clavulanic acid harbours a β-lactam ring fused to a 5-membered ring. Position C-1 of this ring, however, is substituted with an enol ether oxygen. This is an excellent leaving group and therefore promotes secondary ring opening and, in turn, chemical reactions within the β-lactamase active site that disfavour deacylation. In this way, clavulanic acid is an irreversible "suicide" inhibitor (Drawz and Bonomo 2010). Unfortunately, clavulanic acid induces AmpC expression in *P. aeruginosa* (Lister *et al.* 1999).

Penicillanic acid sulfones. Like clavulanic acid, penicillanic acid sulfone BLIs are also β-lactam-based and therefore irreversibly inhibit β-lactamases (Drawz and Bonomo 2010). The

pharmacophore of this inhibitor class differs from that of clavams in that a sulfone replaces the oxygen at position C-1 of the 5-membered ring. Common examples include sulbactam and, of particular relevance to this thesis, tazobactam (English *et al.* 1978; Fisher *et al.* 1980). Unfortunately, they also induce AmpC expression in *P. aeruginosa* (Mark *et al.* 2011). This is why tazobactam is co-administered with the novel antipseudomonal cephalosporin, ceftolozane, which again exhibits remarkable stability against AmpC (van Duin and Bonomo 2016).

Boronic acid. Although the characteristic β-lactam motif is absent from these BLIs, the boron atom that replaces it is still an effective electrophile and can therefore form a reversible covalent bond with the catalytic serine of the β-lactamase (Beesley *et al.* 1983). Indeed, boron-based compounds have been used as serine protease inhibitors since the 1970s (Smoum *et al.* 2012). While these inhibitors show considerable potential – especially since their hydrolysis has yet to be reported – their use in therapeutics is still quite minimal, particularly due to the potential toxicity of the born atom (Papp-Wallace and Bonomo 2016). Vaborbactam is a well-known boronic acid-based BLI currently gaining clinical traction (Lapuebla *et al.* 2015).

Diazabicyclooctanes. Rather than the classical four-membered β-lactam ring, DBOs present the target carbonyl carbon in the form of a five-membered cyclic urea. This unique moiety promotes reversible inhibition of β-lactamases (Ehmann *et al.* 2012) (**Fig. 1.7**). Briefly, upon nucleophilic attack of the DBO scaffold, ring opening occurs and an acyl–enzyme complex forms rapidly through a stable carbamoyl linkage. The open-ring conformation of the DBO is highly similar to that of the unreacted form and is stabilized through favourable interactions with conserved catalytic residues (that is, the same residues responsible for β-lactam binding and catalysis) (Stachyra *et al.* 2010; Lahiri *et al.* 2013). Therefore, rather than eventual hydrolysis and turnover, deacylation of enzyme-bound DBOs promotes slow regeneration of their native

structures, enabling the same inhibitor molecule to perform several rounds of inhibition. It is these features that offer DBOs enhanced potency and spectrum of activity compared to β-lactam based BLIs. Examples include avibactam and the more recent relebactam, which differs from avibactam only through the addition of a piperidine ring to reduce efflux (Blizzard *et al.* 2014).

Avibactam, the BLI of particular relevance to this thesis, is the first FDA-approved DBO BLI (Papp-Wallace and Bonomo 2016). It is also the first BLI with clinically useful inhibitory activity against AmpC β-lactamases (Levasseur *et al.* 2012), as demonstrated by rapid acylation and slow deacylation rates (e.g., k_{on}^{app} of ~10^3 M^{-1} s^{-1} and k_{off}^{app} of ~10^{-5} s^{-1}) (Ehmann *et al.* 2013). Unlike clavulanic acid, sulbactam, and tazobactam, avibactam does not induce AmpC expression in *P. aeruginosa* (Tondi *et al.* 2005). Its co-administration with the novel antipseudomonal cephalosporin ceftazidime therefore yields a remarkably effective β-lactam/BLI combination for targeting infections caused by MDR *P. aeruginosa* (van Duin and Bonomo 2016).

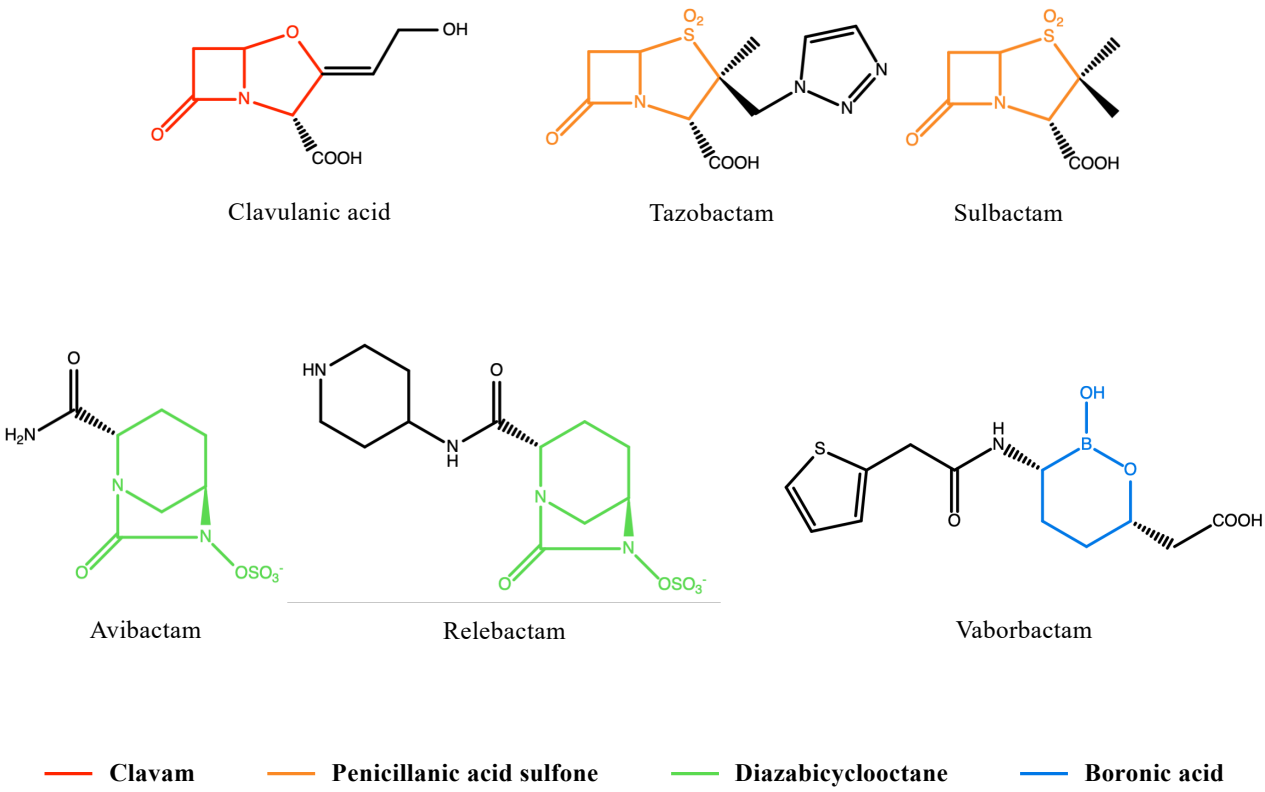

Figure 1.6 – Chemical structures of clinically-relevant β-lactamase inhibitors. The distinctive pharmacophore of each class is colour-coded as follows: clavam (red); penicillanic acid sulfones (orange); diazabicyclooctanes (DBOs) (green); boronic acid (blue). Clavulanic acid is an extended-spectrum clavam produced naturally by *Streptomyces clavuligerus*. Tazobactam and sulbactam are synthetic penicillanic acid sulfones with potent inhibitory activity against class A/group 2 β-lactamases. Avibactam and relebactam are diazabicyclooctane (DBO) non–β-lactam β-lactamase inhibitors with enhanced activity towards class C β-lactamases, including AmpC. The DBO ring contains a carbonyl carbon analogous to that of the β-lactam ring. Vaborbactam is a boronic acid-based serine β-lactamase inhibitor with potent inhibitory activity against KPC carbapenemases. A boron atom takes the place of the carbonyl carbon common to all other classes of β-lactamase inhibitors (Bush and Bradford 2016).

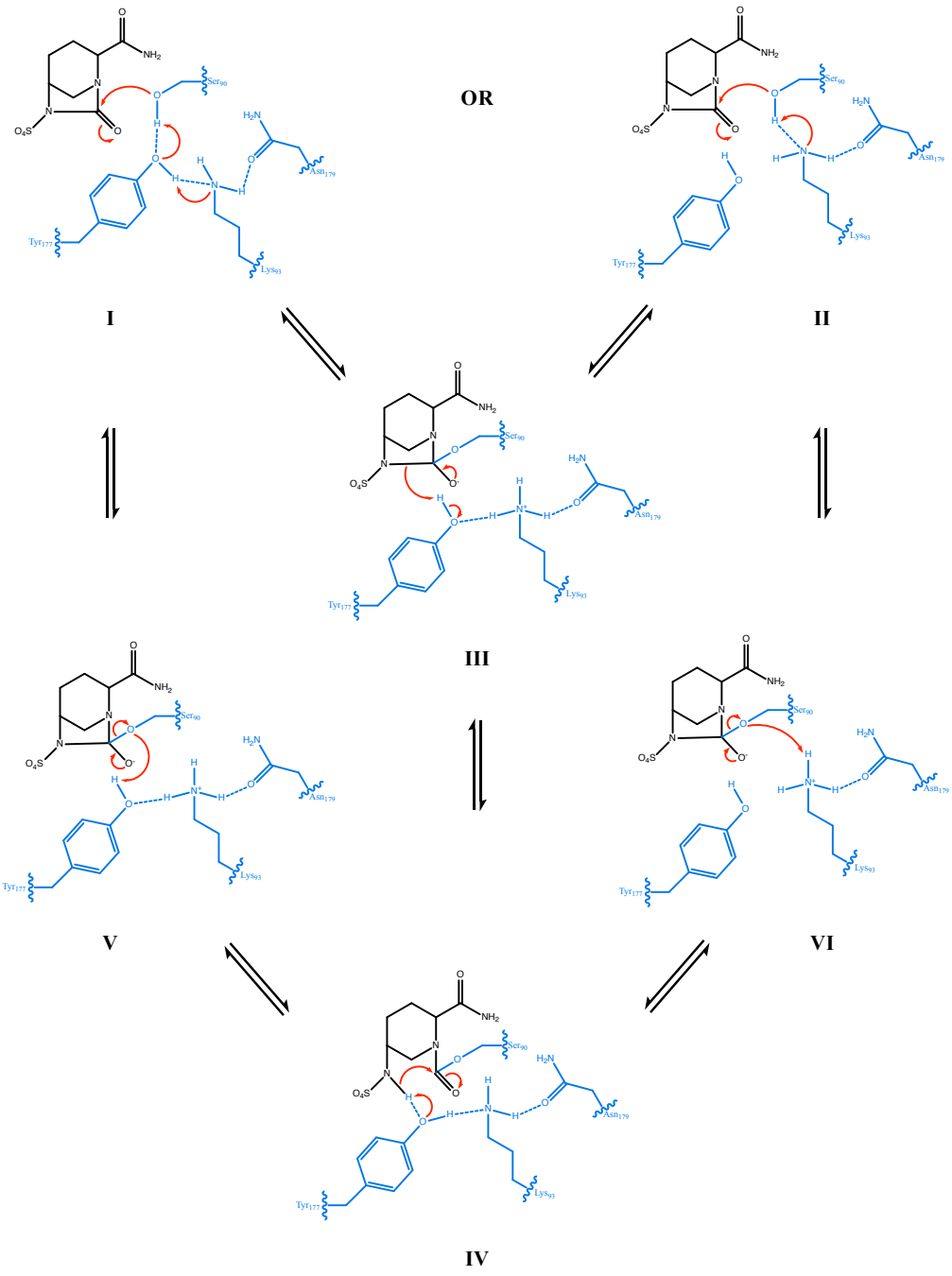

Figure 1.7 – Proposed mechanism of reversible acylation and recyclization of avibactam for class C β-lactamases. Acylation can proceed via one of two mechanisms. The single-base mechanism **(I–III–IV–V)** involves Tyr177 (SANC position 150) acting as both the general acid and the general base to assist the catalytic serine, Ser90 (SANC position 64) in acylation. For the two-base mechanism **(II–III–IV–VI)**, Tyr177 and Lys93 (SANC position 67) function respectively as the general acid and general base to acylate the enzyme. This figure was adapted from "Avibactam and class C β-lactamases: mechanism of inhibition, conservation of the binding pocket, and implications for resistance" by Lahiri *et al.* (2014) in Antimicrob. Agents Chemother., **58(10):**5704–5713 © the American Society for Microbiology.

1.8. Research Premise

To summarize the above literature review, *P. aeruginosa* employs a suite of resistance mechanisms to evade the lethal effects of β-lactam antibiotics, the most common being the production of the β-lactamase AmpC. This highly efficient enzyme hydrolyzes the majority of cephalosporins with near catalytic perfection and resists inhibition by most β-lactamase inhibitors (Jacoby 2009). Two exceptions include the β-lactam/BLI combinations ceftolozane/tazobactam and ceftazidime/avibactam. Indeed, their broad-spectrum activity has made them outstanding treatment options for nosocomial infections caused by MDR/AmpC-expressing *P. aeruginosa* (Bush and Bradford 2016; Papp-Wallace and Bonomo 2016).

Throughout the last few years, however, *P. aeruginosa* clinical isolates expressing mutated forms of AmpC conferring resistance to ceftolozane/tazobactam and cross-resistance to ceftazidime/avibactam have been reported, indicating that the evolution of resistance to these novel antipseudomonal combination therapies is already underway. Specifically, Fraile-Ribot *et al.* (2018) identified three different AmpC mutant enzymes in *P. aeruginosa* strains isolated from patients who were treated with ceftolozane/tazobactam: E247K, T96I, and a 19-amino acid deletion in the omega (Ω) loop, ΔG229–E247. (Notably, microbiological profiling revealed that these isolates all contain the OprD Q142X and AmpR G154R mutations that confer carbapenem resistance (Cabot *et al.* 2016) and promote AmpC overexpression (Cabot *et al.* 2012), respectively [see section 1.4]). Moreover, MacVane *et al.* (2017) reported a *P. aeruginosa* strain expressing an AmpC mutant enzyme, G183D, which arose after only six weeks of exposure to ceftolozane/tazobactam. Interestingly, all four of these AmpC mutations are within or proximal to the Ω loop, suggesting that this domain (which borders the active site) may be a hotspot for generating β-lactam resistance (Jacoby 2009) (**Fig. 1.8**).

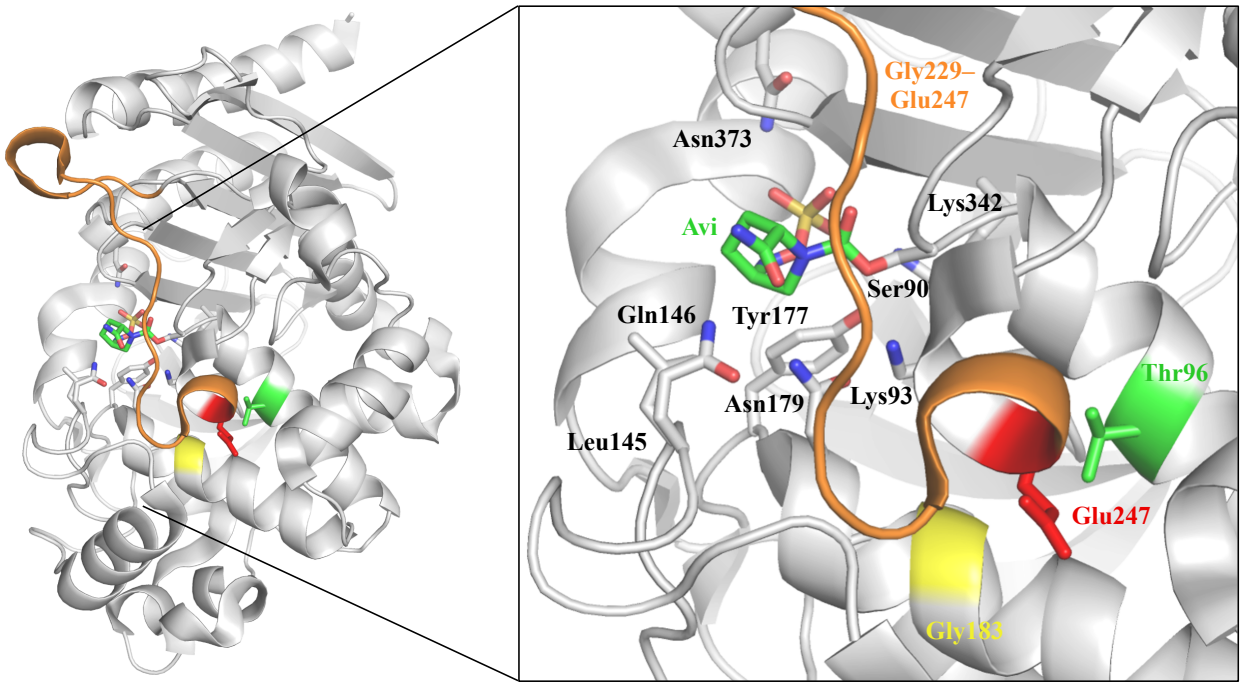

Figure 1.8 – Structural model of *P. aeruginosa* PAO1 AmpC β-lactamase highlighting the AmpC mutations investigated in this work. The amino acids defining the antibiotic resistant mutants investigated in this thesis are coloured red (E247K), yellow (G183D), green (T96I), and orange (ΔG229–E247). (This specific colour-coding scheme is maintained throughout this thesis for the presentation of all kinetic data). Avibactam (Avi) is depicted as green sticks and the conserved amino acids that compose the active site/binding pocket are depicted as grey sticks. The numbering of all amino acids represents their positions in the immature form of the AmpC enzyme (i.e., signal peptide included) as described by Mack *et al.* (2019). This figure was prepared in the PyMOL Molecular Graphic System (v.2.3.4) using the crystal coordinates published by Lahiri *et al.* (2013) (PDB ID: 4HEF).

1.9. Research Objectives

Although these AmpC mutant enzymes have been shown to be associated with a significant reduction in the susceptibility of *P. aeruginosa* to ceftolozane/tazobactam and, consequently, ceftazidime/avibactam, the molecular mechanism of this type of drug resistance remains poorly understood (MacVane *et al.* 2017; Fraile-Ribot *et al.* 2018). This is likely because, with the exception of E247K (Barnes *et al.* 2019), these AmpC mutants have only been characterized by microbiological profiling and molecular modelling (Lahiri *et al.* 2015; Boulant *et al.* 2019; Huang *et al.* 2020). Accordingly, the aim of this thesis is to investigate the catalytic properties of the *P. aeruginosa* AmpC mutant enzymes E247K, G183D, T96I, and ΔG229–E247 (alongside the WT AmpC enzyme) in order to provide a quantitative description of the effects of each mutation on antibiotic catalysis and inhibitor binding. To accomplish this, three main objectives were established:

1. Investigate the influence of the mutations on the ability of AmpC to hydrolyze ceftolozane and ceftazidime using Michaelis–Menten kinetics
2. Elucidate the effects of the mutations on the susceptibility of AmpC to inhibition by avibactam and tazobactam using nitrocefin-based inhibition assays
3. Explore the impact of these mutations on the stability and flexibility of AmpC and how this relates to enzyme activity

2. Materials and Methods

2.1. Preparation of WT and mutant AmpC expression constructs

Wild-type (WT) and mutant AmpC open reading frames (*bla*$_{PDC}$) were amplified by PCR from previously constructed pUCP24 plasmids (Fraile-Ribot *et al.* 2018) (**Table 2.1**). The forward (5'–GATATcatatgGATCGCCTGAAGGC–3' [NdeI cut site in lowercase letters]) and reverse (5'–CTATActcgagTCACAGGCCGC–3' [XhoI cut site in lowercase letters]) oligonucleotide primers used for amplification were designed to exclude DNA encoding the N-terminal signal peptide and the ten C-terminal residues, respectively. The resulting amplicons, therefore, encode amino acids D32–L387 (Morinaka *et al.* 2015). The purified amplicons were directionally cloned into the pET24b(+) bacterial expression vector (Novagen) using the restriction enzymes NdeI and XhoI (New England Biolabs [NEB]) and T4 DNA Ligase (NEB).

The AmpC G183D point mutant was generated by site-directed mutagenesis using the Q5® Site-Directed Mutagenesis Kit (NEB) and the WT AmpC pET24b(+)-based expression vector (pCSW) as the template DNA to generate pCSG (**Table 2.1**). The forward and reverse primers used to introduce this mutation were 5'–GATCTGTTCGGCTATCTCGCCG–3' and 5'–GATGCTCGGGTTGGAATAGAGGC –3', respectively.

Each construct was transformed into $CaCl_2$-competent *Escherichia coli* DH5α (NEB) and subsequently isolated from a single kanamycin-resistant colony (selected from LB agar supplemented with 35 μg/ml kanamycin). The fidelity of each construct was confirmed by Sanger DNA sequencing at The Centre for Applied Genomics (TCAG), SickKids Hospital (Toronto, ON, CAN).

Table 2.1 – Bacterial strains and plasmids used in this work.

	Relevant genotype	**Source**
Strain		
E. coli DH5α	F– *endA1* thi-1 *recA1* relA1 gyrA96 *phoA* *supE44* Φ80d*lacZ*ΔM15 Δ(*lacZYA-argF*)U169 *hsdR17*(r_K^-, m_K^+) λ–	NEB
E. coli BL21–Gold (DE3)	F– *ompT gal dcm endA*, *hsdS*(r_B^-, m_B^-), λ(DE3[*lacI lacUV5-T7p07 ind1 sam7 nin5*]) [$malB^+$]$_{K-12}$(λ^S)	Stratagene
Plasmid		
pUCP24–PDC-1	pUCP24 (gen^R) containing WT *P. aeruginosa* PAO1 bla_{PDC} (GenBank ID: NG_049865)	Fraile-Ribot *et al.* (2018)
pUCP24–PDC-221	pUCP24 containing bla_{PDC} with E247K point mutation (GenBank ID: MF481212)	Fraile-Ribot *et al.* (2018)
pUCP24–PDC-222	pUCP24 containing bla_{PDC} with T96I point mutation (GenBank ID: MF481213)	Fraile-Ribot *et al.* (2018)
pUCP24–PDC-223	pUCP24 containing bla_{PDC} with ΔG229–E247 deletion mutation (GenBank ID: MF481214)	Fraile-Ribot *et al.* (2018)
pET24b(+)	Bacterial expression vector (5309 bp); pBR322 origin; T7 promoter; kan^R	Novagen
pCSW	pET24b(+)/bla_{PDC} (D32–L387)	This work
pCSE	pET24b(+)/bla_{PDC} E247K (D32–L387)	This work
pCSG	pET24b(+)/bla_{PDC} G183D (D32–L387)	This work
pCST	pET24b(+)/bla_{PDC} T96I (D32–L387)	This work
pCSO	pET24b(+)/bla_{PDC} ΔG229–E247 (D32–L387)	This work

2.2. Expression and purification of WT and mutant AmpC enzymes

The WT and mutant AmpC enzymes were expressed and purified using a standardized *E. coli*-based recombinant protein expression system for use in kinetic studies. First, each pET24b(+)-based AmpC expression construct was transformed into $CaCl_2$-competent *E. coli* BL21–Gold (DE3) (Stratagene). Transformants were then grown aerobically at 37˚C in 500 ml Terrific Broth (TB) supplemented with 70 µg/ml kanamycin to late logarithmic phase (optical density at 600 nm [OD_{600}] between 0.8 and 0.9). Expression of the AmpC enzymes was then induced with 1 mM isopropyl-β-D-1-thiogalactopyranoside (IPTG) and the cultures were grown overnight at 18˚C with shaking. Cells were harvested via centrifugation (3,440 × *g*) at 4˚C for 45 min and frozen at –80˚C for >24 hrs before resuspension in lysis buffer (20 mM sodium citrate [pH 5.2], SigmaFAST™ Protease Inhibitor Cocktail [EDTA-free], 1 mM EDTA [pH 8.0], 1 mM PMSF, 50 µg/ml DNase I, and 5 mM $MgCl_2$) and subsequent lysis via sonication (5 × 7 bursts at 50% duty cycle with 30 sec of incubation on ice between each round). The lysate was clarified via high-speed centrifugation (15,400 × *g*) at 4˚C for 30 min and then applied to a 12 ml cation-exchange column containing SP Sepharose High Performance resin (GE Healthcare) pre-equilibrated with 20 mM sodium citrate buffer (pH 5.2). The resin was washed with 20 mM sodium citrate buffer (pH 5.2) and AmpC was subsequently eluted over a linear gradient of 0–0.5 M NaCl in the same buffer. Chromatographic steps were performed at 4˚C using ÄKTA FPLC.

Fractions containing AmpC were identified by SDS–PAGE analysis. The protein concentrations (mg/ml) of these fractions were determined using a NanoDrop™ One (Thermo Fisher Scientific) by measuring the absorbance at λ = 280 nm and using the theoretical mass and extinction coefficient (ε) of the protein (**Table 2.2**). The ProtParam tool of the ExPASy Bioinformatics Resource Portal was used to obtain these values (Artimo *et al.* 2012).

Table 2.2 – Description of WT and mutant AmpC enzymes investigated in this work.

AmpC[a]	Description of Mutation	MW (kDa)	#AA	pI	ε_{280} (M^{-1} cm^{-1})
WT (PDC-1)	N/A; wild-type AmpC	39.219	357	7.84	54,320
E247K (PDC-221)	Substitution in Ω loop	39.219	357	8.83	54,320
G183D (PDC-322)	Substitution in H-5 helix	39.277	357	7.03	54,320
T96I (PDC-222)	Substitution in H-2 helix	39.231	357	7.84	54,320
ΔG229–E247 (PDC-223)	Deletion of 19 AA in Ω loop	37.225	357	8.57	52,830

[a] PDC numbering system as described by Mack *et al.* (2019).

Fractions containing purified AmpC were pooled and dialyzed overnight against 2 L 20 mM HEPES buffer (pH 7.5) at 4˚C. The sample was then concentrated down to ~2 ml using a 10 kDa molecular weight cut-off (MWCO) centrifugal filter unit, clarified via centrifugation (16,000 × *g*) for 15 min, and applied to a 5 ml Hi-Trap Heparin column (GE Healthcare) pre-equilibrated with 20 mM HEPES buffer (pH 7.5) to remove excess nucleic acid. The resin was washed with 20 mM HEPES buffer (pH 7.5) and AmpC was subsequently eluted over a linear gradient of 0–0.4 M NaCl in the same buffer. Chromatographic steps were performed at 4˚C using ÄKTA FPLC.

Fractions containing AmpC were identified by SDS–PAGE analysis and the concentration and purity were determined as described above. Fractions containing AmpC at a reasonable concentration and purity were pooled and concentrated to ~5 mg/ml using a 10 kDa MWCO centrifugal filter unit and clarified via centrifugation (16,000 × *g*) for 15 min at 4˚C. Samples were diluted 1:1 in storage buffer (20 mM HEPES buffer [pH 7.5] containing 50% glycerol [final 25%]), divided into single-use 15 µl aliquots, and stored at –80˚C.

2.3. Kinetic characterization of WT and mutant AmpC enzymes

Kinetic assays were performed at room temperature (~28˚C) in clear-bottom 96-well microtiter plates (far UV transparent Grenier [Monroe, NC, USA] plates for the ceftolozane and ceftazidime hydrolysis assays and Falcon [Tewksbury, MA, USA] plates for the nitrocefin hydrolysis assays) in buffer containing 0.1 M sodium phosphate (pH 7.0) and 0.1 mg/ml bovine serum albumin (BSA). Reaction progress was monitored by absorbance using a SpectraMax® iD5 Multi-Mode Microplate Reader (Molecular Devices, San Jose, CA, USA) and the data were

collected using SoftMax® Pro Software. Data represent averages of at least three technical replicates that were analyzed using SigmaPlot (Systat Software, Inc., CA, USA).

2.3.1. Michaelis–Menten kinetic analysis of WT and mutant AmpC enzymes

The catalytic properties of the WT and mutant AmpC enzymes were investigated using Michaelis–Menten kinetics. Specifically, the hydrolysis of ceftolozane, ceftazidime, and nitrocefin (a chromogenic cephalosporin analogue) by each AmpC enzyme was measured through β-lactamase activity assays, the conditions of which are described below.

Ceftolozane hydrolysis. Initial rates of ceftolozane hydrolysis were measured by monitoring absorbance changes at λ = 283 nm through challenging each AmpC enzyme (WT [2 μM]; E247K [0.05 μM]; G183D, T96I, and ΔG229–E247 [0.1 μM]) with ceftolozane (Merck & Co., Inc.) concentrations ranging from 0–800 μM for 3,600 s at 28˚C. Due to the high absorptivity of ceftolozane, activities above 800 μM (i.e., 2.5 absorbance units) could not be accurately measured. The slopes of the traces (i.e., initial rates) were determined by linear regression using the relationship, $\left(\frac{d[P]}{dt}\right)_{t=0} = \left(\frac{1}{\Delta\varepsilon_{283}}\right)\left(\frac{dA}{dt}\right)_{t=0}$, where $\Delta\varepsilon_{283} = -9{,}740\ M^{-1}\ cm^{-1}$ (Takeda *et al.* 2007).

Ceftazidime hydrolysis. Initial rates of ceftazidime hydrolysis were measured by monitoring absorbance changes at λ = 260 nm through challenging each AmpC enzyme (WT [2 μM]; E247K [0.05 μM]; G183D, T96I, and ΔG229–E247 [0.1 μM]) with ceftazidime (Sigma Aldrich) concentrations ranging from 0–600 μM for 3,600 s at 28˚C. Due to the high absorptivity of ceftazidime, activities above 600 μM (i.e., 2.5 absorbance units) could not be accurately measured. The slopes of the traces (i.e., initial rates) were determined by linear regression using the relationship, $\left(\frac{d[P]}{dt}\right)_{t=0} = \left(\frac{1}{\Delta\varepsilon_{260}}\right)\left(\frac{dA}{dt}\right)_{t=0}$, where $\Delta\varepsilon_{260} = -8{,}660\ M^{-1}\ cm^{-1}$ (Bush *et al.* 1982).

Nitrocefin hydrolysis. Initial rates of nitrocefin hydrolysis were measured by monitoring absorbance changes at λ = 486 nm through challenging each AmpC enzyme (WT [0.250 nM]; E247K, G183D, and T96I [5 nM]; ΔG229–E247 [10 nM]) with nitrocefin (Sigma Aldrich) concentrations ranging from 0–200 μM for 1,200 s at 28˚C. The slopes of the traces (i.e., initial rates) were determined by linear regression using the relationship, $\left(\frac{d[P]}{dt}\right)_{t=0} = \left(\frac{1}{\Delta\varepsilon_{486}}\right)\left(\frac{dA}{dt}\right)_{t=0}$, where $\Delta\varepsilon_{486}$ = 20,500 M^{-1} cm^{-1} (Chow *et al.* 2013).

The initial rates of ceftolozane, ceftazidime, or nitrocefin hydrolysis were plotted as a function of their respective substrate concentrations and the resulting plots were fitted to the Michaelis–Menten equation, Eq. 1:

$$\text{reaction rate} = \frac{d[P]}{dt} = \frac{V_{\max}[S]}{K_m + [S]} \quad \text{(Eq. 1)}$$

Where [*P*] is the concentration of product formed at time *t*, $V_{\max}$ is the maximal velocity at saturating substrate concentration, [*S*], and K_m is the Michaelis constant.

At substrate concentrations well below the K_m, Eq. 1 can be simplified as follows:

$$\frac{d[P]}{dt} = \frac{V_{\max}[S]}{K_m + [S]} = \frac{k_{cat}[E][S]}{K_m + [S]} = \frac{k_{cat}}{K_m}[E][S] \quad \text{(Eq. 2)}$$

Where [*E*] is the concentration of enzyme and $\frac{k_{cat}}{K_m}$ is the specificity constant of the enzyme for a particular substrate, *S*. Therefore, for the cases in which an AmpC enzyme demonstrated linear concentration dependence towards a particular substrate, Eq. 2 (i.e., linear regression analysis) was used in place of Eq. 1 to determine the specificity constant instead (Johnson 2019).

2.3.2. Avibactam inhibition assays

The acylation kinetics of the WT and mutant AmpC enzymes by avibactam were measured as previously described (Ehmann *et al.* 2012). Briefly, hydrolysis of 100 μM nitrocefin

by each AmpC enzyme (5 nM [WT] or 100 nM [mutants]) was measured by monitoring absorbance changes at λ = 486 nm in the presence of different concentrations of avibactam (1–10 μM [WT]; 11–88 μM [E247K]; 50–400 μM [G183D, ΔG229–E247]; 12.5–150 μM [T96I]) for 1,200 s at 28˚C. The resulting progress curves were fitted to Eq. 3 using non-linear regression to obtain the pseudo first-order rate constant, k_{obs}. The rationale for this is described below:

Avibactam is a slow-binding inhibitor of AmpC; therefore, the kinetic profile of AmpC-catalyzed nitrocefin hydrolysis in the presence of avibactam is expected to follow Eq. 3:

$$P = v_S t + (v_0 - v_S)\frac{(1 - e^{-k_{obs}t})}{k_{obs}} \quad \text{(Eq. 3)}$$

Where P is the amount of product formed at time t, v_0 and v_S represent uninhibited and fully inhibited enzyme velocity at infinite substrate concentration, respectively, and k_{obs} is an apparent rate constant that exhibits the following linear dependence on inhibitor concentration:

$$k_{obs} = k_{off}^{app} + k_{on}^{app}\frac{[I]}{\left(1 + \frac{[S]}{K_m}\right)} \quad \text{(Eq. 4)}$$

Where k_{off}^{app} and k_{on}^{app} are the respective apparent rate constants for inhibitor (I) dissociation and binding, [I] is the inhibitor concentration, [S] is the substrate concentration (i.e., 100 μM nitrocefin), and K_m is the Michaelis constant (i.e., the experimentally determined K_m values of each AmpC enzyme for nitrocefin [**Table 3.1**]). The rate constants k_{off}^{app} and k_{on}^{app} are therefore key kinetic parameters for comparing the susceptibility of the WT and mutant AmpC enzymes towards avibactam acylation (Ehmann *et al.* 2012). Accordingly, the k_{obs} values for the WT and mutant AmpC enzymes were plotted as a function of avibactam concentration. The resulting linear dependence allowed for an estimation of the k_{off}^{app} and k_{on}^{app} values associated with the avibactam inhibition reaction.

2.3.3. Tazobactam inhibition assays

The acylation kinetics of the WT and mutant AmpC enzymes by tazobactam were measured as previously described (Papp-Wallace *et al.* 2010). Briefly, hydrolysis of 100 μM nitrocefin by each AmpC enzyme (5 nM [WT] or 100 nM [mutants]) was measured by monitoring absorbance changes at λ = 486 nm in the presence of different concentrations of tazobactam (12.5–150 μM) for 1,200 s at 28˚C. Data were analyzed as described in section 2.3.2.

2.4. Melting temperature determination

Melting temperatures (T_m [˚C]) of the WT and mutant AmpC enzymes were determined through thermal denaturation experiments using a NanoTemper Prometheus NT.48 differential scanning fluorimeter (DSF). Briefly, 1.7 mg/ml (50 μM) of AmpC enzyme in storage buffer (20 mM HEPES buffer [pH 7.5] containing 50% glycerol [final 25%]) was loaded into a capillary tube and protein denaturation was followed by monitoring the ratio of fluorescence intensities measured at 330 nm and 350 nm (excitation 290 nm) as the sample was heated from 20˚C to 95˚C at a rate of 1˚C min^{-1}. The inflection point of the resulting plot defines the melting temperature of the enzyme (Munoz and Sanchez-Ruiz 2004). Reported T_m values represent the averages of three technical replicates.

3. Results

3.1. Expression and purification of WT and mutant AmpC enzymes

3.1.1. WT and mutant AmpC enzymes are stably expressed as soluble monomers.

The WT and mutant AmpC enzymes were expressed and purified using a standardized *E. coli*-based recombinant protein expression system for use in kinetic studies and crystallization trials. Small-scale test inductions were first performed to optimize the conditions for protein expression. The highest expression levels are obtained from *E. coli* BL21–Gold (DE3) cells induced with 1 mM IPTG and grown in Terrific Broth at 18˚C for 16–18 hrs. There is no marked difference in expression levels between the WT and mutant AmpC enzymes; approximately 50% of each enzyme is expressed as insoluble inclusion bodies (**Fig. 3.1**). Despite this, sufficient yields of each enzyme can be obtained from the soluble fractions.

The WT and mutant AmpC enzymes were isolated from clarified cell lysate via cation exchange chromatography using SP Sepharose resin and further purified using Heparin chromatography. All five enzymes elute as single peaks during both rounds of purification, suggesting that they are expressed as a single, monomeric species. Elution begins and ends rather abruptly at around 0.15 M and 0.35 M NaCl, respectively, and peaks between 0.2 M and 0.25 M NaCl (**Fig 3.2**). While the Heparin chromatography step does result in a loss of some enzyme (~20–30%), it is highly effective in removing not only excess nucleic acid but also any traces of unwanted proteins from the sample; this is evident in the SDS–PAGE analysis of the Heparin-purified AmpC fractions (**Fig 3.2**). Finally, the purification profiles of all the AmpC mutants are comparable to those of WT AmpC with respect to elution range, yield (i.e., mg quantities), and purity (A260/280 and A260/230). All enzymes remain stable throughout the entire purification process, with trace amounts of precipitation observed.

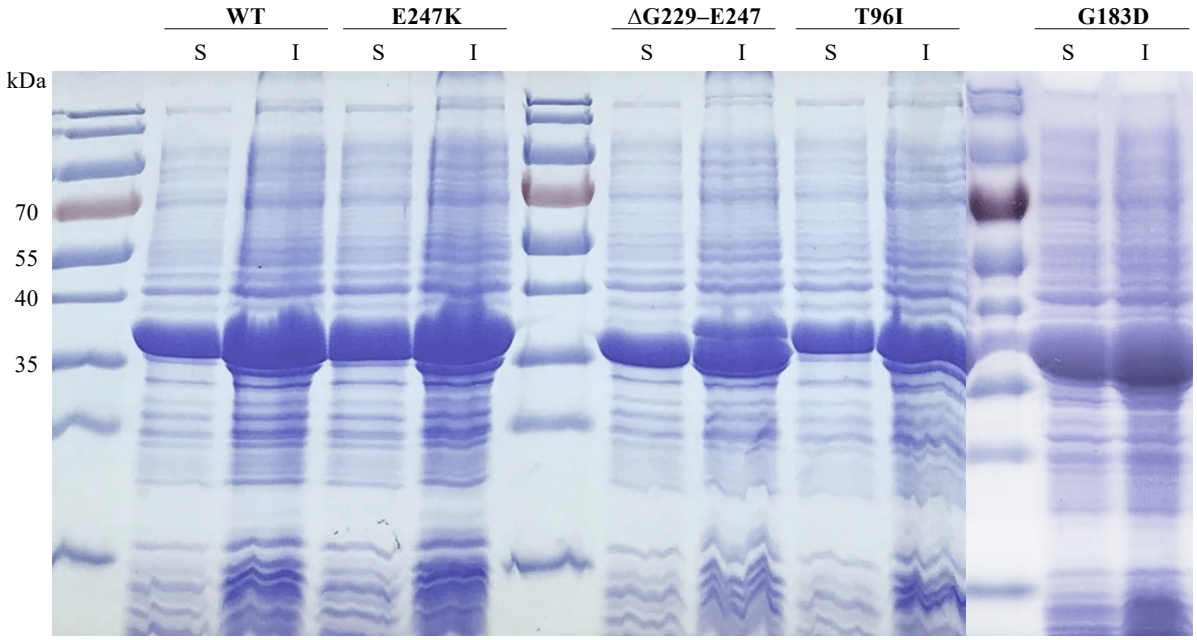

Figure 3.1 – Expression of WT and mutant AmpC enzymes. SDS–PAGE of soluble (S) and insoluble (I) fractions of WT and mutant AmpC enzymes obtained from clarified *E. coli* BL21–Gold (DE3) lysate. Protein band sizes were estimated by comparison to PageRuler™ Pre-stained Protein Ladder (10–180 kDa) (Thermo Fisher Scientific). The size of the AmpC enzyme is ~39.2 kDa; therefore, the large bands between 35 and 40 kDa indicate successful overexpression.

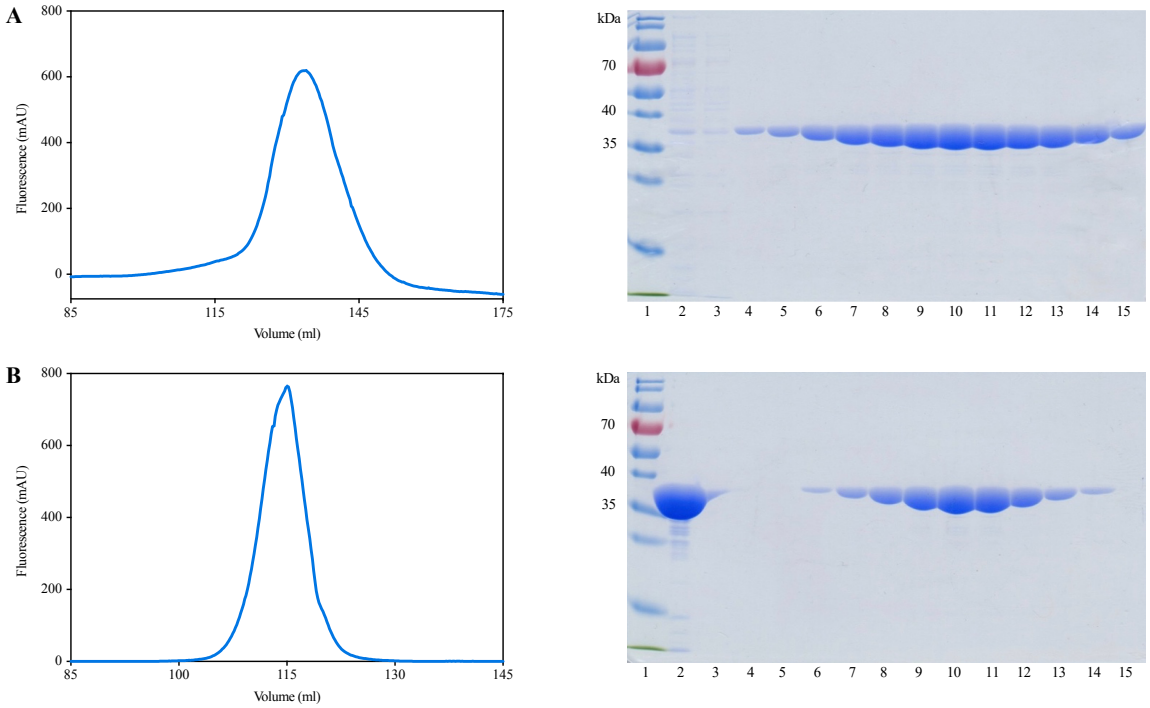

Figure 3.2 – Purification of WT AmpC. (A) SP Sepharose isolation and chromatography of WT AmpC from clarified *E. coli* BL21–Gold (DE3) lysate. Fractions within the fluorescence peak (top left) were analyzed via SDS–PAGE (top right) to confirm the presence of AmpC (~39.2 kDa). (1) PageRuler™ Prestained Protein Ladder (10–180 kDa); (2) sample flow-through; (3) buffer wash; (4–15) fractions containing WT AmpC. **(B)** Heparin purification and chromatography of WT AmpC. Fractions within the fluorescence peak (bottom left) were analyzed via SDS–PAGE (bottom right) to confirm the presence and purity of AmpC. (1) PageRuler™ Prestained Protein Ladder (10–180 kDa); (2) WT AmpC sample obtained from (A); (3) sample flow-through; (4, 5) buffer washes; (6–15) fractions containing WT AmpC.

3.2. Hydrolysis of ceftolozane and ceftazidime by WT and mutant AmpC enzymes

Resistance to ceftolozane/tazobactam (and cross resistance to ceftazidime/avibactam) has been reported in several *P. aeruginosa* clinical isolates, and while it has been confirmed to be the result of the mutant AmpC enzymes that they overexpress, the molecular mechanism by which these mutations promote AmpC-mediated resistance is poorly understood. Accordingly, the first objective of this thesis was to use Michaelis–Menten kinetics to investigate the effects of these mutations on the catalytic activity of AmpC towards ceftolozane and ceftazidime. (Figures S1 and S2 respectively display typical traces of ceftolozane and ceftazidime hydrolysis by the WT and mutant AmpC enzymes that were used in Michaelis–Menten kinetic analysis).

3.2.1. WT AmpC displays a modest difference in its specificity towards ceftolozane and ceftazidime, with a slight preference for ceftazidime.

The rates of ceftolozane and ceftazidime hydrolysis by WT AmpC demonstrate hyperbolic concentration dependence (**Fig. 3.3 and 3.4**), permitting determination of the Michaelis–Menten kinetic parameters V_{max} (maximal velocity), k_{cat} (enzyme turnover number or catalytic rate constant), and K_m (Michaelis constant) (**Table 3.1**). The k_{cat} values of WT AmpC for the hydrolysis of ceftolozane and ceftazidime differ from one another only by a factor of 2, with ceftolozane having the larger turnover. The K_m of WT AmpC for ceftolozane, however, is 6-fold larger than that for ceftazidime, indicating that the enzyme has a much lower affinity for ceftolozane. On balance, the specificity constant $\left(\frac{k_{cat}}{K_m}\right)$ of WT AmpC for ceftolozane is nearly 3-fold lower than that for ceftazidime. Since enzyme specificity is proportional to enzyme efficiency and proficiency (Fersht 1999; Miller and Wolfenden 2002), it can be said that WT AmpC demonstrates slightly higher catalytic efficiency towards ceftazidime than ceftolozane.

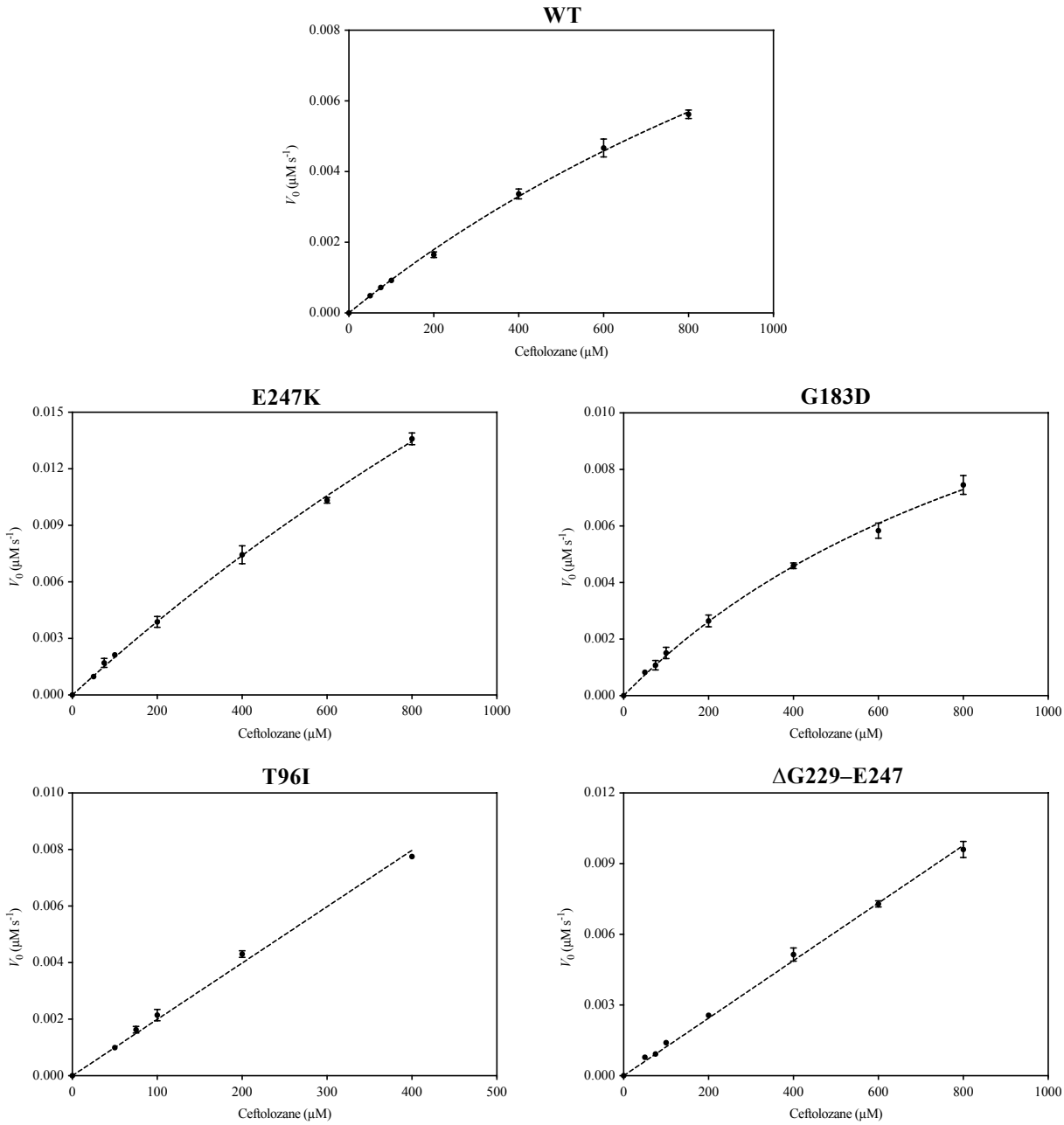

Figure 3.3 – Michaelis–Menten plots of WT and mutant AmpC enzymes towards ceftolozane. Each enzyme was challenged with ceftolozane ranging from 0–800 μM and initial rates of ceftolozane hydrolysis were measured at λ = 283 nm for 3,600 s at 28˚C. The slope of each trace was determined by linear regression analysis and plotted against the corresponding ceftolozane concentration to obtain the plots displayed above. Data points represent averages of at least three technical replicates and error bars represent the standard deviation. To obtain Michaelis–Menten kinetic parameters, the plots were analyzed either by linear regression (T96I and ΔG229–E247) or fitted to Eq. 1 (WT, E247K, and G183D).

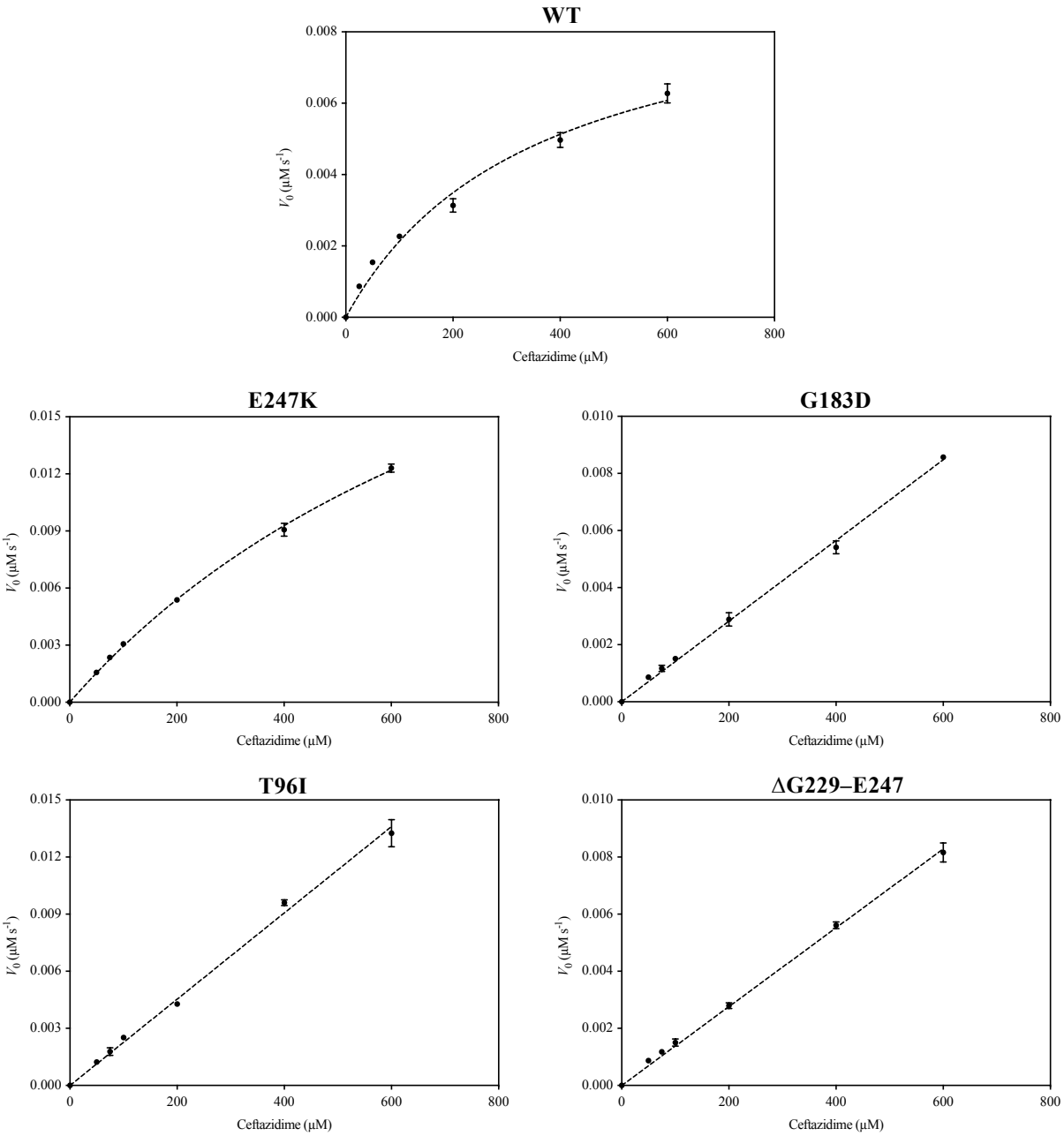

Figure 3.4 – Michaelis–Menten plots of WT and mutant AmpC enzymes towards ceftazidime. Each enzyme was challenged with ceftazidime ranging from 0–600 μM and initial rates of ceftazidime hydrolysis were measured at λ = 260 nm for 3,600 s at 28˚C. The slope of each trace was determined by linear regression analysis and plotted against the corresponding ceftazidime concentration to obtain the plots displayed above. Data points represent averages of at least three technical replicates and error bars represent the standard deviation. To obtain Michaelis–Menten kinetic parameters, the plots were analyzed either by linear regression (G183D, T96I, and ΔG229–E247) or fitted to Eq. 1 (WT and E247K).

Table 3.1 – Michaelis–Menten kinetic parameters of WT and mutant AmpC enzymes for ceftolozane, ceftazidime, and nitrocefin.

Kinetic Parameter[a]	Substrate		
	Ceftolozane	Ceftazidime	Nitrocefin
WT			
V_{max} (μM s^{-1})	$(2.10 \pm 0.26) \times 10^{-2}$	$(9.70 \pm 1.10) \times 10^{-3}$	$(8.12 \pm 0.796) \times 10^{-3}$
k_{cat} (s^{-1})	$(1.04 \pm 0.13) \times 10^{-2}$	$(4.85 \pm 0.55) \times 10^{-3}$	32.48 ± 3.2
K_m (μM)	2107.3 ± 341.2	353.5 ± 81.1	126.12 ± 23.63
k_{cat}/K_m (μM^{-1} s^{-1})	$(4.91 \pm 1.01) \times 10^{-6}$	$(1.37 \pm 0.35) \times 10^{-5}$	$(2.58 \pm 0.54) \times 10^{-1}$
Fold change[b]	1	1	1
E247K			
V_{max} (μM s^{-1})	$(7.42 \pm 1.23) \times 10^{-2}$	$(3.29 \pm 0.20) \times 10^{-2}$	$(6.84 \pm 0.880) \times 10^{-3}$
k_{cat} (s^{-1})	1.48 ± 0.25	$(6.58 \pm 0.40) \times 10^{-1}$	1.37 ± 0.18
K_m (μM)	3610.2 ± 704.3	1016.9 ± 90.3	62.86 ± 17.67
k_{cat}/K_m (μM^{-1} s^{-1})	$(4.11 \pm 1.05) \times 10^{-4}$	$(6.47 \pm 0.70) \times 10^{-4}$	$(2.18 \pm 0.67) \times 10^{-2}$
Fold change	83.7	47.2	0.085
G183D			
V_{max} (μM s^{-1})	$(1.80 \pm 0.17) \times 10^{-2}$	ND	$(6.27 \pm 0.355) \times 10^{-3}$
k_{cat} (s^{-1})	$(1.80 \pm 0.17) \times 10^{-1}$	ND	1.25 ± 0.07
K_m (μM)	1174.3 ± 165.1	ND	73.53 ± 8.34
k_{cat}/K_m (μM^{-1} s^{-1})	$(1.53 \pm 0.26) \times 10^{-4}$	$(1.41 \pm 0.02) \times 10^{-4}$	$(1.71 \pm 0.22) \times 10^{-2}$
Fold change	31.2	10.3	0.066
T96I			
V_{max} (μM s^{-1})	ND[c]	ND	$(6.43 \pm 0.247) \times 10^{-3}$
k_{cat} (s^{-1})	ND	ND	1.29 ± 0.05
K_m (μM)	ND	ND	46.22 ± 4.51
k_{cat}/K_m (μM^{-1} s^{-1})	$(1.99 \pm 0.04) \times 10^{-4}$	$(2.27 \pm 0.04) \times 10^{-4}$	$(2.78 \pm 0.29) \times 10^{-2}$
Fold change	40.5	16.6	0.107
ΔG229–E247			
V_{max} (μM s^{-1})	ND	ND	$(1.00 \pm 0.231) \times 10^{-2}$
k_{cat} (s^{-1})	ND	ND	1.00 ± 0.23
K_m (μM)	ND	ND	222.66 ± 80.67
k_{cat}/K_m (μM^{-1} s^{-1})	$(1.22 \pm 0.02) \times 10^{-4}$	$(1.38 \pm 0.02) \times 10^{-4}$	$(4.50 \pm 1.93) \times 10^{-3}$
Fold change	24.8	10.1	0.017

[a] Experiments were performed in triplicate; ± values represent the standard errors reported from regression analysis.
[b] Ratio of enzyme specificity constant (k_{cat}/K_m) of mutant AmpC relative to WT AmpC.
[c] ND, not determined.

3.2.2. AmpC mutants exhibit increased catalytic efficiency towards ceftolozane and ceftazidime compared to WT AmpC.

Ceftolozane. The ceftolozane hydrolysis rates of the E247K and G183D AmpC mutants demonstrate hyperbolic concentration dependence, while those of T96I and ΔG229–E247 are linear (**Fig. 3.3 and 3.4**). Due to this observed linearity, only the specificity constants $\left(\frac{k_{cat}}{K_m}\right)$ can be calculated from the Michaelis–Menten plots of the T96I and ΔG229–E247 mutants; however, it is clear that the K_m values of these mutants for ceftolozane must be larger than 3610.2 μM (Fersht 1999) (**Table 3.1**). Therefore, with the exception of G183D, these mutations appear to weaken the affinity of AmpC for ceftolozane. These AmpC mutations also appear to influence enzyme turnover. Indeed, the respective catalytic rate constants (k_{cat}) of the G183D and E247K point mutants for ceftolozane hydrolysis are one and two orders of magnitude larger than that of WT AmpC (**Table 3.1**). Although the k_{cat} values of the T96I and ΔG229–E247 mutants cannot be determined directly, they can be estimated using the limiting K_m value of 3610.2 μM. Specifically, the ceftolozane turnover rates of these mutants are likely to be greater than 0.44 s^{-1} under saturating conditions, which is more than a 40-fold increase in k_{cat} relative to WT AmpC. Therefore, all AmpC mutations appear to increase ceftolozane turnover rate by at least an order of magnitude relative to the WT enzyme. The overall effect of these changes is apparent in the ceftolozane specificity constants of the AmpC mutants, all of which are at least 25-fold larger than that of WT AmpC. The E247K point mutant demonstrates the largest increase in catalytic efficiency towards ceftolozane, with a remarkable 84-fold increase in $\frac{k_{cat}}{K_m}$. To summarize, the AmpC mutants (with the exception of G183D) have reduced affinities for ceftolozane; however, since they all exhibit higher ceftolozane turnover rates, their catalytic efficiencies towards this antibiotic are greater than that of the WT enzyme. Figure S1 compares the rates of ceftolozane

hydrolysis by WT AmpC with those of the AmpC mutants to further illustrate their increased specificity towards this antibiotic.

Ceftazidime. The catalysis of ceftazidime by the AmpC mutants is quite similar to that of ceftolozane, with a few notable disparities. Specifically, only the E247K point mutant demonstrates hyperbolic concentration dependence, while the rates of ceftazidime hydrolysis by the G183D, T96I, and ΔG229–E247 mutants are linear (**Fig. 3.3 and 3.4**). The ceftazidime K_m values of these mutants are therefore greater than that of the E247K mutant (1016.9 μM) (**Table 3.1**). Notably, the G183D point mutant shows significantly reduced affinity for ceftazidime, while its affinity for ceftolozane is nearly 2-fold higher than that of WT AmpC. Overall, these results indicate that all four mutations reduce the affinity of AmpC for ceftazidime. To continue, the ceftazidime turnover rate (k_{cat}) of the E247K point mutant is more than two orders of magnitude larger than that of WT AmpC (**Table 3.1**). This parameter can be estimated for the other three AmpC mutants, which again demonstrate linear rates of ceftazidime hydrolysis. With the limiting K_m value of 1016.9 μM, the G183D, T96I, and ΔG229–E247 mutants are estimated to hydrolyze ceftazidime at a rate of at least 0.14 s^{-1} under saturating conditions. This is nearly a 30-fold increase in enzyme turnover relative to WT AmpC. Finally, all AmpC mutants hydrolyze ceftazidime with greater catalytic efficiency than WT AmpC. Indeed, each mutant enzyme exhibits at least a 10-fold increase in ceftazidime $\frac{k_{cat}}{K_m}$ compared to the WT enzyme, with the E247K point mutant displaying an impressive 47-fold enhancement. To summarize, although all AmpC mutants have reduced affinities for ceftazidime, their rates of ceftazidime turnover are higher, and as a result, their catalytic efficiencies towards this antibiotic are greater than that of the WT enzyme. Figure S2 compares the rates of ceftazidime hydrolysis by WT AmpC with those of the AmpC mutants to further illustrate their increased specificity towards this antibiotic.

In this way, it is clear that these mutations affect the hydrolysis of ceftolozane and ceftazidime by AmpC similarly, with the one exception being the opposing changes in affinity of the G183D point mutant towards these antibiotics. In fact, the ranking of the AmpC mutants in terms of largest to smallest fold change in ceftazidime $\frac{k_{cat}}{K_m}$ relative to WT AmpC is identical to that of ceftolozane: E247K > T96I > G183D > ΔG229–E247. This can be clearly observed in Figure 3.5, which compares the catalytic activity of WT AmpC towards ceftolozane (A) and ceftazidime (B) with that of each AmpC mutant.

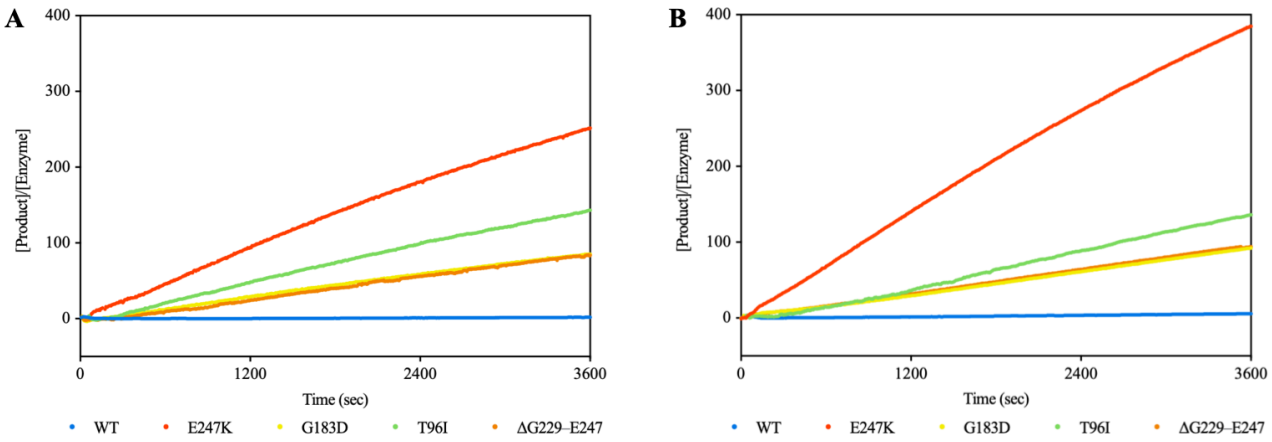

Figure 3.5 – Hydrolysis of 200 µM (A) ceftolozane and (B) ceftazidime by WT and mutant AmpC enzymes. Each enzyme was challenged with 200 µM ceftolozane or ceftazidime and hydrolysis was measured by monitoring absorbance changes at λ = 283 nm or λ = 260 nm, respectively, for 3,600 s at 28˚C. Kinetic traces were converted into product concentration (i.e., hydrolyzed antibiotic [µM]) using the Beer–Lambert law, divided by enzyme concentration (WT [2 µM]; E247K [0.05 µM]; G183D, T96I, and ΔG229–E247 [0.1 µM]), and plotted as a function of time (sec).

3.3. Hydrolysis of nitrocefin by WT and mutant AmpC enzymes

Inhibition assays were performed in order to investigate the effect of each AmpC mutation on the inhibition potency of avibactam and tazobactam towards AmpC. These assays involved measuring the hydrolysis of the chromogenic cephalosporin analogue, nitrocefin, by each AmpC enzyme in the presence of different concentrations of avibactam or tazobactam. Since estimation of the apparent acylation rate (k_{on}^{app}) of the inhibitor considers the K_m of the enzyme for nitrocefin (Ehmann *et al.* 2012), Michaelis–Menten kinetics were used to determine the kinetic parameters of the WT and mutant AmpC enzymes towards this substrate.

3.3.1. AmpC mutants exhibit decreased catalytic efficiency towards nitrocefin compared to WT AmpC.

The nitrocefin hydrolysis rates of the WT and mutant AmpC enzymes exhibit hyperbolic behaviour (**Fig. 3.6**), enabling determination of their individual V_{max}, k_{cat}, and K_m values for this substrate (**Table 3.1**). These results indicate that nitrocefin is a much "better" substrate for AmpC than both ceftolozane and ceftazidime. Indeed, the three AmpC point mutants (E247K, G183D, and T96I) show a modest increase in nitrocefin affinity compared to WT AmpC, as demonstrated by a 2- to 3-fold reduction in K_m. Conversely, the ΔG229–E247 deletion mutant has a lower affinity for nitrocefin, with a K_m nearly 2-fold larger than that of WT AmpC. Moreover, all the AmpC mutants exhibit at least an order of magnitude reduction in nitrocefin turnover (k_{cat}) relative to WT AmpC. However, since the maximal velocity (V_{max}) of nitrocefin hydrolysis by each AmpC mutant does not differ appreciably from that of WT AmpC, and $k_{cat} = \frac{V_{max}}{[E]}$ (Johnson 2019), this considerable decrease in enzyme turnover rate can be related to the disparate enzyme concentrations ([E]) required for Michaelis–Menten kinetic analysis.

Specifically, 5 nM to 10 nM of mutant AmpC enzyme is needed to hydrolyze the same range of nitrocefin concentrations as 0.25 nM of the WT AmpC enzyme; this is a 20- to 40-fold increase in [E], respectively (see section 2.3.1). This speaks to the difference in nitrocefin specificity between the WT and mutant AmpC enzymes. Indeed, relative to WT AmpC, all four AmpC mutants demonstrate at least an order of magnitude reduction in catalytic efficiency towards nitrocefin, with the ΔG229–E247 deletion mutant showing the largest decrease (**Table 3.1**).

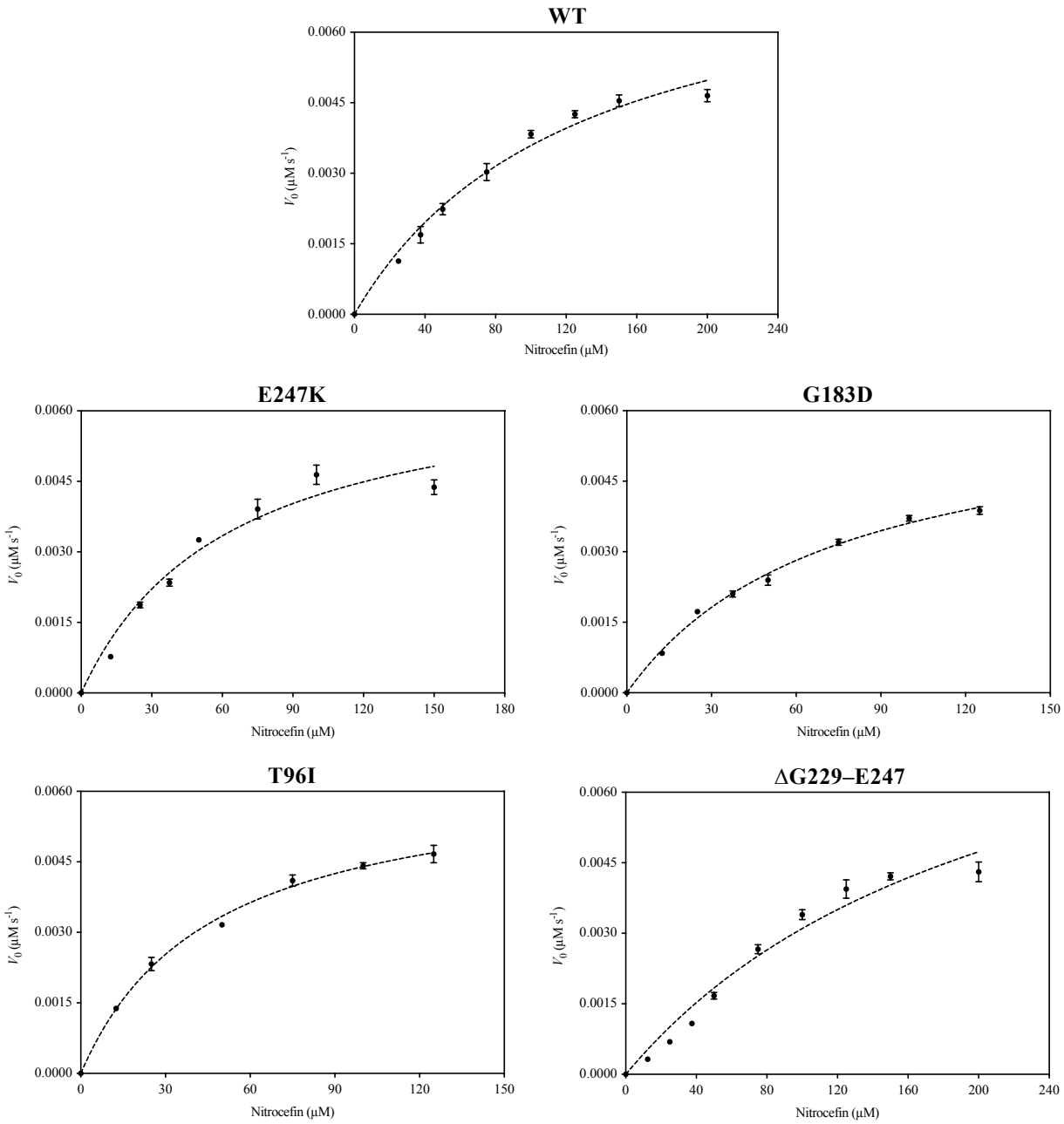

Figure 3.6 – Michaelis–Menten plots of WT and mutant AmpC enzymes towards nitrocefin. Each enzyme was challenged with nitrocefin ranging from 0–200 μM and initial rates of ceftolozane hydrolysis were measured at λ = 486 nm for 1,200 s at 28˚C. The slope of each trace was determined by linear regression analysis and plotted against the corresponding nitrocefin concentration to obtain the plots displayed above. Data points represent averages of at least three technical replicates and error bars represent the standard deviation. To obtain Michaelis–Menten kinetic parameters, the plots were fitted to Eq. 1.

3.4. Inhibition of WT and mutant AmpC enzymes by avibactam and tazobactam

The second objective of this thesis was to elucidate the influence of the AmpC mutations on the ability of avibactam and tazobactam – the respective inhibitors co-administered with ceftazidime and ceftolozane – to inhibit AmpC. Inhibition assays were performed with each enzyme using either avibactam or tazobactam as the inhibitor and nitrocefin as the substrate. Figures S3 and S4 respectively display typical traces of nitrocefin hydrolysis by the WT and mutant AmpC enzymes in the presence of different concentrations of avibactam and tazobactam.

3.4.1. AmpC mutants demonstrate reduced susceptibility to inhibition by avibactam.

The progress curves obtained from the avibactam inhibition assays (**Fig. S3**) were fitted to an integrated rate equation (Eq. 3) by non-linear regression to determine the apparent rate constant, k_{obs}, for each reaction. The results of these fits are displayed in Table 3.2. The k_{obs} values for the WT and mutant AmpC enzymes were then plotted as a function of avibactam concentration (**Fig. 3.7**). The resulting linear dependence allows for an estimation of the apparent avibactam acylation rate (k_{on}^{app}) and the apparent avibactam dissociation rate (k_{off}^{app}) (**Table 3.3**). These rate constants are therefore key kinetic parameters for differentiating the susceptibility of the WT and mutant AmpC enzymes towards inhibition by avibactam.

Avibactam exhibits the highest rate of enzyme acylation towards WT AmpC, as demonstrated by a k_{on}^{app} value of 6.03 x 10^3 M^{-1} s^{-1} (**Table 3.3**). Remarkably, acylation of all four AmpC mutant enzymes by avibactam is reduced by at least an order of magnitude relative to WT AmpC. Specifically, while the respective avibactam acylation rates of the E247K, T96I, and G183D point mutants are 8-, 12-, and 44-fold lower than that of WT AmpC, the most profound reduction in avibactam acylation is as large as two orders of magnitude, as observed in the

ΔG229–E247 deletion mutant. Moreover, the apparent rate of avibactam dissociation (k_{off}^{app}) of all the AmpC mutants is around one order of magnitude higher than that of WT AmpC, indicating that these mutations also accelerate the release of avibactam from the enzyme. The overall effect of these rate changes is most clearly demonstrated by the changes in the apparent avibactam inhibition binding constant, $K_{avi-binding} = \frac{k_{off}^{app}}{k_{on}^{app}}$ (i.e., the dissociation constant, K_d), which informs the binding affinity of avibactam for AmpC (Corzo 2006) (**Table 3.3**). Specifically, the $K_{avi-binding}$ of each AmpC mutant is between two and three orders of magnitude larger than that of WT AmpC, indicating that avibactam experiences a marked reduction in affinity towards the AmpC mutants. In other words, these AmpC mutations reduce the inhibitory potency of avibactam from the nanomolar to the micromolar concentration scale.

Table 3.2 – Non-linear regression analysis results of fitting the kinetic profiles of nitrocefin hydrolysis by WT and mutant AmpC enzymes in the presence of different concentrations of avibactam to Eq. 3[b] ($P = Y_0 + a(1 - e^{-bx}) + dx$).

Avibactam (M)	Parameter[a]				
	b (k_{obs}) (s^{-1})	Y_0	a	d	R^2
WT					
1.0×10^{-6}	$(4.90 \pm 0.00) \times 10^{-3}$	$(2.26 \pm 0.00) \times 10^{-6}$	$(1.12 \pm 0.00) \times 10^{-5}$	$(1.37 \pm 0.00) \times 10^{-9}$	0.9999
1.5×10^{-6}	$(5.85 \pm 0.25) \times 10^{-3}$	$(2.52 \pm 0.06) \times 10^{-6}$	$(9.40 \pm 0.38) \times 10^{-6}$	$(2.37 \pm 0.32) \times 10^{-9}$	0.9997
2.0×10^{-6}	$(6.80 \pm 0.30) \times 10^{-3}$	$(2.22 \pm 0.34) \times 10^{-6}$	$(7.84 \pm 0.62) \times 10^{-6}$	$(3.16 \pm 0.61) \times 10^{-9}$	0.9996
3.0×10^{-6}	$(9.30 \pm 0.50) \times 10^{-3}$	$(2.20 \pm 0.29) \times 10^{-6}$	$(5.51 \pm 0.80) \times 10^{-6}$	$(3.86 \pm 0.28) \times 10^{-9}$	0.9996
4.0×10^{-6}	$(1.33 \pm 0.00) \times 10^{-2}$	$(1.74 \pm 0.00) \times 10^{-6}$	$(3.18 \pm 0.00) \times 10^{-6}$	$(4.15 \pm 0.00) \times 10^{-9}$	0.9999
5.0×10^{-6}	$(1.69 \pm 0.06) \times 10^{-2}$	$(2.33 \pm 0.25) \times 10^{-6}$	$(3.27 \pm 0.34) \times 10^{-6}$	$(3.62 \pm 0.25) \times 10^{-9}$	0.9998
7.5×10^{-6}	$(2.41 \pm 0.00) \times 10^{-2}$	$(1.98 \pm 0.28) \times 10^{-6}$	$(1.71 \pm 0.34) \times 10^{-6}$	$(2.96 \pm 0.28) \times 10^{-9}$	0.9999
1.0×10^{-5}	$(3.54 \pm 0.05) \times 10^{-2}$	$(1.99 \pm 0.26) \times 10^{-6}$	$(1.24 \pm 0.07) \times 10^{-6}$	$(2.63 \pm 0.18) \times 10^{-9}$	0.9992
E247K					
1.1×10^{-5}	$(6.00 \pm 0.28) \times 10^{-3}$	$(2.81 \pm 0.23) \times 10^{-6}$	$(8.74 \pm 0.35) \times 10^{-6}$	$(7.16 \pm 0.49) \times 10^{-10}$	0.9993
2.2×10^{-5}	$(8.73 \pm 0.21) \times 10^{-3}$	$(2.72 \pm 0.10) \times 10^{-6}$	$(5.73 \pm 0.08) \times 10^{-6}$	$(2.59 \pm 0.49) \times 10^{-10}$	0.9994
3.1×10^{-5}	$(1.14 \pm 0.01) \times 10^{-2}$	$(2.57 \pm 0.17) \times 10^{-6}$	$(4.32 \pm 0.08) \times 10^{-6}$	$(1.75 \pm 0.83) \times 10^{-10}$	0.9996
4.4×10^{-5}	$(1.49 \pm 0.07) \times 10^{-2}$	$(2.15 \pm 0.06) \times 10^{-6}$	$(3.01 \pm 0.20) \times 10^{-6}$	$(1.66 \pm 1.28) \times 10^{-10}$	0.9991
6.2×10^{-5}	$(1.91 \pm 0.01) \times 10^{-2}$	$(2.17 \pm 0.22) \times 10^{-6}$	$(2.01 \pm 0.21) \times 10^{-6}$	$(6.89 \pm 6.89) \times 10^{-11}$	0.9941
8.8×10^{-5}	$(2.82 \pm 0.11) \times 10^{-2}$	$(1.97 \pm 0.19) \times 10^{-6}$	$(1.11 \pm 0.08) \times 10^{-6}$	$(1.01 \pm 0.34) \times 10^{-10}$	0.9912
G183D					
4.0×10^{-5}	$(6.10 \pm 0.10) \times 10^{-3}$	$(3.23 \pm 0.03) \times 10^{-6}$	$(8.89 \pm 0.40) \times 10^{-6}$	$(9.88 \pm 0.15) \times 10^{-10}$	0.9989
5.0×10^{-5}	$(6.43 \pm 0.34) \times 10^{-3}$	$(2.85 \pm 0.09) \times 10^{-6}$	$(7.88 \pm 0.28) \times 10^{-6}$	$(6.70 \pm 0.56) \times 10^{-10}$	0.9993
1.0×10^{-4}	$(9.85 \pm 0.55) \times 10^{-3}$	$(2.52 \pm 0.09) \times 10^{-6}$	$(4.87 \pm 0.38) \times 10^{-6}$	$(2.59 \pm 1.30) \times 10^{-10}$	0.9968
1.5×10^{-4}	$(1.21 \pm 0.05) \times 10^{-2}$	$(2.24 \pm 0.11) \times 10^{-6}$	$(3.36 \pm 0.29) \times 10^{-6}$	$(6.63 \pm 1.85) \times 10^{-11}$	0.9995
2.0×10^{-4}	$(1.64 \pm 0.02) \times 10^{-2}$	$(1.90 \pm 0.04) \times 10^{-6}$	$(2.18 \pm 0.49) \times 10^{-6}$	$(4.98 \pm 0.40) \times 10^{-11}$	0.9734
3.0×10^{-4}	$(2.09 \pm 0.06) \times 10^{-2}$	$(1.36 \pm 0.23) \times 10^{-6}$	$(9.68 \pm 1.72) \times 10^{-7}$	$(4.65 \pm 2.22) \times 10^{-11}$	0.9940
4.0×10^{-4}	$(2.67 \pm 0.03) \times 10^{-2}$	$(1.13 \pm 0.27) \times 10^{-6}$	$(6.48 \pm 1.04) \times 10^{-7}$	$(7.64 \pm 3.93) \times 10^{-11}$	0.9939
T96I					
1.25×10^{-5}	$(7.40 \pm 0.14) \times 10^{-3}$	$(2.99 \pm 0.25) \times 10^{-6}$	$(8.52 \pm 0.42) \times 10^{-6}$	$(5.18 \pm 1.24) \times 10^{-10}$	0.9993
2.50×10^{-5}	$(1.01 \pm 0.01) \times 10^{-2}$	$(2.79 \pm 0.25) \times 10^{-6}$	$(6.06 \pm 0.13) \times 10^{-6}$	$(6.32 \pm 4.81) \times 10^{-11}$	0.9991
5.00×10^{-5}	$(1.29 \pm 0.03) \times 10^{-2}$	$(2.50 \pm 0.23) \times 10^{-6}$	$(4.81 \pm 0.17) \times 10^{-6}$	$(6.10 \pm 4.43) \times 10^{-11}$	0.9983
7.50×10^{-5}	$(1.87 \pm 0.04) \times 10^{-2}$	$(3.05 \pm 0.36) \times 10^{-6}$	$(3.45 \pm 0.08) \times 10^{-6}$	$(6.78 \pm 7.05) \times 10^{-11}$	0.9935
1.00×10^{-4}	$(2.24 \pm 0.05) \times 10^{-2}$	$(2.66 \pm 0.21) \times 10^{-6}$	$(2.35 \pm 0.14) \times 10^{-6}$	$(7.02 \pm 4.24) \times 10^{-11}$	0.9918
1.50×10^{-4}	$(2.85 \pm 0.16) \times 10^{-2}$	$(2.33 \pm 0.34) \times 10^{-6}$	$(1.05 \pm 0.11) \times 10^{-6}$	$(3.71 \pm 3.23) \times 10^{-11}$	0.9942
ΔG229–E247					
5.0×10^{-5}	$(2.83 \pm 0.12) \times 10^{-3}$	$(6.54 \pm 0.98) \times 10^{-7}$	$(9.97 \pm 0.45) \times 10^{-6}$	$(1.76 \pm 2.19) \times 10^{-10}$	0.9999
1.0×10^{-4}	$(4.33 \pm 0.26) \times 10^{-3}$	$(4.79 \pm 1.54) \times 10^{-7}$	$(6.54 \pm 0.16) \times 10^{-6}$	$(1.63 \pm 1.71) \times 10^{-26}$	0.9997
1.5×10^{-4}	$(5.85 \pm 0.11) \times 10^{-3}$	$(5.73 \pm 1.26) \times 10^{-7}$	$(4.48 \pm 0.11) \times 10^{-6}$	$(2.85 \pm 4.02) \times 10^{-11}$	0.9997
2.0×10^{-4}	$(7.55 \pm 0.23) \times 10^{-3}$	$(5.73 \pm 0.44) \times 10^{-7}$	$(3.16 \pm 0.15) \times 10^{-6}$	$(3.27 \pm 5.66) \times 10^{-11}$	0.9962
3.0×10^{-4}	$(1.02 \pm 0.03) \times 10^{-2}$	$(6.56 \pm 1.50) \times 10^{-7}$	$(1.97 \pm 0.07) \times 10^{-6}$	$(1.92 \pm 1.92) \times 10^{-11}$	0.9993
4.0×10^{-4}	$(1.25 \pm 0.04) \times 10^{-2}$	$(5.60 \pm 0.38) \times 10^{-7}$	$(1.22 \pm 0.04) \times 10^{-6}$	$(3.05 \pm 3.40) \times 10^{-11}$	0.9984

[a] Parameter values represent averages of at least three technical replicates and ± values represent the standard deviation.

[b] See section 2.3.2 for details.

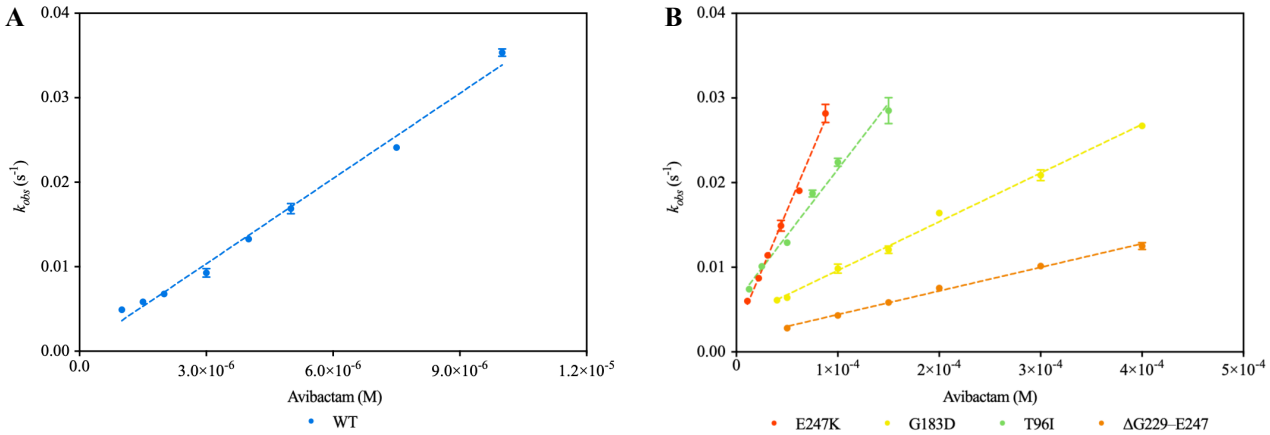

Figure 3.7 – Plots of k_{obs} vs. avibactam concentration for (A) WT and (B) mutant AmpC enzymes. The data points correspond to the values in Table 3.2 and represent averages of at least three technical replicates. The error bars represent the standard deviation (some are smaller than the size of the data points). The lines represent the best linear correlation.

Table 3.3 – Inhibition kinetics of WT and mutant AmpC enzymes by avibactam and tazobactam.

Kinetic Parameter[a]	Inhibitor	
	Avibactam	Tazobactam
WT		
k_{on}^{app} (M^{-1} s^{-1})	$(6.03 \pm 1.21) \times 10^{3}$	$(1.96 \pm 0.27) \times 10^{2}$
k_{off}^{app} (s^{-1})	$(2.7 \pm 6.90) \times 10^{-4}$	$(5.0 \pm 0.31) \times 10^{-3}$
$K_{I\text{–}binding}$ (M)[b]	$(4.48 \pm 11) \times 10^{-8}$	$(2.55 \pm 0.35) \times 10^{-5}$
R^2	0.9907	0.9938
E247K		
k_{on}^{app} (M^{-1} s^{-1})	$(7.35 \pm 2.27) \times 10^{2}$	$(4.56 \pm 0.78) \times 10^{2}$
k_{off}^{app} (s^{-1})	$(2.5 \pm 0.53) \times 10^{-3}$	$(5.3 \pm 0.70) \times 10^{-3}$
$K_{I\text{–}binding}$ (M)	$(3.40 \pm 1.30) \times 10^{-6}$	$(1.16 \pm 0.25) \times 10^{-5}$
R^2	0.9945	0.9909
G183D		
k_{on}^{app} (M^{-1} s^{-1})	$(1.36 \pm 0.14) \times 10^{2}$	$(1.47 \pm 0.22) \times 10^{2}$
k_{off}^{app} (s^{-1})	$(3.9 \pm 0.36) \times 10^{-3}$	$4.3 \pm 0.22) \times 10^{-3}$
$K_{I\text{–}binding}$ (M)	$(2.87 \pm 0.40) \times 10^{-5}$	$(2.93 \pm 0.46) \times 10^{-5}$
R^2	0.9958	0.9926
T96I		
k_{on}^{app} (M^{-1} s^{-1})	$(4.93 \pm 0.52) \times 10^{2}$	$(4.45 \pm 0.30) \times 10^{2}$
k_{off}^{app} (s^{-1})	$(6.0 \pm 0.69) \times 10^{-3}$	$(5.9 \pm 0.41) \times 10^{-3}$
$K_{I\text{–}binding}$ (M)	$(1.22 \pm 0.19) \times 10^{-5}$	$(1.33 \pm 0.13) \times 10^{-5}$
R^2	0.9889	0.9952
ΔG229–E247		
k_{on}^{app} (M^{-1} s^{-1})	$(4.04 \pm 1.50) \times 10^{1}$	$(6.28 \pm 1.9) \times 10^{1}$
k_{off}^{app} (s^{-1})	$(1.6 \pm 0.19) \times 10^{-3}$	$(2.5 \pm 0.05) \times 10^{-3}$
$K_{I\text{–}binding}$ (M)	$(3.96 \pm 1.54) \times 10^{-5}$	$(3.98 \pm 1.2) \times 10^{-5}$
R^2	0.9962	0.9997

[a] Parameters were obtained by fitting the data in Figure 3.6 or Figure 3.7 to Eq. 3; ± values represent the standard errors reported from regression analysis.

[b] Apparent inhibition binding constant for inhibitor I (avibactam [avi] or tazobactam [tazo]); ± values represent the standard error.

3.4.2. Tazobactam inhibitory potency does not differ appreciably between the WT and mutant AmpC enzymes.

Although tazobactam is known to be a poor inhibitor of AmpC (Bebrone *et al.* 2010), its activity towards the WT and mutant AmpC enzymes was still measured, particularly for comparative purposes. The progress curves obtained from the tazobactam inhibition assays (**Fig. S4**) were analyzed in the same way as those from the avibactam inhibition assays (section 3.4.1). The results of these fits are displayed in Table 3.4. The k_{obs} values for the WT and mutant AmpC enzymes were then plotted as a function of tazobactam concentration (**Fig. 3.8**). Again, the resulting linear relationship between these variables allows for an estimation of k_{on}^{app} (tazobactam acylation rate) and k_{off}^{app} (tazobactam turnover rate) (**Table 3.3**).

Acylation of WT AmpC by tazobactam is relatively slow, as demonstrated by a k_{on}^{app} value of 1.96 x 10^2 M^{-1} s^{-1} (**Table 3.3**). (Comparatively, the avibactam acylation rate of WT AmpC is 30-fold faster). Relative to that of WT AmpC, the tazobactam acylation rate is lower for the G183D and ΔG229–E247 mutants, but higher for E247K and T96I mutants. However, none of these changes in k_{on}^{app} are large enough to suggest that the tazobactam acylation rate differs significantly between the WT and mutant AmpC enzymes. Indeed, the largest change in k_{on}^{app} is the 3-fold decrease observed in the ΔG229–E247 mutant. Similarly, the tazobactam turnover rate (k_{off}^{app}) of each AmpC mutant is virtually unchanged from that of WT AmpC, suggesting that these mutations do not affect the ability of AmpC to slowly break down tazobactam. It follows, then, that the apparent tazobactam inhibition binding constant, $K_{tazo-binding} = \frac{k_{off}^{app}}{k_{on}^{app}}$, also does not differ appreciably between the WT and mutant AmpC enzymes. Indeed, the affinity of tazobactam for the AmpC mutants varies no more than 2-fold from that for WT AmpC. Thus, these mutations do not appear to affect the already poor inhibition potency of tazobactam towards AmpC.

Table 3.4 – Non-linear regression analysis results of fitting the kinetic profiles of nitrocefin hydrolysis by WT and mutant AmpC enzymes in the presence of different concentrations of tazobactam to Eq. 3[b] ($P = Y_0 + a(1 - e^{-bx}) + dx$).

Tazobactam (M)	Parameter[a]				
	b (k_{obs}) (s^{-1})	Y_0	a	d	R^2
WT					
1.25×10^{-5}	$(6.03 \pm 0.19) \times 10^{-3}$	$(1.77 \pm 0.17) \times 10^{-6}$	$(1.06 \pm 0.14) \times 10^{-5}$	$(1.98 \pm 0.15) \times 10^{-10}$	0.9993
2.5×10^{-5}	$(8.23 \pm 0.39) \times 10^{-3}$	$(1.59 \pm 0.18) \times 10^{-6}$	$(7.90 \pm 1.64) \times 10^{-6}$	$(3.16 \pm 2.13) \times 10^{-10}$	0.9997
5.0×10^{-5}	$(1.04 \pm 0.03) \times 10^{-2}$	$(1.68 \pm 0.27) \times 10^{-6}$	$(5.13 \pm 0.21) \times 10^{-6}$	$(7.00 \pm 2.58) \times 10^{-11}$	0.9998
7.5×10^{-5}	$(1.34 \pm 0.04) \times 10^{-2}$	$(1.38 \pm 0.30) \times 10^{-6}$	$(3.77 \pm 0.48) \times 10^{-6}$	$(1.68 \pm 0.27) \times 10^{-11}$	0.9988
1.0×10^{-4}	$(1.59 \pm 0.02) \times 10^{-2}$	$(1.36 \pm 0.27) \times 10^{-6}$	$(2.79 \pm 0.43) \times 10^{-6}$	$(8.05 \pm 5.42) \times 10^{-11}$	0.9765
E247K					
1.25×10^{-5}	$(7.33 \pm 0.09) \times 10^{-3}$	$(2.76 \pm 0.55) \times 10^{-6}$	$(7.78 \pm 0.86) \times 10^{-6}$	$(6.89 \pm 0.84) \times 10^{-10}$	0.9994
2.5×10^{-5}	$(1.09 \pm 0.02) \times 10^{-2}$	$(2.58 \pm 0.46) \times 10^{-6}$	$(4.87 \pm 0.59) \times 10^{-6}$	$(4.19 \pm 0.34) \times 10^{-10}$	0.9992
5.0×10^{-5}	$(1.40 \pm 0.08) \times 10^{-2}$	$(2.52 \pm 0.42) \times 10^{-6}$	$(3.56 \pm 0.26) \times 10^{-6}$	$(3.38 \pm 0.49) \times 10^{-10}$	0.9983
7.5×10^{-5}	$(1.72 \pm 0.08) \times 10^{-2}$	$(2.10 \pm 0.44) \times 10^{-6}$	$(2.38 \pm 0.29) \times 10^{-6}$	$(2.75 \pm 0.28) \times 10^{-10}$	0.9959
1.0×10^{-4}	$(2.27 \pm 0.03) \times 10^{-2}$	$(2.40 \pm 0.13) \times 10^{-6}$	$(1.36 \pm 0.33) \times 10^{-6}$	$(2.36 \pm 0.40) \times 10^{-10}$	0.9940
1.5×10^{-4}	$(3.24 \pm 0.09) \times 10^{-2}$	$(1.31 \pm 0.13) \times 10^{-6}$	$(7.77 \pm 0.35) \times 10^{-7}$	$(1.77 \pm 0.13) \times 10^{-10}$	0.9823
G183D					
1.25×10^{-5}	$(5.13 \pm 0.21) \times 10^{-3}$	$(2.44 \pm 0.32) \times 10^{-6}$	$(1.01 \pm 0.05) \times 10^{-5}$	$(1.49 \pm 0.33) \times 10^{-9}$	0.9993
2.5×10^{-5}	$(6.00 \pm 0.19) \times 10^{-3}$	$(2.29 \pm 0.40) \times 10^{-6}$	$(8.24 \pm 0.47) \times 10^{-6}$	$(9.08 \pm 0.64) \times 10^{-10}$	0.9991
5.0×10^{-5}	$(7.03 \pm 0.05) \times 10^{-3}$	$(2.31 \pm 0.41) \times 10^{-6}$	$(7.12 \pm 0.26) \times 10^{-6}$	$(6.41 \pm 1.30) \times 10^{-10}$	0.9988
7.5×10^{-5}	$(8.90 \pm 0.40) \times 10^{-3}$	$(1.99 \pm 0.45) \times 10^{-6}$	$(5.23 \pm 0.37) \times 10^{-6}$	$(3.25 \pm 1.20) \times 10^{-10}$	0.9994
1.0×10^{-4}	$(1.10 \pm 0.03) \times 10^{-2}$	$(1.83 \pm 0.40) \times 10^{-6}$	$(3.99 \pm 0.42) \times 10^{-6}$	$(2.16 \pm 0.05) \times 10^{-10}$	0.9993
1.5×10^{-4}	$(1.35 \pm 0.01) \times 10^{-2}$	$(1.12 \pm 0.16) \times 10^{-6}$	$(2.37 \pm 0.23) \times 10^{-6}$	$(7.62 \pm 0.55) \times 10^{-11}$	0.9951
T96I					
1.25×10^{-5}	$(7.63 \pm 0.36) \times 10^{-3}$	$(3.09 \pm 0.40) \times 10^{-6}$	$(9.18 \pm 1.12) \times 10^{-6}$	$(9.23 \pm 0.35) \times 10^{-10}$	0.9992
2.5×10^{-5}	$(9.00 \pm 0.70) \times 10^{-3}$	$(3.04 \pm 0.08) \times 10^{-6}$	$(7.31 \pm 1.18) \times 10^{-6}$	$(6.99 \pm 1.47) \times 10^{-10}$	0.9991
5.0×10^{-5}	$(1.28 \pm 0.03) \times 10^{-2}$	$(2.78 \pm 0.25) \times 10^{-6}$	$(4.67 \pm 0.46) \times 10^{-6}$	$(6.52 \pm 0.60) \times 10^{-10}$	0.9995
7.5×10^{-5}	$(1.73 \pm 0.02) \times 10^{-2}$	$(2.29 \pm 0.17) \times 10^{-6}$	$(3.25 \pm 0.16) \times 10^{-6}$	$(5.39 \pm 1.20) \times 10^{-10}$	0.9976
1.0×10^{-4}	$(2.03 \pm 0.04) \times 10^{-2}$	$(2.22 \pm 0.24) \times 10^{-6}$	$(2.18 \pm 0.23) \times 10^{-6}$	$(4.73 \pm 0.92) \times 10^{-10}$	0.9962
1.5×10^{-4}	$(2.66 \pm 0.00) \times 10^{-2}$	$(1.56 \pm 0.01) \times 10^{-6}$	$(1.13 \pm 0.05) \times 10^{-6}$	$(3.24 \pm 0.49) \times 10^{-10}$	0.9971
ΔG229–E247					
2.5×10^{-5}	$(3.57 \pm 0.01) \times 10^{-3}$	$(4.61 \pm 0.45) \times 10^{-7}$	$(8.66 \pm 0.40) \times 10^{-6}$	$(1.52 \pm 0.87) \times 10^{-10}$	0.9988
5.0×10^{-5}	$(4.63 \pm 0.19) \times 10^{-3}$	$(4.19 \pm 1.36) \times 10^{-7}$	$(6.41 \pm 0.85) \times 10^{-6}$	$(1.04 \pm 0.36) \times 10^{-10}$	0.9998
1.0×10^{-5}	$(6.88 \pm 0.08) \times 10^{-3}$	$(4.50 \pm 1.22) \times 10^{-7}$	$(4.05 \pm 0.06) \times 10^{-6}$	$(1.52 \pm 0.71) \times 10^{-10}$	0.9998
1.5×10^{-4}	$(9.07 \pm 0.09) \times 10^{-3}$	$(4.12 \pm 1.80) \times 10^{-7}$	$(2.50 \pm 0.26) \times 10^{-6}$	$(5.62 \pm 1.43) \times 10^{-11}$	0.9970
2.0×10^{-4}	$(1.11 \pm 0.00) \times 10^{-2}$	$(2.16 \pm 0.00) \times 10^{-8}$	$(1.77 \pm 0.00) \times 10^{-6}$	$(1.25 \pm 0.00) \times 10^{-10}$	0.9986

[a] Parameter values represent averages of at least three technical replicates and ± values represent the standard deviation.

[b] See section 2.3.2 for details.

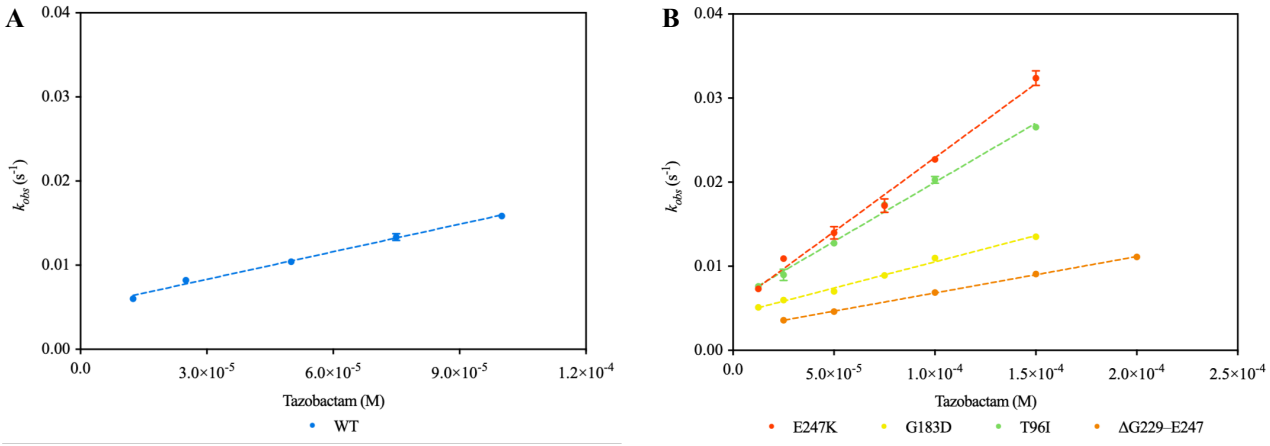

Figure 3.8 – Plots of k_{obs} vs. tazobactam concentration for (A) WT and (B) mutant AmpC enzymes. The data points correspond to the values in Table 3.4 and represent averages of at least three technical replicates. The error bars represent the standard deviation (some are smaller than the size of the data points). The lines represent the best linear correlation.

3.5. Thermal stability of WT and mutant AmpC enzymes

3.5.1. AmpC mutants have lower thermal stabilities compared to WT AmpC.

To investigate whether mutations in AmpC compromise enzyme stability, the melting temperatures (T_m) of the WT and mutant AmpC enzymes were determined by monitoring the ratio of fluorescence intensities measured at 330 nm and 350 nm as the enzymes were heated from 20˚C to 95˚C at a rate of 1˚C min^{-1}. The inflection point of the resulting plot defines the melting temperature of the enzyme (Munoz and Sanchez-Ruiz 2004) (**Fig. 3.9**). Intriguingly, each AmpC mutant has a melting temperature lower than that of WT AmpC (T_m = 55.33˚C) (**Table 3.5**). The E247K point mutant demonstrates the largest reduction in thermal stability, with a T_m nearly 10˚C lower than that of WT AmpC. The other AmpC point mutants, G183D and T96I, appear to be slightly more stable than E247K, with respective T_m values of 50.43˚C and 49.23˚C. Interestingly, the ΔG229–E247 deletion mutant exhibits the highest thermal stability of all the AmpC mutants, with a T_m = 51.77˚C.

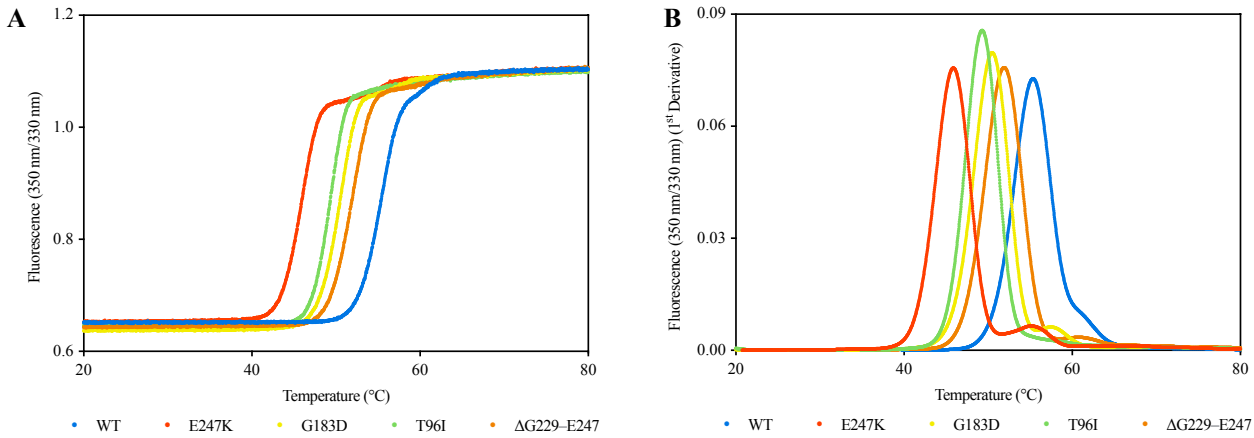

Figure 3.9 – Melting temperature determination of WT and mutant AmpC enzymes. Each enzyme (50 μM) was heated from 20˚C to 95˚C at a rate of 1˚C min^{-1} using a NanoTemper Prometheus NT.48 DSF and protein denaturation was followed by monitoring the ratio of fluorescence intensities measured at 330 nm and 350 nm (excitation 290 nm). The melt curves represent one technical replicate for each enzyme. The T_m values are represented by the inflection points in melt curve (**A**) and the fluorescence peaks in melt curve (**B**).

Table 3.5 – Melting temperatures of WT and mutant AmpC enzymes.

AmpC Enzyme	T_m (˚C)[a]	ΔT_m (˚C)[b]
WT	55.33 ± 0.06	0.00 ± 0.080
E247K	45.80 ± 0.00	–9.53 ± 0.060
G183D	50.43 ± 0.15	–4.90 ± 0.200
T96I	49.23 ± 0.06	–6.10 ± 0.080
ΔG229–E247	51.77 ± 0.06	–3.56 ± 0.080

[a] Values represent averages of three technical replicates; ± values represent the standard deviation.
[b] Changes in T_m relative to WT AmpC; ± values represent the standard error.

4. Discussion

The AmpC mutant enzymes E247K, G183D, T96I, and ΔG229–E247 were identified in *P. aeruginosa* clinical isolates that arose in response to ceftolozane/tazobactam exposure. MIC experiments revealed that these isolates are indeed resistant to ceftolozane/tazobactam and exhibit cross-resistance to ceftazidime/avibactam, and microbiological profiling confirmed that the AmpC mutant enzymes are responsible for conferring this resistance profile (MacVane *et al.* 2017; Fraile-Ribot *et al.* 2018). While computational efforts such as molecular modelling have begun to decipher the mechanism by which these mutations promote this resistance, it is evident that detailed kinetic studies of the actual AmpC mutant enzymes are warranted for complete elucidation. Accordingly, the goal of this thesis was to investigate the catalytic properties of these mutant AmpC enzymes (alongside WT AmpC) in order to provide a quantitative description of the effects of each mutation on both antibiotic hydrolysis and inhibitor binding.

4.1. Catalytic activity of WT AmpC towards ceftolozane and ceftazidime

The first goal of this thesis was to investigate the catalytic activity of the WT AmpC enzyme towards ceftolozane and ceftazidime using Michaelis–Menten kinetics, particularly to serve as a means of comparison to the AmpC mutant enzymes. First, while the rate of ceftolozane turnover (k_{cat}) by WT AmpC is twice as fast as the rate of ceftazidime turnover, the affinity (K_m) of this enzyme for ceftolozane is 6-fold lower than that for ceftazidime. The considerable difference in enzyme affinity for ceftolozane and ceftazidime reflects the distinctive properties of their R2 side chains. Specifically, the 2-methyl-3-aminopyrazolium side chain of ceftolozane offers an additional positive charge in the form of a basic 2-aminoethyluredio moiety (pK_a = 7.95) (Murano *et al.* 2008) (**Fig. 1.3**). As a consequence of its larger bulk and increased

net charge at neutral pH, ceftolozane introduces greater steric hindrance and therefore interacts less favourably with the AmpC active site compared to ceftazidime (Murano *et al.* 2008). It follows, then, that WT AmpC demonstrates a modest difference in its specificity $\left(\frac{k_{cat}}{K_m}\right)$ towards ceftolozane and ceftazidime, with higher activity towards ceftazidime. These observations are consistent with the results of a previous study in which the affinity and catalytic efficiency of *P. aeruginosa* WT AmpC towards ceftolozane are both 20-fold lower than those for ceftazidime (Takeda *et al.* 2007).

These differences notwithstanding, the activity of WT AmpC towards ceftolozane and ceftazidime is still quite low compared to its catalytic efficiency towards earlier-generation cephalosporins. The $\frac{k_{cat}}{K_m}$ of WT AmpC for the first-generation cephalosporin cephalothin, for instance, is 5.1×10^{-1} μM^{-1} s^{-1} (Rodríguez-Martínez *et al.* 2009), which is 4 orders of magnitude larger than that for ceftazidime (**Table 3.1**). This further highlights the increased protection against β-lactamase-mediated hydrolysis afforded by the continued structural modification of cephalosporins. One such optimization common to both ceftolozane and ceftazidime (but missing from earlier-generation cephalosporins like cephalothin) is the oxime moiety, which contributes to their identical hydrophilic R1 side chains and heightens protection against β-lactamases by increasing overall stability (**Fig. 1.3**) (Toda *et al.* 2008). Indeed, crystal structures (Powers *et al.* 2001) and molecular models (Barnes *et al.* 2019) of AmpC complexed with ceftazidime and ceftolozane, respectively, reveal that this R1 side chain interacts unfavourably with Ω loop residues Gly248 and Tyr249 (SANC positions 220 and 221, respectively), thereby preventing these drugs from adopting catalytically competent conformations in the enzyme active site. Ultimately, as ceftolozane and ceftazidime are designed to resist hydrolysis by AmpC β-lactamases, it is not surprising that WT AmpC exhibits poor catalytic activity towards them.

4.2. Effects of mutations on the hydrolysis of ceftolozane and ceftazidime by AmpC

While the above results provide further insight into the catalytic properties of WT AmpC, the overarching goal of this study is to understand how AmpC mutations affect these properties. As such, Michaelis–Menten kinetics were also used to characterize the AmpC mutant enzymes E247K, G183D, T96I, and ΔG229–E247. First, this analysis revealed that the AmpC mutants have lower affinities for both ceftolozane and ceftazidime compared to WT AmpC. The one exception is the G183D point mutant, which demonstrates enhanced affinity for ceftolozane. This is not surprising, however, and provides some insight into the mutational strategy of AmpC. To elaborate, the substitution of glycine for aspartic acid at position 183 in AmpC introduces a negative formal charge in the H-5 helix, which is proximal to the enzyme active site (**Fig. 4.1**). Given that the R2 side chain of ceftolozane has a significant net positive charge at neutral pH (**Fig. 1.3**), it is conceivable that the G183D mutation improves accommodation of this drug into the enzyme active site. The absence of this additional charge in the R2 side chain of ceftazidime also explains why the G183D mutant instead shows reduced affinity for this antibiotic.

Despite having lower affinities for ceftolozane and ceftazidime, all the AmpC mutants hydrolyze both drugs with highly improved activity compared to WT AmpC; this is clearly demonstrated by faster enzyme turnover rates (k_{cat}) and, in turn, at least an order of magnitude increase in catalytic efficiency ($\frac{k_{cat}}{K_m}$). These results can be further explained using the wealth of structural and functional information available for AmpC. First, Glu247 contributes to the Ω loop (**Fig. 4.1**) (Fraile-Ribot *et al.* 2018) and is obviously directly adjacent to Gly248 and Tyr249 which, as previously mentioned, interact unfavourably with ceftolozane and ceftazidime (Powers *et al.* 2001). Barnes *et al.* (2019) propose that the substitution of glutamic acid to lysine at position 247 in AmpC (i.e., E247K) orients Tyr249 in such a way that improves stabilization and

hydrolysis of ceftolozane/ceftazidime in the active site. Gly183 is also in close contact with Gly248 and Tyr249, and Lahiri *et al.* (2015) suggest that substituting this glycine residue for aspartic acid (i.e., G183D) re-positions these Ω loop residues to reduce steric clashing with ceftolozane and ceftazidime, leading to improved hydrolytic efficiency. It follows, then, that the Ω loop truncation mutant, ΔG229–E247, also reduces steric hindrance to facilitate the breakdown of these cephalosporins. Thr96, on the other hand, resides in the H-2 helix, which also contains the catalytic serine, Ser90 (SANC position 64), and interacts with the Ω loop via hydrogen bonding (**Fig. 4.1**) (Raimondi *et al.* 2001). Substituting this threonine residue for isoleucine (i.e., T96I) is thought to increase the pliability of the H-2 helix, thereby improving the ability of Ser90 to launch a nucleophilic attack on the β-lactam carbonyl carbon (Raimondi *et al.* 2001). It is also worth mentioning that extended-spectrum AmpC enzymes containing point mutations in the Ω loop or H-2 helix have also been reported in other prominent Gram-negative pathogens like *Serratia marcescens* and *Enterobacter cloacae* and display the same altered catalytic properties as those exhibited by AmpC mutants investigated in this thesis (that is, reduced affinity and heightened enzyme turnover towards ceftazidime and other extended-spectrum cephalosporins) (Matsumura *et al.* 1998; Raimondi *et al.* 2001; Hidri *et al.* 2005).

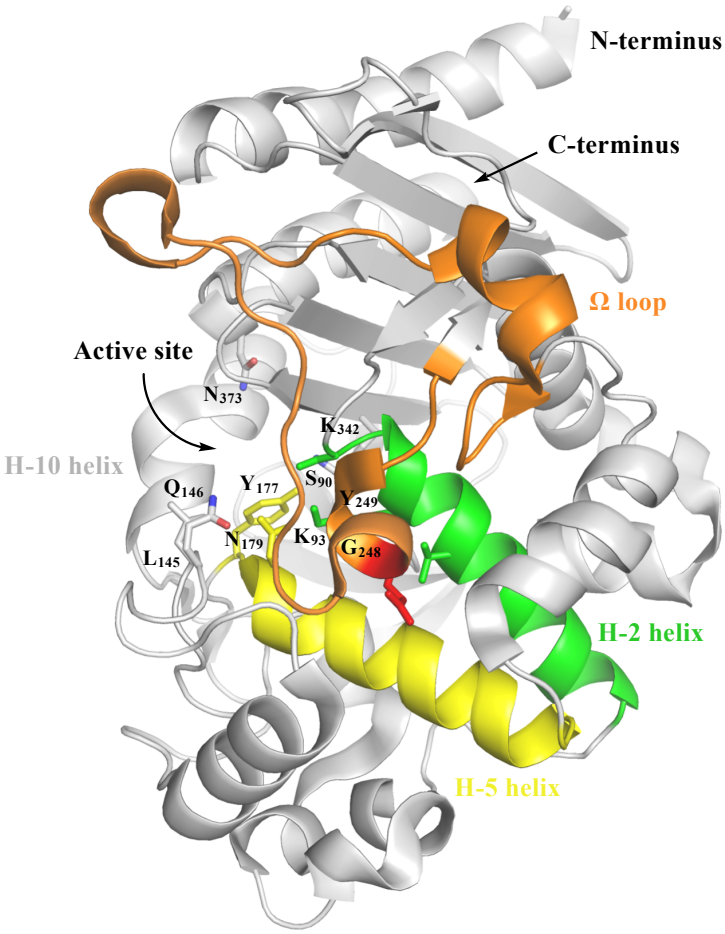

APADRLKALV DAAVQPVMKA NDIPGLAVAI SLKGEPHYFS YGLASKEDGR RVTPETLFEI

H-2 helix

GSVSKTFTAT LAGYALTQDK MRLDDRASQH WPALQGSRFD GISLLDLATY TAGGLPLQFP

H-5 helix

DSVQKDQAQI RDYYRQWQPT YAPGSQRIYS NPSIGLFGYL AARSLGQPFE RLMEQQVFPA

Ω loop

LGLEQTHLDV PEAALAQYAQ GYGKRDRPLR VGPGPLDAEG YGVKTSAADL LRFVDANLHP

H-10 helix

ERLDRPWAQA LDATHRGYYK VGDMTQGLGW EAYDWPISLK RLQAGNSTPM ALQPHRIARL

PAPQALEGQR LLNKTGSTNG FGAYVAFVPG RDLGLVILAN RNYPNAERVK IAYAILSGLE

Figure 4.1 – Structural model and corresponding amino acid sequence of *P. aeruginosa* PAO1 AmpC β-lactamase. The structural domains in which the AmpC mutations occur are colour-coded as follows: Ω loop (orange; location of ΔG229–E247K deletion and E247K [red]); H-5 helix (yellow; location of G183D); H-2 helix (green; location of T96I). Key active-site residues (and the Ω loop residues discussed in the text, Gly248 and Tyr249) are labelled on the model and bolded in the sequence. The coloured boxes indicate the residues that compose each domain and the residues that represent the AmpC mutants are colour-coded as described above. This figure was prepared in the PyMOL Molecular Graphic System (v.2.3.4) using the crystal coordinates published by Lahiri *et al.* (2013) (PDB ID: 4HEF).

4.3. Effects of mutations on the hydrolysis of nitrocefin by AmpC

Hydrolysis of the chromogenic cephalosporin analogue, nitrocefin, by the WT and mutant AmpC enzymes was also investigated using Michaelis–Menten kinetics. Although the AmpC mutants (save the ΔG229–E247 deletion mutant) demonstrate a modest increase in affinity for nitrocefin compared to WT AmpC, they all exhibit more than an order of magnitude reduction in enzyme turnover. The net result of these competing contributions is revealed by the specificity constants of the AmpC mutants, which signify at least an order of magnitude reduction in nitrocefin hydrolysis efficiency relative to WT AmpC. These results contrast significantly with those obtained for ceftolozane and ceftazidime hydrolysis. Indeed, as previously discussed, the AmpC mutants demonstrate enhanced catalytic efficiency towards ceftolozane and ceftazidime compared to WT AmpC but have reduced affinities for them. It should be emphasized, however, that the AmpC mutant enzymes arose in the presence of ceftolozane/tazobactam, so it makes sense that their mutations are catered towards improving ceftolozane catalysis. The ceftazidime cross-resistance that these mutations confer is also not surprising considering the high structural similarity between ceftolozane and ceftazidime (**Fig. 4.1**). The opposing effects of these mutations on the activity of AmpC towards these different substrates, however, can be better understood if the rate-limiting step of the nitrocefin hydrolysis mechanism differs from that of ceftolozane/ceftazidime. This is a reasonable prediction considering that, unlike ceftolozane and ceftazidime, nitrocefin is not a “natural” antibiotic substrate for AmpC; therefore, its hydrolytic mechanism cannot be expected to proceed identically to that of ceftolozane/ceftazidime. This is discussed in greater detail later.

4.4. Influence of mutations on avibactam inhibitory potency towards AmpC

To further elucidate the molecular mechanism for how AmpC mutations confer resistance to β-lactam/BLI combination therapy, the susceptibility of the WT and mutant AmpC enzymes to inhibitor acylation was evaluated. Specifically, the effect of avibactam (or tazobactam) on nitrocefin hydrolysis by each of the AmpC mutants was compared to that of WT AmpC. First, avibactam exhibits the highest rate of acylation towards – and the slowest rate of dissociation from – the WT AmpC enzyme. This is not surprising, as avibactam is known for its rapid acylation of and slow deacylation from a wide range of β-lactamases, including AmpC enzymes (Stachyra *et al.* 2010). Indeed, the inhibition kinetics of avibactam towards WT AmpC from *P. aeruginosa* PAO1 were previously investigated by Ehmann *et al.* (2013), who reported k_{on}^{app} and k_{off}^{app} values of $(2.9 \pm 0.1) \times 10^3$ M^{-1} s^{-1} and $(1.9 \pm 0.6) \times 10^{-3}$ s^{-1}, respectively. These results are consistent with the values reported in this thesis (**Table 3.3**), providing further support for the inhibitory efficacy of avibactam towards WT AmpC. Intriguingly, the rate of avibactam acylation of each AmpC mutant is at least an order of magnitude lower than that of WT AmpC, revealing that these mutations compromise the ability avibactam to rapidly bind AmpC. Moreover, the notable increase in avibactam deacylation rate observed in the AmpC mutants indicates that their mutations also accelerate the release of avibactam from the enzyme. Since avibactam is a reversible inhibitor, it is only effective while enzyme bound; therefore, slow deacylation is an important facet of the avibactam inhibition cycle (Stachyra *et al.* 2010; Ehmann *et al.* 2012). By accelerating the rate at which avibactam dissociates from AmpC, then, these mutations effectively reduce the lifespan of the acyl–enzyme complex, which in turn increases the opportunity for the unbound enzyme to hydrolyze the co-administered β-lactam, ceftazidime. Since the job of a BLI is to "protect" its partner β-lactam from β-lactamase-mediated hydrolysis

(Drawz and Bonomo 2010), it is clear that the AmpC mutations directly interfere with the overall functionality of avibactam.

To continue, the avibactam binding constant, $K_{\text{avi–binding}} = \frac{k_{\text{off}}^{\text{app}}}{k_{\text{on}}^{\text{app}}}$, also known as the inhibition binding constant, K_{d}, informs the binding affinity of avibactam for AmpC, and is therefore another useful parameter for comparing the susceptibility of the WT and mutant AmpC enzymes towards avibactam inhibition (Corzo 2006). The $K_{\text{avi–binding}}$ for WT AmpC is relatively low ($4.48 \pm 11 \times 10^{-8}$ M) and is consistent with the measurements reported by Ehmann *et al.* (2013) ($K_{\text{avi–binding}} = 6.6 \times 10^{-7}$ M). Remarkably, the $K_{\text{avi–binding}}$ for each AmpC mutant is at least two orders of magnitude larger than that for WT AmpC, indicating that avibactam has reduced affinity for the AmpC mutants. In other words, while nanomolar concentrations of avibactam are sufficient to achieve equilibrium between bound and free WT AmpC, avibactam is required in micromolar concentrations to accomplish this with the AmpC mutants. This is the net result of a reduction in avibactam acylation rate ($k_{\text{on}}^{\text{app}}$) and an acceleration in avibactam deacylation rate ($k_{\text{off}}^{\text{app}}$). It is worth emphasizing that avibactam interacts with the same active site residues as those responsible for β-lactam binding and catalysis (**Fig. 1.7 and 4.1**), and since the AmpC mutations decrease enzyme affinity for ceftolozane and ceftazidime, it makes sense that they also reduce avibactam binding affinity. However, the reduction in avibactam affinity is far greater than that of either ceftolozane or ceftazidime. This can be attributed to the rigid binding mode and highly restricted rotational freedom of avibactam, which limit its ability to adapt to the structural or electrostatic changes that the AmpC mutations impose on the active site (Ehmann *et al.* 2012; Lahiri *et al.* 2014). Since ceftolozane and ceftazidime are much more flexible (Powers *et al.* 2001), their accommodation into the active site is not affected as significantly by these mutations (which improve their catalytic turnover, nonetheless). This argument was initially made by

Lahiri *et al.* (2014), who describe an AmpC mutant (N346Y) that reduces avibactam inhibition potency while still accommodating and efficiently hydrolyzing the monobactam aztreonam.

The effects of the AmpC mutations on the inhibitory properties of tazobactam, the BLI co-administered with ceftolozane, were also measured. None of the mutations, however, cause an appreciable change in the inhibitory activity (i.e., the k_{on}^{app} and k_{off}^{app}) of tazobactam towards AmpC. This is not surprising, as tazobactam is known to be a poor inhibitor of AmpC and other class C β-lactamases (Bebrone *et al.* 2010). This does, however, further suggest that ceftolozane is the selective pressure guiding the evolution of these AmpC mutant enzymes. Moreover, the difference in the respective inhibition binding constants of avibactam and tazobactam for WT AmpC further emphasizes the low inhibitory potency of tazobactam towards this enzyme. Specifically, the affinity of avibactam for WT AmpC is over two orders of magnitude higher than that of tazobactam. These observations are consistent with the results of a previous study in which amino acid substitutions in the class C β-lactamase from *Acinetobacter baumannii* (ADC-7) are found to significantly reduce the inhibitory potency of avibactam – but not tazobactam – towards this enzyme (Skalweit *et al.* 2015).

4.5. Relationship between AmpC stability, flexibility, and activity

Enzyme active sites, while optimal for substrate recognition, are intentionally strained and poorly packed (Richards 1977). Typically, this is due to electrostatic repulsion resulting from the juxtaposition of active site residues carrying the same formal charge (Elcock 2001). Conformational strain is also present among residues responsible for substrate binding (Herzberg and Moult 1991). Substituting amino acids within or proximal to the active site is therefore likely to increase this strain and, consequently, reduce enzyme stability (Wang *et al.* 2002).

Accordingly, to investigate whether the AmpC mutations affect enzyme stability, the melting temperatures (T_m) of the WT and mutant AmpC enzymes were measured. The T_m determined for WT AmpC (i.e., PDC-1 from *P. aeruginosa* PAO1) (55.33˚C) is comparable to those of other WT AmpC analogues, including *E. coli* AmpC (54.6˚C) (Beadle *et al.* 1999) and *P. aeruginosa* PDC-3 (52.0˚C) (Barnes *et al.* 2019). The T_m values of the AmpC mutants, however, are noticeably lower than that of WT AmpC, indicating that these mutations do in fact decrease the melting point of this enzyme. This change in protein melting point (ΔT_m) between the WT and mutant AmpC enzymes can be related to changes in protein folding free energy ($\Delta\Delta G_{unfolding} = \Delta G^{mutant}_{unfolding} - \Delta G^{WT}_{unfolding}$) through the equation, $\Delta\Delta G_{unfolding} = \frac{\Delta H_{unfolding}}{T_m}\Delta T_m$ (Francisco *et al.* 2019), where $\Delta H_{unfolding}$ is the unfolding enthalpy, which is positive during thermal denaturation (Pica and Graziamo 2016), and T_m is the melting temperature of the WT AmpC enzyme. That is to say, these mutations decrease the stability of AmpC which in turn increases its flexibility and dynamics at room temperature.

Furthermore, increases in enzyme flexibility have been shown to facilitate enzyme function by permitting substrate access to and product release from the active site (Nicholson *et al.* 1995). Since the AmpC mutations clearly enhance enzyme flexibility, the relationship between enzyme flexibility and enzyme activity for WT AmpC and for the AmpC point mutants (E247K, G183D, and T96I) was investigated. Single point mutations have negligible effects on the $\Delta H_{unfolding}$ of an enzyme (Whitford 2005); therefore, the $\Delta\Delta G_{unfolding}$ of each AmpC point mutant is proportional to ΔT_m. The log of the specificity constants (i.e., catalytic efficiencies) of the WT and point mutant AmpC enzymes for ceftolozane, ceftazidime, and nitrocefin can therefore be related to the respective changes in protein melting point (**Fig. 4.2**). It is clear that the catalytic efficiency of AmpC towards ceftolozane and ceftazidime uniformly increases as the

enzyme becomes more flexible and dynamic (that is, as its melting temperature decreases). This trend is not observed for nitrocefin hydrolysis. This is not particularly surprising, however, as nitrocefin is not a "natural" substrate for AmpC, nor is it related to the appearance of the AmpC mutants. In fact, this further supports the notion that these mutations are catered towards enhancing the catalytic activity of AmpC towards ceftolozane (and, consequently, ceftazidime). This also suggests that the rate-limiting step of the ceftolozane/ceftazidime catalytic cycle is different from that of nitrocefin and is likely coupled to a protein dynamic process.

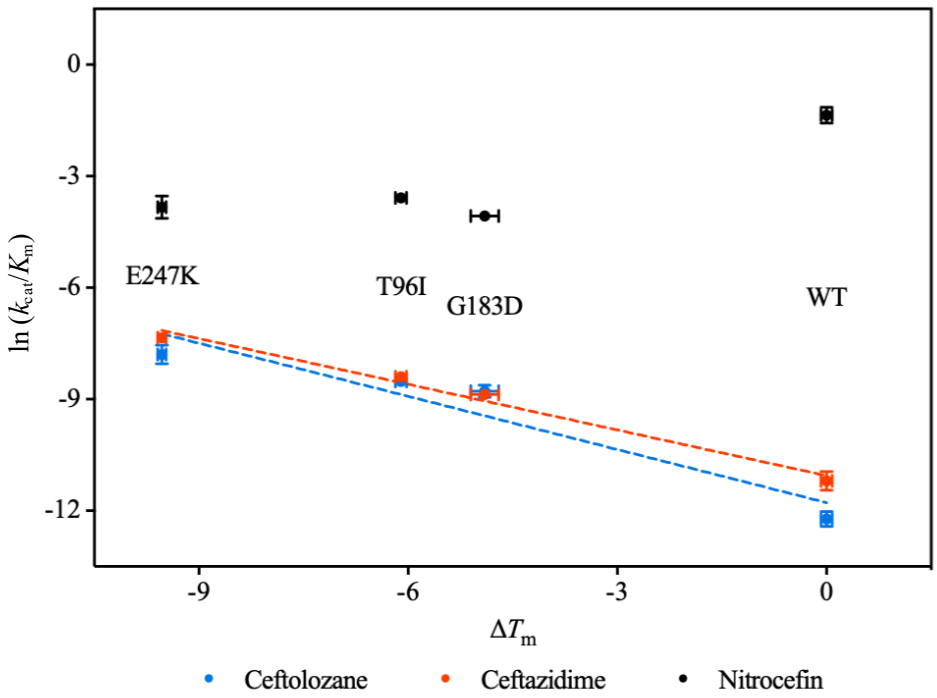

Figure 4.2 – Plot of the log of specificity constants of the WT and point mutant AmpC enzymes against their ΔT_m as defined in the text. The vertical and horizontal error bars represent the standard error and standard deviation, respectively. The lines represent the best linear fits to the ceftolozane ($R^2 = 0.9086$) and ceftazidime ($R^2 = 0.9853$) data.

Finally, while enzyme activity is often facilitated by a limited number of highly conserved residues, enzyme stability results from the contribution of a variety of structural domains (Schreiber *et al.* 1994). The tolerance of an enzyme for mutations in structural residues is therefore far greater than it is for functional or active site residues (Wang *et al.* 2002). Mutations in the catalytic residues of AmpC, for example, have been shown to decrease enzyme activity 10^3–10^5-fold compared to the WT enzyme (Beadle and Shoichet 2002). This explains why the AmpC mutants presented in this study contain structural mutations (i.e., in the Ω loop or a helical domain) instead of active site mutations (**Fig. 4.1; Table 2.2**). As previously discussed, these mutations introduce structural or electrostatic changes to the active site that enhance enzyme activity without altering the conserved catalytic residues. While this does reduce enzyme stability, there are various structural domains that work to maintain the integrity of the enzyme.

4.6. Effects of mutations on the catalytic cycle of AmpC

β-lactam hydrolysis proceeds by a mechanism involving acylation and subsequent deacylation of the β-lactamase (**Fig. 1.4**) (Minasov *et al.* 2002). Acylation occurs when the active site serine, Ser90, launches a nucleophilic attack on the β-lactam carbonyl carbon, forming a high-energy acylation intermediate. This leads to opening of the β-lactam ring and the formation of a low-energy acyl–enzyme complex. Deacylation occurs when a catalytic water attacks this complex, facilitating the formation of a high-energy deacylation intermediate that promotes the release of the inactive β-lactam product from the enzyme. This can be represented by Scheme 1:

$$E + S \underset{k_{-1}}{\overset{k_1}{\rightleftharpoons}} E{\cdot}S \underset{k_{-2}}{\overset{k_2}{\rightleftharpoons}} E{-}S \xrightarrow{k_3} E + P \qquad \text{(Scheme 1)}$$

Where k_1 and k_{-1} are the respective association and dissociation rate constants for the Michaelis complex ($E{\cdot}S$), k_2 is the rate of AmpC acylation via nucleophilic attack on the β-lactam, and k_3 is

the rate of deacylation/hydrolysis of the AmpC–β-lactam complex (Draws and Bonomo 2010). Since avibactam binding to AmpC is reversible and involves ring opening through acylation of the catalytic serine (Ehmann *et al.* 2012), the first two steps of Scheme 1 can also represent avibactam inhibition (hence the inclusion of k_{-2} to represent reversibility). In Scheme 1, two limiting cases can be considered: (1) the rate-limiting step is k_2, where the specificity constant is $\frac{k_2}{K_m}$; (2) the rate-limiting step is k_3, where the specificity constant is $\frac{k_3}{K_m}$. In case (1), the AmpC mutations should affect the apparent activation energies of the β-lactam hydrolysis reaction and the avibactam binding rates in a similar fashion. This was tested by generating a log-log plot of the specificity constants of the WT and mutant AmpC enzymes for ceftolozane, ceftazidime, and nitrocefin as a function of k_{on}^{app} (**Fig. 4.3**). It is clear from this analysis that only the effects of the AmpC mutations on the hydrolysis of nitrocefin are correlated with avibactam binding, suggesting that k_2 (acylation) is the rate-limiting step for the hydrolysis of nitrocefin by AmpC. Moreover, the lack of correlation between avibactam binding and the catalysis of ceftolozane and ceftazidime confirms that the rate-limiting step of the ceftolozane/ceftazidime catalytic cycle is different from that of nitrocefin. This suggests that k_3 (deacylation) is the rate-limiting step for the breakdown of ceftolozane and ceftazidime by AmpC. This is consistent with results obtained by Chow *et al.* (2013) for BlaC, the β-lactamase from *Mycobacterium tuberculosis*, which indicate that k_2 is the rate-limiting step for nitrocefin hydrolysis and k_3 is the rate-limiting step for the breakdown of cefoxitin, a second-generation cephalosporin. Taken together, these results indicate that by increasing both the rate of β-lactam deacylation and the activation barrier of enzyme acylation, these mutations allow AmpC to hydrolyze ceftolozane and ceftazidime with improved catalytic activity while simultaneously evading inhibition by avibactam.

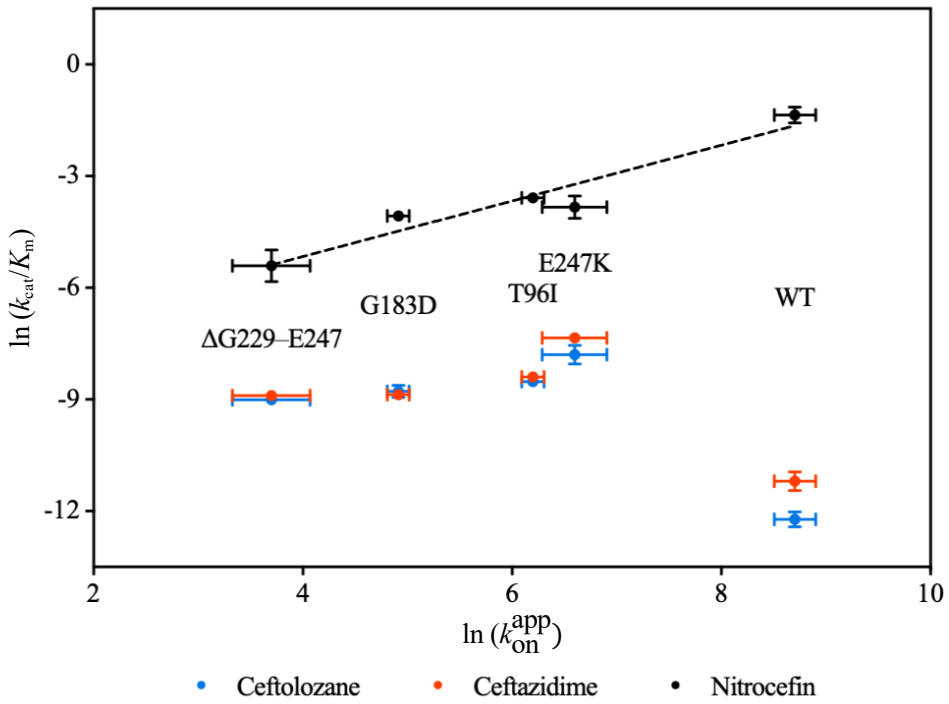

Figure 4.3 – Log–log plot of the specificity constants of the WT and mutant AmpC enzymes as a function of avibactam k_{on}^{app} as defined in the text. The vertical and horizontal error bars represent the standard errors reported from regression analysis. The line represents the best linear fit to the nitrocefin data ($R^2 = 0.9268$).

5. Conclusion

5.1. Summary of Findings

The unfortunate emergence of *P. aeruginosa* clinical isolates overexpressing mutated forms of AmpC is compromising the efficacy of the novel antipseudomonal β-lactam/BLI combinations ceftolozane/tazobactam and ceftazidime/avibactam. Although these isolates have been characterized by MIC experiments, the AmpC mutations defining them (E247K, G183D, T96I, and ΔG229–E247) had yet to be described in detail. While molecular modelling has begun to elucidate the structural implications of these mutations, it is evident that a kinetic description of their influence is warranted. Accordingly, the objective of this thesis was to study the catalytic properties of these mutant AmpC enzymes (alongside WT AmpC) to understand the effects of each mutation on antibiotic catalysis and inhibitor binding. It was hypothesized that these mutations enhance the activity of AmpC towards ceftolozane and ceftazidime.

Remarkably, it was found that not only do these mutations increase the catalytic efficiency of AmpC towards both ceftolozane and ceftazidime, they also reduce the enzyme's susceptibility to inhibition by avibactam. Thus, the E247K, G183D, T96I, and ΔG229–E247 mutations exert a two-fold effect on the catalytic cycle of AmpC. First, they reduce the affinity of avibactam for AmpC by increasing the activation energy of the enzyme acylation step. This does not influence the catalytic turnover of ceftolozane and ceftazidime significantly, however, as deacylation appears to be the rate-limiting step for the breakdown of these antibiotics. Second, these mutations reduce the stability of AmpC, thereby increasing its flexibility. This appears to accelerate β-lactam deacylation, resulting in larger catalytic efficiencies towards ceftolozane and ceftazidime compared to WT AmpC. It is the contribution of these two effects that allows the AmpC mutants to evade avibactam while hydrolyzing cephalosporins with enhanced efficiency.

5.2. Future Directions

Originally, this thesis had a fourth objective: to crystallize the WT and mutant AmpC enzymes and subsequently complex them with ceftolozane (± tazobactam) and ceftazidime (± avibactam) in order to visualize the structural influence of the mutations on the molecular interactions of AmpC with these antibiotics and inhibitors. Encouragingly, crystals of WT AmpC and the AmpC mutants G183D, T96I, and ΔG229–E247 were obtained from primary commercial crystallization screens; AmpC consistently formed highly branched, needle-like crystals (colloquially referred to as "sea urchins"). Optimization of these crystals proved to be considerably more difficult than anticipated, and in the interest of time, this objective was abandoned, and the enzyme kinetic studies were prioritized. That being said, a reasonable future direction of this work would be to continue with this optimization in order to obtain AmpC crystals with sufficient diffraction quality. Since all the AmpC expression constructs used in this study were initially designed to generate AmpC crystals with optimal diffraction quality (section 2.1) (Morinaka *et al.* 2015), this experimental endeavor certainly holds promise. Crystal structures of the WT and mutant AmpC enzymes complexed with ceftolozane/tazobactam and ceftazidime/avibactam would provide detailed structural insights into how the mutations affect the accommodation and positioning of these compounds in the active site. This could in turn aid the design of β-lactams and BLIs with reduced susceptibility to mutational resistance (e.g., inform potential modifications to the R2 side chains of ceftolozane and ceftazidime to increase stability against β-lactamases). Although crystal structures of the AmpC mutant enzymes did not result from this study, speculation of the effects of their mutations on the structural and catalytic properties of AmpC was still possible, as the crystal structure of WT AmpC from *P. aeruginosa* (PDC-1) is already available and well-understood (sections 4.1 and 4.2).

It is also worth mentioning that a useful product of this study is a highly optimized procedure for the expression, purification, and kinetic characterization of AmpC enzymes. Therefore, this methodology could be used as a means of surveillance—that is, to characterize any other AmpC mutant enzymes that may arise in response to ceftolozane/tazobactam and ceftazidime/avibactam in the future. This would further elucidate the mutational strategy of AmpC and therefore provide more information for the design and optimization of new antipseudomonal β-lactams and broad-spectrum BLIs. Moreover, as other novel β-lactam/BLI combination therapies with promising activity against AmpC β-lactamases are gaining clinical traction, it would be beneficial to use this methodology to characterize any AmpC mutations that may arise in response to them as well. Specifically, imipenem-relebactam and meropenem-vaborbactam are two β-lactam/BLI combination therapies that demonstrate clinically useful activity against class C β-lactamases like AmpC (**Fig 1.6**; section 1.7.2) (Zhanel *et al.* 2018). As the therapeutic utility of these drugs increases, it is conceivable that AmpC mutations may begin to arise and promote resistance to them, thereby necessitating the kinetic characterization of these mutant enzymes (which we believe can be accomplished using the methodology developed for this thesis).

Appendix

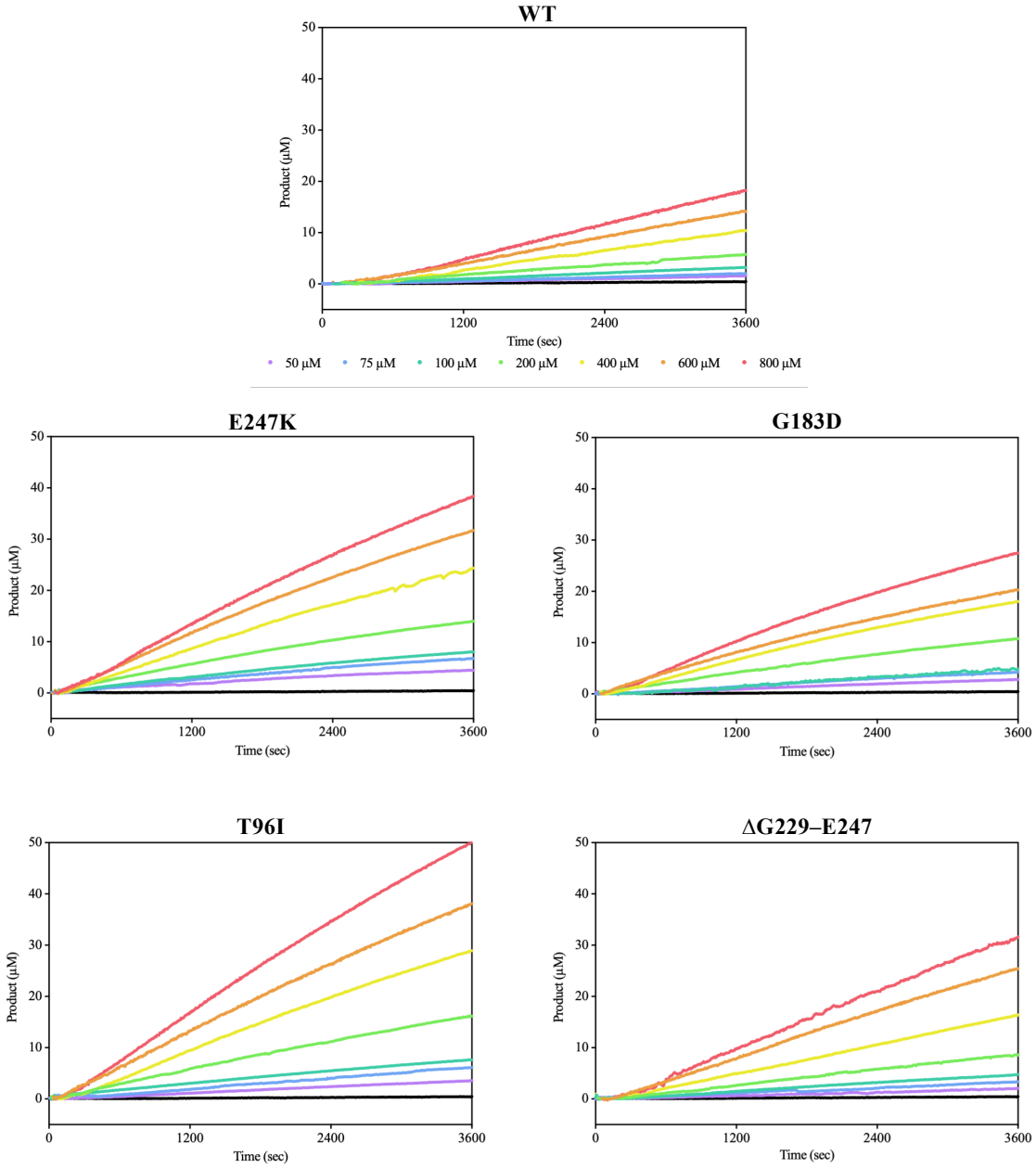

Figure S1 – Traces of ceftolozane hydrolysis by WT and mutant AmpC enzymes. Each enzyme was challenged with ceftolozane ranging from 50–800 μM and initial rates of ceftolozane hydrolysis were measured at λ = 283 nm for 3,600 s at 28˚C in triplicate. The kinetic traces represent one technical replicate for each enzyme. Traces in black represent 50 μM ceftolozane alone (i.e., no AmpC enzyme) to serve as negative controls.

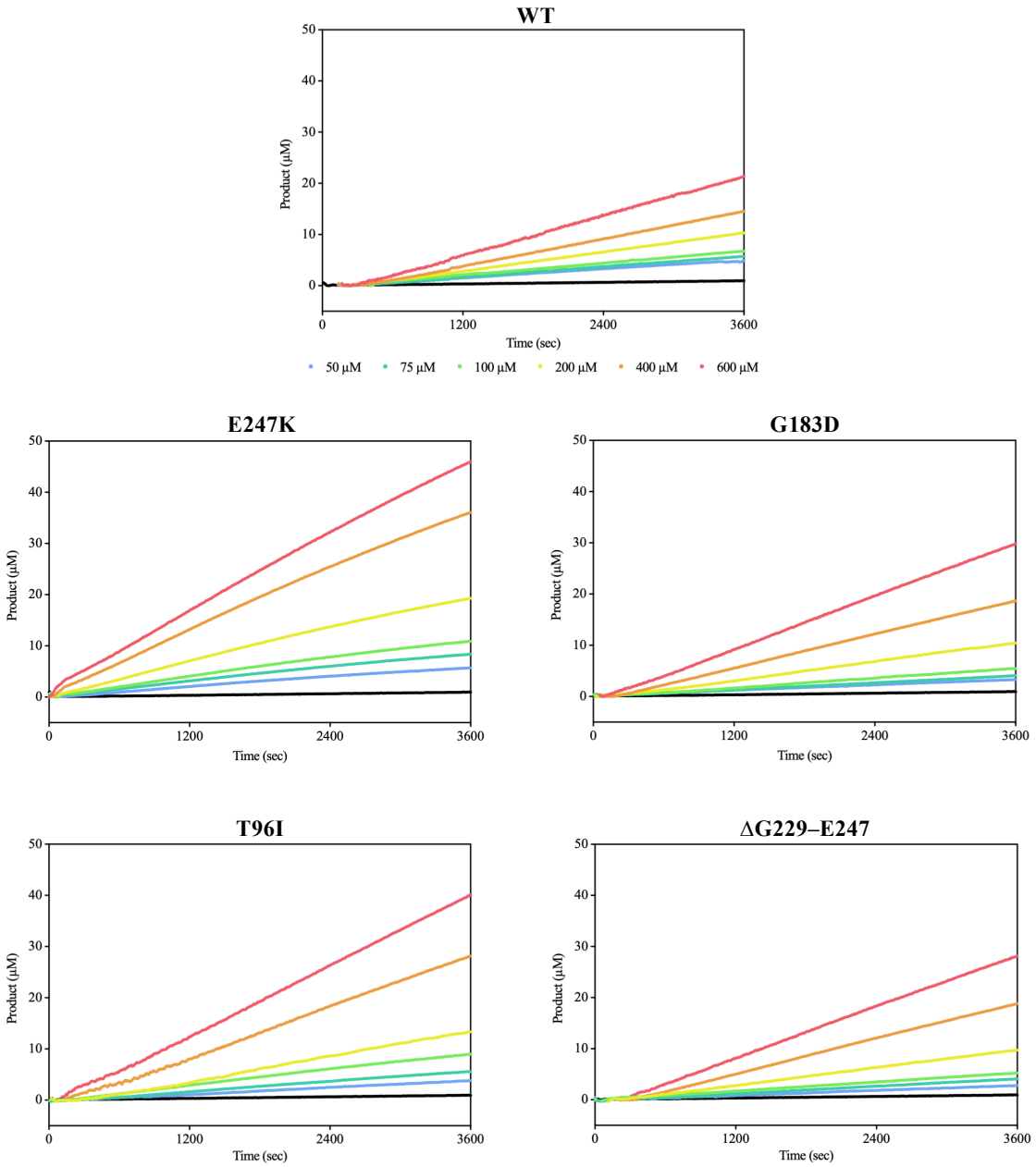

Figure S2 – Traces of ceftazidime hydrolysis by WT and mutant AmpC enzymes. Each enzyme was challenged with ceftazidime ranging from 50–600 μM and initial rates of ceftazidime hydrolysis were measured at λ = 260 nm for 3,600 s at 28˚C in triplicate. The kinetic traces represent one technical replicate for each enzyme. Traces in black represent 50 μM ceftazidime alone (i.e., no AmpC enzyme) to serve as negative controls.

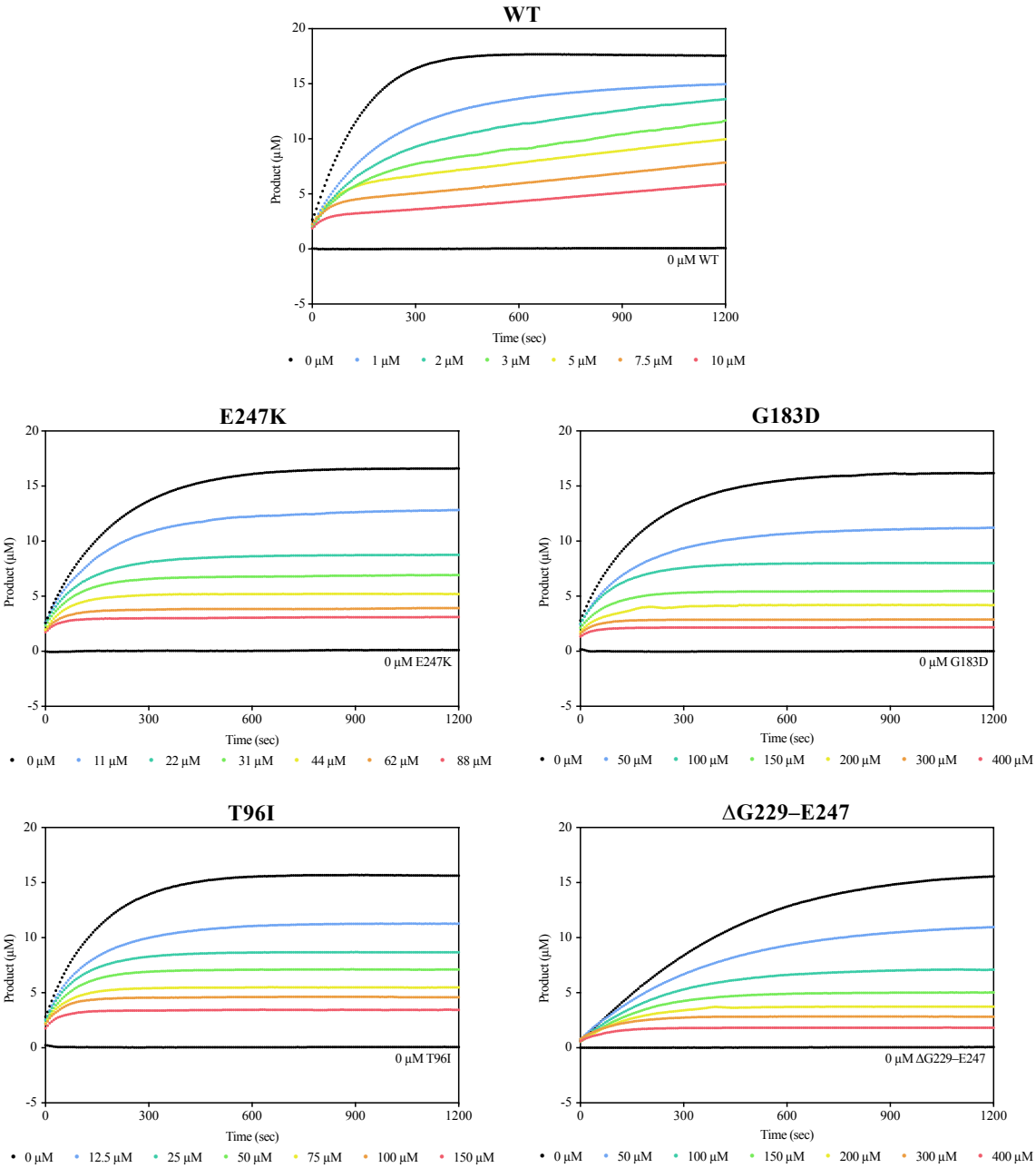

Figure S3 – Typical time courses of the hydrolysis of 100 μM nitrocefin by WT and mutant AmpC enzymes in the presence of different concentrations of avibactam. Each enzyme was challenged with 100 μM nitrocefin and avibactam ranging from 0–400 μM and nitrocefin hydrolysis was measured at λ = 486 nm for 1,200 s at 28˚C in triplicate. The kinetic traces represent one technical replicate for each enzyme. Each trace was fitted to Eq. 3 to obtain k_{obs} values, which were plotted against their respective avibactam concentrations to yield the plots in Figure 3.7.

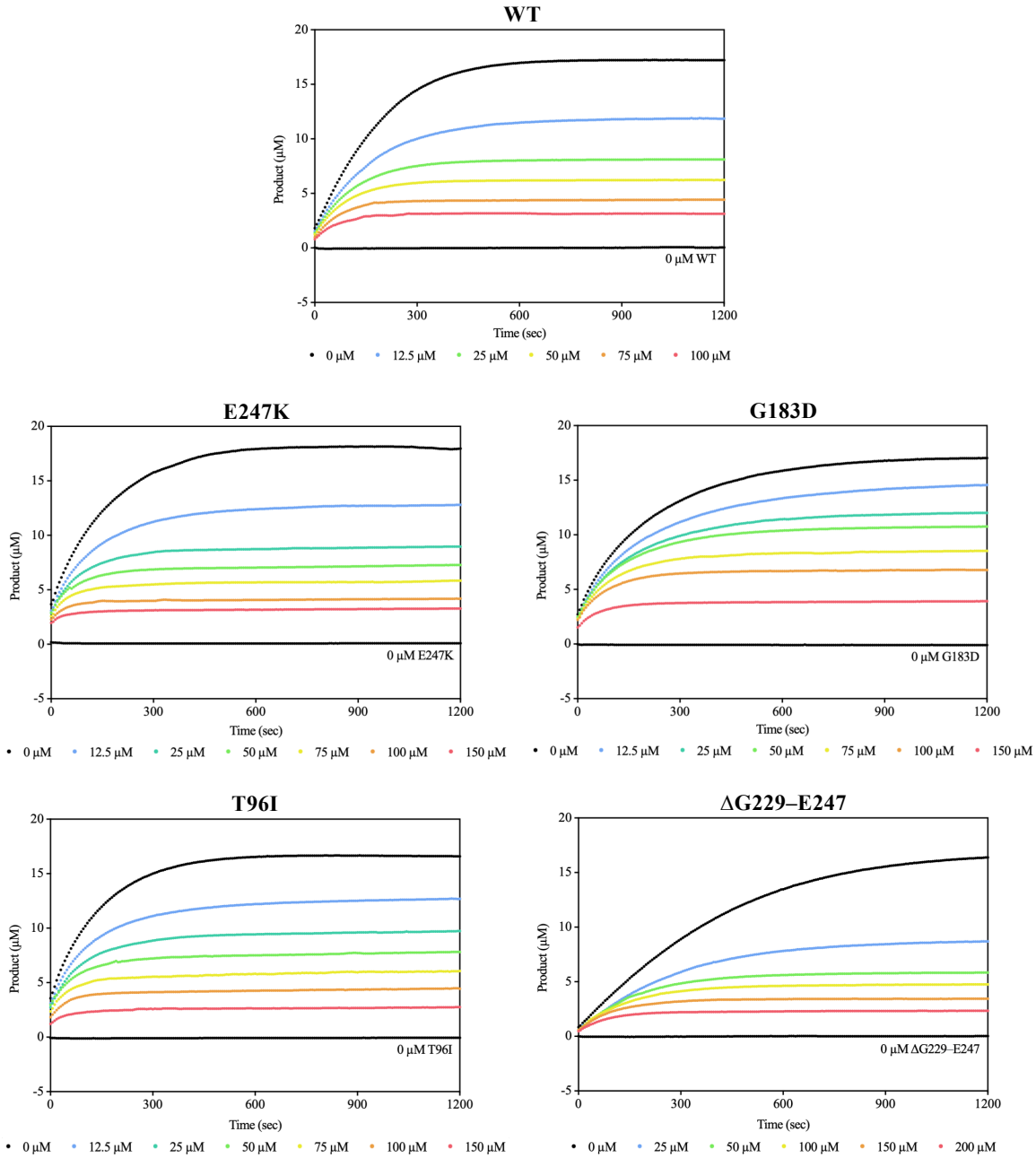

Figure S4 – Typical time courses of the hydrolysis of 100 μM nitrocefin by WT and mutant AmpC enzymes in the presence of different concentrations of tazobactam. Each enzyme was challenged with 100 μM nitrocefin and tazobactam ranging from 0–150 μM and nitrocefin hydrolysis was measured at λ = 486 nm for 1,200 s at 28˚C in triplicate. The kinetic traces represent one technical replicate for each enzyme. Each trace was fitted to Eq. 3 to obtain k_{obs} values, which were plotted against their respective tazobactam concentrations to yield the plots in Figure 3.8.

References

Abraham, E.P. and Newton, G.G. 1961. The structure of cephalosporin C. Biochem. J. **79:**377–393.

Ambler, R.P. 1980. The structure of β-lactamases. Phil. Trans. R. Soc. Lond. B Biol. Sci. **289(1036):**321–331.

Aslam, B., Wang, W., Arshad, M.I., Khurshid, M., Muzammil, S., Rasool, M.H., Nisar, M.A., Alvi, R.F., Aslam, M.A., Qamar, M.U., Salamat, M.K.F., and Baloch, Z. 2018. Antibiotic resistance: a rundown of a global crisis. Infect Drug Resist. **11:**1645–1658.

Artimo, P., Jonnalagedda, M., Arnold, K., Baratin, D., Csardi, G., de Castro, E., Duvaud, S., Flegel, V., Fortier, A., Gasteiger, E., Grosdidier, A., Hernandez, C., Ioannidis, V., Kuznetsov, D., Liechti, R., Moretti, S., Mostaguir, K., Redaschi, N., Rossier, G., Xenarios, I., and Stockinger, H. 2012. ExPASy: SIB bioinformatics resource portal. Nucleic Acids Res. **40(W1):**W597–W603. doi:10.1093/nar/gks400.

Babic, M., Hujer, A.M., and Bonomo, R.A. 2006. What's new in antibiotic resistance? Focus on β-lactamases. Drug Resist. Updat. **9:**142–156.

Barnes, M.D., Taracila, M.A., Rutter, J.D., Bethel, C.R., Galdadas, I., Hujer, A.M., Caselli, E., Prati, F., Dekker, J.P., Papp-Wallace, K.M., Haider, S., and Bonomo, R.A. 2018. Deciphering the evolution of cephalosporin resistance to ceftolozane-tazobactam in *Pseudomonas aeruginosa*. mBio. **9(6):**e02085-18.

Beadle, B.M., McGovern, S.L., Patera, A., and Shoichet, B.K. 1999. Functional analyses of AmpC β-lactamase through differential stability. Protein Sci. **8:**1816–1824.

Beadle, B.M. and Shoichet, B.K. 2002. Structural bases of stability-function tradeoffs in enzymes. J. Mol. Biol. **321:**285–296.

Bebrone, C., Lassaux, P., Vercheval, L., Sohier, J., Jehaes, A., Sauvage, E., and Galleni, M. 2010. Current challenges in antimicrobial chemotherapy: focus on β-lactamase inhibition. Drugs. **70(6):**651–679.

Beesley, T., Gascoyne, N., Knott-Hunziker, V., Petursson, S., Waley, S.G., Jaurin, B., and Grundström, T. 1983. The inhibition of class C β-lactamases by boronic acids. Biochem. J. **209(1):**229–233.

Blizzard, T.A., Chen, H., Kim, S., Wu, J., Bodner, R., Gude, C., Imbriglio, J., Young, K., Park, Y.W., Ogawa, A., Raghoobar, S., Hairston, N., Painter, R.E., Wisniewski, D., Scapin, G., Fitzgerald, P., Sharma, N., Lu, J., Ha, S., Hermes, J., and Hammond, M.L. 2014. Discovery of MK-7655, a β-lactamase inhibitor for combination with Primaxin®. Bioorg Med Chem Lett. **24(3):**780–785.

Boulant, T., Jousset, A.B., Bonnin, R.A., Barrail-Tran, A., Borgel, A., Oueslati, S., Naas, T., and Dortet, L. 2019. A 2.5-year within-patient evolution of *Pseudomonas aeruginosa* isolates *in vivo* acquisition of ceftolozane-tazobactam and ceftazidime-avibactam resistance upon treatment. Antimicrob Agents Chemother. **63(12)**.

Breidenstein, E.B., de la Fuente-Nunez, C., and Hancock, R.E. 2011. *Pseudomonas aeruginos*a: all roads lead to resistance. Trends Microbiol. **19:**419–426.

Bulychev, A. and Mobashery, S. 1999. Class C β-lactamases operatre at the diffusion limit for turnover of their preferred cephalosporin substrates. Antimicrob. Agents Chemother. **43:**1743–1746.

Bush, K., Freudenberger, J.S., and Sykes, R.B. 1982. Interaction of azthreonam and related monobactams with β-lactamases from Gram-negative bacteria. Antimicrob. Agents Chemother. **22:**414–420.

Bush, K., and G. A. Jacoby. 2009. Updated functional classification of β-lactamases. Antimicrob. Agents Chemother. doi:10.1128/AAC.01009-09.
Bush, K. and Bradford, P.A. 2016. β-lactams and β-lactamase inhibitors: an overview. Cold Spring Harb. Perspect. Med. **6:**a025247.
Caprile, K.A. 1988. The cephalosporin antimicrobial agents: a comprehensive review. J. Vet. Pharmacol. Ther. **11(1):**1–32.
Chambers, H.F. 1999. Penicillin-binding protein-mediated resistance in pneumococci and staphylococci. J. Infect. Dis. **179(Suppl. 2):**S353–S359.
Chen, Y., Minasov, G., Roth, T.A., Prati, F., and Shoichet, B.K. 2006. The deacylation mechanism of AmpC β-lactamase at ultrahigh resolution. J. Am. Chem. Soc. **128(9):**2970–2976.
Cheng, Q., Li, H., Merdek, K., and Park, J.T. 2000. Molecular characterization of the β-*N*-acetylglucosaminidase of *Escherichia coli* and its role in cell wall recycling. J. Bacteriol. **182(17):**4836–4840.
Cheng, Q. and Park, J.T. 2002. Substrate specificity of the AmpG permease required for recycling of cell wall anhydro-muropeptides. J. Bacteriol. **184(23):**6434–6436.
Chow, C., Xu, H., and Blanchard, J.S. 2013. Kinetic characterizations of nitrocefin, cefoxitin, and meopenem hydrolysis by β-lactamase from *Mycobacterium tuberculosis*. Biochemistry. **52(23):**4097–4104.
Corzo, J. 2006. Time, the forgotten dimension of ligand binding teaching. BAMBED. **34(6):**413–416.
Danel, F., Page, M.G., and Livermore, D.M. 2007. Class D β-lactamases. In Bonomo, R.A. and Tolmasky, M.E. (ed.), Enzyme-mediated resistance to antibiotics: mechanisms, dissemination, and prospects for inhibition. ASM Press, Washington, DC. 163–194.
Datta, N. and Kontomichalou, P. 1965. Penicillinase synthesis controlled by infectious R factors in Enterobacteriaceae. Nature. **208:**239–241.
de la Fuente-Nunez, C. 2019. Toward autonomous antibiotic discovery. mSystems. **4(3)**.
Dietz, H., Pfeifle, D., and Wiedemann, B. 1997. The signal molecule for β-lactamase induction in *Enterobacter cloacae* is the anhydromuramylpentapeptide. Antimicrob. Agents Chemother. **41(10):**2113–2120.
Doumith, M., Ellington, M.J., Livermore, D.M., and Woodford, N. 2009. Molecular mechanisms disrupting porin expression in ertapenem-resistant *Klebsiella* and *Enterobacter* spp. clinical isolates from the UK. J. Antimicrob. Chemother. **63:**659–667.
Drawz, S.M. and Bonomo, R.A. 2010. Three decades of β-lactamase inhibitors. Clin. Microbiol. Rev. **23(1):**160–201.
Drenkard, E. 2003. Antimicrobial resistance of *Pseudomonas aeruginosa* biofilms. Microbes Infect. **5:**1213–1219.
Dryjanski, M. and R. F. Pratt. 1995. Steady-state kinetics of the binding of β-lactams and penicilloates to the second binding site of the *Enterobacter cloacae* P99 β-lactamase. Biochemistry. **34:**3561–3568.
Dubus, A., Ledent, P., Lamotte-Brasseur, J., and Frère, J.M. 1996. The roles of residues Tyr150, Glu272, and His314 in class C β-lactamases. Proteins. **25:**473–485.
Ehmann, D.E., Jahić, H., Ross, P.L., Gu, R.F., Hu, J., Kern, G., Walkup, G.K., and Fisher, S.L. 2012. Avibactam is a covalent, reversible, non–β-lactam β-lactamase inhibitor. PNAS. **109(29):**11663–11668.
Ehmann, D.E., Jahić, H., Ross, P.L., Gu, R.F., Hu, J., Durand-Réville, T.F., Lahiri, S., Thresher,

J., Livchak, S., Gao, N., Palmer, T., Walkup, G.K., and Fisher, S.L. 2013. Kinetics of avibactam inhibition against Class A, C, and D β-lactamases. J. Biol. Chem. **288(39):**27960–27971.
Elcock, A. H. 2001. Prediction of functionally important residues based solely on the computed energetics of protein structure. J. Mol. Biol. **312:**885–896.
English, A.R., Retsema, J.A., Girard, A.E., Lynch, J.E., and Barth, W.E. 1978. CP-45899, a β-lactamase inhibitor that extends the antibacterial spectrum of β-lactams: initial bacteriological characterization. Antimicrob. Agents Chemother. **14:**414–419.
Fisher, J., Belasco, J.G., Charnas, R.L., Khosla, S., and Knowles, J.R. 1980. β-lactamase inactivation by mechanism-based reagents. Philos. Trans. R. Soc. Lond. B. Biol. Sci. **289:**309–319.
Fraile-Ribot, P.A., Cabot, G., Mulet, X., Perianez, L., Martin-Pena, M.L., Juan, C, Perez, J.L., and Oliver, A. 2018. Mechanisms leading to *in vivo* ceftolozane/tazobactam resistance development during the treatment of infections caused by MDR *Pseudomonas aeruginosa*. J. Antimicrob. Chemother. **73:**658–663.
Francisco, O.A., Clark, C.J., Glor, H.M., and Khajehpour, M. 2019. Do soft anions promote protein denaturation through binding interactions? A case study using ribonuclease A. RSC Adv. **9:**3416–3428.
Frère, J.M. 2004. *Streptomyces* R61 D-Ala–D-Ala carboxypeptidase. Handbook of Proteolytic Enzymes. 2nd ed. (Barrett, A.J., Rawlings, N.D., and Woessner, J.F., eds). Elsevier, London. 1959–1962.
Gilchrist, T. 1987. Heterocyclic Chemistry. Harlow: Longman Scientific. ISBN:0-582-01421-2.
Golemi, D., Maveyraud, L., Vakulenko, S., Samama, J.P., and Mobashery, S. 2001. Critical involvement of a carbamylated lysine in catalytic function of class D β-lactamases. Proc. Natl. Acad. Sci. U.S.A. **98:**14280–14285.
Gordon, E., Mouz, N., Duee, E., and Dideberg, O. 2000. The crystal structure of the penicillin-binding protein 2x from *Streptococcus pneumoniae* and its acyl-enzyme form: implication in drug resistance. J. Mol. Biol. **299:**477–485.
Govardhan, C. P. and R. F. Pratt. 1987. Kinetics and mechanism of the serine β-lactamase catalyzed hydrolysis of depsipeptides. Biochemistry. **26:**3385–3395.
Hancock, R.E. and Speert, D.P. 2000. Antibiotic resistance in *Pseudomonas aeruginosa*: mechanisms and impact on treatment. Drug Resist. Updat. **3:**247–255.
Holmes, A.H., Moore, L.S., Sundsfjord, A., Steinbakk, M., Regmi, S., Karkey, A., Guerin, P.J., and Piddock, L.J.V. 2016. Understanding the mechanisms and drivers of antimicrobial resistance. Lacet. **387(10014):**176–187.
Helfand, M.S., Totir, M.A., Carey, M.P., Hujer, A.M., Bonomo, R.A., and Carey, P.R. 2003. Following the reactions of mechanism-based inhibitors with β-lactamase by Raman crystallography. Biochemistry. **42:**13386–13392.
Henrichfreise, B., Wiegand, I., Pfister, W., and Wiedemann, B. 2007. Resistance mechanisms of multiresistant *Pseudomonas aeruginosa* strains from Germany and correlation with hypermutation. Antimicrob. Agents Chemother. **51(11):**4062–4070.
Herzberg, O. and Moult, J. 1987. Bacterial resistance to β-lactam antibiotics: crystal structure of β-lactamase from *Staphylococcus aureus* PC1 at 2.5 Å resolution. Science. **236:**694–701.
Hidri, N., Barnaud, G., Decré, D., Cerceau, C., Lalande, V., Petit, J.C., Labia, R., and Arlet, G.

2005. Resistance to ceftazidime is associated with a S220Y substitution in the omega loop of the AmpC β-lactamase of a *Serratia marcescens* clinical isolate. J. Antimicrob. Chemother. **55:**496–499.

Hocquet, D., Berthelot, P., Roussel-Delvallez, M., Favre, R., Jeannot, K., Bajolet, O., Marty, N., Grattard, F., Mariani-Kurkdjian, P., Bingen, E., Husson, M.O., Couetdic, G., and Plesiat, P. 2007. *Pseudomonas aeruginosa* may accumulate drug resistance mechanisms without losing its ability to cause bloodstream infections. Antimicrob. Agents Chemother. **51(10):**3531–3536.

Holtje, J.V., Kopp, U., Ursinus, A., and Wiedemann, B. 1994. The negative regulator of β-lactamase induction AmpD is a *N*-acetylanhydromuramyl-l-alanine amidase. FEMS Microbiol. Lett. **122(1–2):**159–164.

Holtje, J.V. 1998. Growth of the stress-bearing and shape-maintaining murein sacculus of *Escherichia coli*. Microbiol. Mol. Biol. Rev. **62(1):**181–203.

Huang, W., El Hamouche, J., Wang, G., Smith, M., Yin, C., Dhand, A., Dimitrova, N., and Fallon, J.T. 2020. Integrated genome-wide analysis of an isogenic pair of *Pseudomonas aeruginosa* clinical isolates with differential antimicrobial resistance to ceftolozane/tazobactam, ceftazidime/avibactam, and piperacillin/tazobactam. Int. J. Mol. Sci. **21:**1026.

Jacobs, C., Joris, B., Jamin, M., Klarsov, K., Van Beeumen, J., Mengin-Lecreulx, D., van Heijenoort, J., Park, J.T., Normak, S., and Frère, J.M. 1995. AmpD, essential for both β-lactamase regulation and cell wall recycling, is a novel cytosolic *N*-acetylmuramyl-l-alanine amidase. Mol. Microbiol. **15(3):**553–559.

Jacobs, C., Frère, J.M., and Normark, S. 1997. Cytosolic intermediates for cell wall biosynthesis and degradation control inducible beta-lactam resistance in Gram-negative bacteria. Cell. **88(6):**823–832.

Jacoby, G.A., Mills, D.M., and Chow, N. 2004. Role of β-lactamases and porins in resistance to ertapenem and other β-lactams in *Klebsiella pneumoniae*. Antimicrob. Agents Chemother. **48:**3203–3206.

Jacoby, G.A. 2009. AmpC β-lactamases. Clin. Microbiol. Rev. **22(1):**161–182.

Johnson, K.A. 2019. New standards for collecting and fitting steady state kinetic data. Beilstein J. Org. Chem. **15:**16–29.

Juan, C., Macia, M.D., Gutierrez, O., Vidal, C., Perez, J.L., and Oliver A. 2005. Molecular mechanisms of β-lactam resistance mediated by AmpC hyperproduction in *Pseudomonas aeruginosa* clinical strains. Antimicrob. Agents Chemother. **49(11):**4733–4738.

Juan, C., Moya, B., Perez, J.L., and Oliver, A. 2006. Stepwise upregulation of the *Pseudomonas aeruginosa* chromosomal cephalosporinase conferring high-level β-lactam resistance involves three AmpD homologues. Antimicrob. Agents Chemother. **50(5):**1780–1787.

Juan, C., Zamorano, L., Pérez, J.L., Ge, Y., and Oliver, A. 2009. Activity of a new antipseudomonal cephalosporin, CXA-101 (FR264205), against carbapenem-resistant and multidrug-resistant *Pseudomonas aeruginosa* clinical strains. Antimicrob. Agents Chemother. **54(2):**846–851.

Knox, J.R., Moews, P.C., and Frère, J.M. 1996. Molecular evolution of bacterial β-lactam resistance. Chem. Biol. **3:**937–947.

Kong, K.F., Jayawardena, S.R., Indulkar, S.D., Del Puerto, A., Koh, C.L., Høiby, N., and

Mathee, K. 2005. *Pseudomonas aeruginosa* AmpR is a global transcriptional factor that regulates expression of AmpC and PoxB β-lactamases, proteases, quorum sensing, and other virulence factors. Antimicrob. Agents Chemother. **49(11):**4567–4575.

Kuga, A., Okamoto, R., and Inoue, M. 2000. ampR gene mutations that greatly increase class C β-lactamase activity in *Enterobacter cloacae*. Antimicrob. Agents Chemother. **44(3):**561–567.

Lahiri, S.D., Mangani, S., Durand-Reville, T., Benvenuti, M., De Luca, F., Sanyal, G., and Docquier, J.D. 2013. Structural insight into potent broad-spectrum inhibition with reversible recyclization mechanism: avibactam in complex with CTX-M-15 and *Pseudomonas aeruginosa* AmpC β-lactamases. Antimicrob. Agents Chemother. **57(6):**2496–2505.

Lahiri, S.D., Johnstone, M.R., Ross, P.L., McLaughlin, R.E., Olivier, N.B., Alm, R.A. 2014. Avibactam and class C β-lactamases: mechanism of inhibition, conservation of binding pocket and implications for resistance. Antimicrob. Agents Chemother. **58:**5704–13.

Lahiri, S.D., Walkup, G.K., Whiteaker, J.D., Palmer, T., McCormack, K., Tanudra, M.A., Nash, T.J., Thresher, J., Johnstone, M.R., Hajec, L., Livchak, S., McLaughlin, R.E., and Alm, R.A. 2015. Selection and molecular characterization of ceftazidime/avibactam resistant mutants in *Pseudomonas aeruginosa* strains containing derepressed AmpC. J. Antimicrob. Chemother. **70:**1650–1658.

Lapuebla, A., Abdallah, M., Olafisoye, O., Cortes, C., Urban, C., Quale, J., and Landman, D. 2015. Activity of meropenem combined with RPX7009, a novel β-lactamase inhibitor, against Gram-negative clinical isolates in New York City. Antimicrob. Agents Chemother. **59:**4856–4860.

Lee, B. 1971. Conformation of penicillin as a transition-state analog of the substrate of peptidoglycan transpeptidase. J. Mol. Biol. **61:**463–469.

Levasseur, P., Girard, A.M., Claudon, M., Goossens, H., Black, M.T., Coleman, K., and Miossec, C. 2012. *In vitro* antibacterial activity of the ceftazidime-avibactam (NXL104) combination against *Pseudomonas aeruginosa* clinical isolates. Antimicrob. Agents Chemother. **56(3):**1606–1608.

Li, X.Z., Zhang, L., and Poole, K. 2000. Interplay between the MexA-MexB-OprM multidrug efflux system and the outer membrane barrier in the multiple antibiotic resistance of *Pseudomonas aeruginosa*. J. Antimicrob. Chemother. **45:**433–436.

Lister, P.D., Gardner, V.M., and Sanders, C.C. 1999. Clavulanate induces expression of the *Pseudomonas aeruginosa* AmpC cephalosporinase at physiologically relevant concentrations and antagonizes the antibacterial activity of ticarcillin. J. Antimicrob. Chemother. **43(4):**882–889.

Lister, P.D., Wolter, D.J., and Hanson, N.D. 2009. Antibacterial-resistant *Pseudomonas aeruginosa*: clinical impact and complex regulation of chromosomally encoded resistance mechanisms. Clin. Microbiol. Rev. **22(4):**582–610.

Livermore, D.M. 2001. Of *Pseudomonas*, porins, pumps and carbapenems. J. Antimicrob. Chemother. **47:**247–250.

Mack, A.R, Barnes, M.D., Taracila, M.A., Hujer, A.M., Hujer, K.M., Cabot, G., Feldgaren, M., Haft, D.H., Klimke, W., van den Akker, F., Vila, A.J., Smania, A., Haider, S., Papp-Wallace, K.M., Bradford, P.A., Rossolini, G.M., Docquier, J.D., Frère, J.M., Galleni, M., Hanson, N.D., Oliver, A., Plésiat, P., Poirel, L., Nordmann, P., Palzkill, T.G., Jacoby,

G.A., Bush, K., and Bonomo, R.A. 2019. A standard numbering scheme for class C β-lactamases. Antimicrob. Agents Chemother. doi:10.1128/AAC.01841-19.
MacVane, S.H., Pandey, R., Steed, L.L., Kreiswirth, B.N., and Chen, L. 2017. Emergence of ceftolozane-tazobactam-resistant *Pseudomonas aeruginosa* during treatment is mediated by a single AmpC structural mutation. Antimicrob. Agents Chemother. **61(12):**e01183-17.
Mandell G.L. and Perti, W.A. 1996. Antimicrobial agents: penicillins, cephalosporins, and other β-lactam antibiotics. In: Hardman, J.G., Limbird, L.E., Molinoff, P.B., Ruddon, R.W., et al., eds. Goodman and Gilman's The pharmacologic basis of therapeutics. 9th ed. New York: McGraw-Hill, Health Professions Division. 1073–1101.
Mark, B.L., Vocadlo, D.J., and Oliver, A. 2011. Providing β-lactams a helping hand: targeting the AmpC β-lactamase induction pathway. Future Microbiol. **6(12):**1215–1427.
Martinez-Martinez L. 2008. Extended-spectrum β-lactamases and the permeability barrier. Clin. Microbiol. Infect. **14(Suppl. 1):**82–89.
Matsumura, N., Minami, S., and Mitsuhashi, S. 1998. Sequences of homologous β-lactamases from clinical isolates of *Serratia marcescens* with different substrate specificities. Antimicrob. Agents Chemother. **42:**176–179.
Minasov, G., Wang, X., and Shoichet. 2002. An ultrahigh resolution structure of TEM-1 β-lactamase suggests a role for Glu166 as the general base in acylation. J. Am. Chem. Soc. **124:**5333–5340.
Morar, M. and Wright, G.D. 2010. The genomic enzymology of antibiotic resistance. Annu. Rev. Genet. **44:**25–51.
Morinaka, A., Tsutsumi, Y., Yamada, M., Suzuki, K., Watanabe, T., Abe, T., Furuuchi, T., Inamura, S., Sakamaki, Y., Mitsuhashi, N., Ida, T., and Livermore, D.M. 2015. OP0595, a new diazabicyclooctane: mode of action as a serine β-lactamase inhibitor, antibiotic and β-lactam 'enhancer'. J. Antimicrob. Chemother. **70(10):**2779–2786.
Mulcahy, L.R., Burns, J.L., Lory, S., and Lewis, K. 2010. Emergence of *Pseudomonas aeruginosa* strains producing high levels of persister cells in patients with cystic fibrosis. J. Bacteriol. **192:**6191–6199.
Muñoz, V. and Sanchez-Ruiz, J.M. 2004. Exploring protein-folding ensembles: a variable-barrier model for the analysis of equilibrium unfolding experiments. PNAS. **101(51):**17646–17651.
Murano, K., Yamanaka, T., Toda, A., Ohki, H., Okuda, S., Kawabata, K., Hatano, K., Takeda, S., Akamatsu, H., Itoh, K., Misumi, K., Inoue, S., and Takagi, T. 2008. Structural requirements for the stability of novel cephalosporins to AmpC β-lactamase based on 3D-structure. Bioorg. Med. Chem. **16(5):**2261–2275.
Murphy, B.P. and Pratt, R.F. 1991. *N*-(phenylacetyl)glycyl-D-aziridine-2-carboxylate, an acyclic amide substrate of β-lactamases: importance of the shape of the substrate in β-lactamase evolution. Biochemistry. **30:**3640–3649.
Neu, H.C. 1990. β-lactamases, β-lactamase inhibitors, and skin and skin-structure infections. J. Am. Acad. Dermatol. **22:**869–904.
Nicholson, L.K., Yamazaki, T., Torchia, D.A., Grzesiek, S., Bax, A., Stahl, S.J., Kaufman, J.D., Wingfield, P.T., Lam, P.Y.S., Jadhav, P.K., Hodge, C.N., Domaille, P.J., and Chang, C.H. 1995. Flexibility and function in HIV-1 protease. Nat. Struct. Mol. Biol. **2:**274–280.
Nikaido, H., Liu, W., and Rosenberg, E.Y. 1990. Outer membrane permeability and β-lactamase

stability of dipolar ionic cephalosporins containing methoxyimino substituents. Antimicrob. Agents Chemother. **34:**337–342.
O'Callaghan, C.H. 1979. Description and classification of the newer cephalosporins and their relationships with the established compounds. J. Antimicrob. Chemother. **5:**635–671.
Papp-Wallace, K.M., Bethel, C.R., Distler, A.M., Kasuboski, C., Taracila, M., and Bonomo, R.A. 2010. Inhibitor resistance in the KPC-2 β-lactamase, a preeminent property of this class A β-lactamase. Antimicrob. Agents Chemother. **54(2):**890–897.
Papp-Wallace, K.M., Endimiani, A., Taracila, M.A., and Bonomo, R.A. 2011. Carbapenems: past, present, and future. Antimicrob. Agents Chemother. **55(11):**4943–4960.
Papp-Wallace, K.M. and Bonomo, M.D. 2016. New β-lactamase inhibitors in the clinic. Infect. Dis. Clin. North. Am. **30(2):**441–464.
Park, J.T. and Uehara, T. 2008. How bacteria consume their own exoskeletons (turnover and recycling of cell wall peptidoglycan). Microbiol. Mol. Biol. Rev. **72(2):**211–227.
Pica, A. and Graziamo, G. 2016. Shedding light on the extra thermal stability of thermophilic proteins. Biopolymers. **105:**856–863.
Poole, K. 2004. Efflux-mediated multiresistance in Gram-negative bacteria. Clin. Microbiol. Infect. **10:**12–26.
Powers, R.A., Caselli, E., Focia, P.J., Prati, F., and Shoichet, B.K. 2001. Structures of ceftazidime and its transition-state analogue in complex with AmpC β-lactamase: implications for resistance mutations and inhibitor design. Biochemistry. **40:**9207–9214.
Prabaker, K. and Weinstein, R.A. 2011. Trends in antimicrobial resistance in intensive care units in the United States. Curr. Opin. Crit. Care. **17:**472–479.
Raimondi, A., Sisto, F., and Nikaido, H. 2001. Mutation in *Serratia marcescens* AmpC β-lactamase producing high-level resistance to ceftazidime and cefpirome. Antimicrob. Agents Chemother. **45:**2331–2339.
Rammelkamp, C.H. and Keefer, C.S. 1943. Penicillin: Its antibacterial effect in whole blood and serum for the hemolytic *Streptococcus* and *Staphylococcus aureus*. J. Clin. Investig. **22:**649–657.
Reading, C. and Cole. M. 1977. Clavulanic acid: a β-lactamase-inhibiting β-lactam from *Streptomyces clavuligerus*. Antimicrob. Agents Chemother. **11:**852–857.
Rice, L.B. 2009. The clinical consequences of antimicrobial resistance. Curr. Opin. Microbiol. **12(5)**:476–481.
Richards, F.M. 1977. Areas, volumes, packing, and protein structure. Annu. Rev. Biophys. Bioeng. **6:**151–176.
Rodríguez-Martínez, J.M., Poirel, L., and Nordmann, P. 2009. Extended-spectrum cephalosporinases in *Pseudomonas aeruginosa.* Antimicrob Agents Chemother. **53(5):**1766–1771.
Sader, H.S., Rhomberg, P.R., Farrell, D.J., and Jones, R.N. 2011. Antimicrobial activity of CXA-101, a novel cephalosporin tested in combination with tazobactam against Enterobacteriaceae, *Pseudomonas aeruginosa*, and *Bacteroides fragilis* strains having various resistance phenotypes. Antimicrob. Agents Chemother. **55(5):**2390–2394.
Sauvage, E., Kerff, F., Terrak, M., Ayala, J.A., and Charlier, P. 2008. The penicillin-binding proteins: structure and role in peptidoglycan biosynthesis. FEMS Microbiol. Rev. **32:**234–258.
Schreiber, G., Buckle, A.M., and Fersht, A.R. 1994. Stability and function: two constraints in the evolution of barstar and other proteins. Structure. **2:**945–951.

Skalweit, M.J., Li, M., and Taracila, M.A. 2015. Effect of asparagine substitutions in the YXN loop of a class C β-lactamase of *Acinetobacter baumannii* on substrate and inhibitor kinetics. Antimicrob. Agents Chemother. **59(3):**1472–1477.

Smoum, R., Rubinstein, A., Dembitsky, V.M., and Srebnki, M. 2012. Boron containing compounds as protease inhibitors. Chem. Rev. **112(7):**4156–4220.

Stachyra, T., Péchereau, M.C., Bruneau, J.M., Claudon, M., Frère, J.M., Miossec, C., Coleman, K., and Black, M.T. 2010. Mechanistic studies of the inactivation of TEM-1 and P99 by NXL104, a novel non–β-lactam β-lactamase inhibitor. Antimicrob. Agents Chemother. **54:**5132–5138.

Starteva, T. and Yordanov, D. 2009. *Pseudomonas aeruginosa* – a phenomenon of bacterial resistance. J. Med. Microbiol. **58:**1133–1148.

Takeda, S., Ishii, Y., Hatano, K., Tateda, K., and Yamaguchi, K. 2007. Stability of FR264205 against AmpC β-lactamase of *Pseudomonas aeruginosa.* Int. J. Antimicrob. Agents. **30:**443–445.

Talwalkar, J.S., and Murray, T.S. 2016. The approach to *Pseudomonas aeruginosa* in cystic fibrosis. Clin. Chest Med. **37:**69–81.

Thaden, J.T., Park, L.P., Maskarinec, S.A., Ruffin, F., Fowler, V.G., and van Duin, D. 2017. Results from a 13-year prospective cohort study show increased mortality associated with bloodstream infections caused by *Pseudomonas aeruginosa* compared to other bacteria. Antimicrob. Agents Chemother. **61(6):**e02671-16.

Toda, A., Ohki, H., Yamanaka, T., Murano, K., Okuda, S., Kawabata, K., Hatano, K., Matsuda, K., Misumi, K., Itoh, K., Satoh, K., and Inoue, S. 2008. Synthesis and SAR of novel parenteral anti-pseudomonal cephalosporins: discovery of FR264205. Bioorg. Med. Chem. Lett. **18:**4849–4852.

Tomanicek, S.J., Wang, K.K., Weiss, K.L., Blakeley, M.P., Cooper, J., Chen, Y., and Coates, L. 2011. The active site protonation states of perdeuterated Toho-1 β-lactamase determined by neutron diffraction support a role for Glu166 as the general base in acylation. FEBS Lett. **585:**364–368.

Tondi, D., Morandi, F., Bonnet, R., Costi, M.P., and Shoichet, B.K. 2005. Structure-based optimization of a non-β-lactam lead results in inhibitors that do not up-regulate β-lactamase expression in cell culture. J. Am. Chem. Soc. **127:**4632–4639.

Urbach, C., Evrard, C., Pudzaitis, V., Fastrez, J., Soumillion, P., and Declercq, J.P. 2009. Structure of PBP-A from *Thermosynechococcus elongatus*, a penicillin-binding protein closely related to class A β-lactamases. J. Mol. Biol. **386:**109–120.

Vadlamani, G., Thomas, M.D., Patel, T.R., Donald, L.J., Reeve, T.M., Stetefeld, J., Standing, K.G., Vocadlo, D.J., and Mark, B.L. 2015. The β-lactamase gene regulator AmpR is a tetramer that recognizes and binds the D-Ala–D-Ala motif of its repressor UDP-*N*-acetylmuramic acid (MurNAc)-pentapeptide. J. Biol. Chem. **290(5):**2630–2643.

van Duin, D., and Bonomo, A.R. 2016. Ceftazidime/avibactam and ceftolozane/tazobactam: second generation β-lactam/β-lactamase inhibitor combinations. Clin. Infect. Dis. **63(2):**234–241.

Vollmer, W., Joris, B., Charlier, P., and Foster, S. 2008. Bacteria peptidoglycan (murein) hydrolases. FEMS Microbiol. Rev. **32:**259–286.

Votsch, W. and Templin, M.F. 2000. Characterization of a β-N-acetylglucosaminidase of *Escherichia coli* and elucidation of its role in muropeptide recycling and β-lactamase induction. J. Biol. Chem. **275(50):**39032–39038.

Walsh, T. R., Toleman, M.A., Poirel, L., and Nordmann, P. 2005. Metallo-β-lactamases: the quiet before the storm? Clin. Microbiol. Rev. **18:**306–325.
Walther-Rasmussen, J., and Hoiby, N. 2006. OXA-type carbapenemases. J. Antimicrob. Chemother. **57:**373–383.
Wang, X., Minasov, G., and Shoichet, B.K. 2002. Evolution of an antibiotic resistance enzyme constrained by stability and activity trade-offs. J. Mol. Biol. **320:**85–95.
Whitford, D. 2005. Proteins: structure and function. Wiley Publishing Co, Hoboken, NJ.
World Health Organization. 2017. WHO publishes list of bacteria for which new antibiotics are urgently needed. Geneva, Switzerland.
Zhanel, G.G., Chung, P., Adam, H., Zelenitsky, S., Denisuik, A., Schweizer, F., Lagacé-Wiens, P.R.S., Rubinstein, E., Gin, A.S., Walkty, A., Hoban, D.J., Lynch 3rd, J.P., and Karlowsky, J.A. 2014. Ceftolozane/tazobactam: a novel cephalosporin/β-lactamase inhibitor combination with activity against multidrug-resistant gram-negative bacilli. Drugs. **74:**31–51.
Zhanel, G.G., Lawrence, C.K., Adam, H., Schweizer, F., Zelenitsky, S., Zhanel, M., Lagacé-Wiens, P.R.S., Walkty, A., Denisuik, A., Golden, A., Gin, A.S., Hoban, D.J., Lynch III, J.P., and Karlowsky, J.A. 2018. Imipenem-relebactam and meropenem-vaborbactam: two novel carbapenem-β-lactamase inhibitor combinations. Drugs. **78:**65–98.